THEORETICAL INVESTIGATION OF HIGHLY POTENT HIV-1 RT INHIBITORS IN THE CLASS OF EFAVIRENZ DERIVATIVES, BASED ON QUANTUM CHEMICAL CALCULATIONS AND MOLECULAR MODELING

AURADEE PUNKVANG

A THESIS SUBMITTED IN PARTIAL FULFILLMENT OF THE REQUIREMENTS

FOR THE DEGREE OF MASTER OF SCIENCE

MAJOR IN CHEMISTRY

FACULTY OF SCIENCE

UBON RAJATHANEE UNIVERSITY

YEAR 2006

THESIS APPROVAL

UBON RAJATHANEE UNIVERSITY

MASTER OF SCIENCE

MAJOR IN CHEMISTRY FACULTY OF SCIENCE

TITLE THEORETICAL INVESTIGATION OF HIGHLY POTENT HIV-1 RT INHIBITORS IN THE CLASS OF EFAVIRENZ DERIVATIVES, BASED ON QUANTUM CHEMICAL CALCULATIONS AND MOLECULAR MODELING

NAME MS.AURADEE PUNKVANG

THIS THESIS HAS BEEN ACCEPTED BY

..... CHAIR

(ASSOC.PROF.DR.SUPA HANNONGBUA)

..... COMMITTEE

(DR.PORNPAN PUNGPO)

..... COMMITTEE

(DR.CHAN INNTAM)

..... COMMITTEE

(DR.SIRIPORN JUNGSUTTIWONG)

..... DEAN

(DR. JANPEN INTARAPRASERT)

APPROVAL BY UBON RAJATHANEE UNIVERSITY

.....

(ASST.PROF.DR.UTITH INPRASIT)

VICE PRESIDENT FOR ACADEMIC AFFAIRS

FOR THE PRESIDENT OF UBON RAJATHANEE UNIVERSITY

ACADEMIC YEAR 2006

ACKNOWLEDGEMENT

I would like to express my deepest gratitude to my advisor, Dr. Pornpan Pungpo for her continuous support, encouragement, and guidance throughout in my study. Furthermore, I would to thank Associate Professor Dr.Supa Hannongbua for her helpful guidance and continuous supports in various ways.

I would like to thank my thesis committees, Dr.Siriporn Jungsuttiwong and Dr.Chan Inntam for their helpful suggestion.

Special thank to Dr. Patcheenart Saparpakorn for valuable assistance and continuing supports in various way. Dr. Songwut Suramitr is also appreciated for his suggestion on my work.

The Thailand Research Fund (BRG4780007) and Faculty of Science, Ubonrajathanee University, are gratefully acknowledged for partially financial supports for the study.

Department of Chemistry, Faculty of Science, Ubonrajathanee University, the Laboratory for Computational and Applied Chemistry (LCAC) at Kasetsart University, the High Performance Computing Center of the National Electronics and Computer Technology (NECTEC) and the Computer Center of University of Vienna are also gratefully acknowledged for computational resource and software facilities.

Finally, I thank my family, who always love and understand whatever I am. They always encourage and unconditional support me throughout in my study.

Auradee Punkvang

(Miss Auradee Punkvang)

Researcher

บทคัดย่อ

ชื่อเรื่อง : การศึกษาทางทฤษฎีของตัวยับยั้งเอนไซม์การถ่ายแบบเอชไอวี-1 ที่ออกฤทธิ์สูงในกลุ่มของสารอนุพันธ์อีฟาวิเร็นซ์โดยใช้การคำนวณเคมีควอนตัมและการจำลองแบบโมเลกุล

โดย : อรดี พันธ์กว้าง

ชื่อปริญญา : วิทยาศาสตรมหาบัณฑิต

สาขาวิชา : เคมี

ประธานกรรมการที่ปรึกษา : รองศาสตราจารย์ ดร.สุภา หารหนองบัว

ศัพท์สำคัญ : ตัวยับยั้งเอนไซม์การถ่ายแบบเอชไอวี-1 อีฟาวิเร็นซ์ โมเลคูลาร์ด็อกกิ้ง ค่ากัมมันตภาพ คอนฟอร์เมชัน

การศึกษานี้ได้ทำการศึกษาคอนฟอร์เมชันของตัวยับยั้งเอนไซม์การถ่ายแบบเอชไอวี-1 ในกลุ่มของสารยับยั้งอีฟาวิเร็นซ์ และสารอนุพันธ์อีฟาวิเร็นซ์ที่ออกฤทธิ์สูงในการยับยั้งเอนไซม์การถ่ายแบบเอชไอวี-1 ทั้งชนิดดั้งเดิมและชนิดที่มีการกลายพันธุ์ของกรดอะมิโนที่ตำแหน่ง 103 จากไลซินเป็นแอสพาราจีน (K103N) โดยอาศัยระเบียบวิธีการคำนวณทางเคมีควอนตัมในการสร้างแผนภาพพลังงานศักย์ในเชิงสองมิติและสามมิติ ผลการศึกษาพบว่าแผนภาพพลังงานศักย์ที่ได้จากการคำนวณด้วยระเบียบวิธีการคำนวณขั้นสูง สามารถทำให้เข้าใจถึงคอนฟอร์เมชันที่เป็นไปได้ของสารยับยั้งอีฟาวิเร็นซ์และสารอนุพันธ์อีฟาวิเร็นซ์ และชี้ให้เห็นว่าโมเลกุลของสารยับยั้งอีฟาวิเร็นซ์และสารอนุพันธ์มีความยืดหยุ่นในโมเลกุลสูงซึ่งจะแสดงบทบาทสำคัญในการยับยั้งเอนไซม์การถ่ายแบบเอชไอวี-1 ทั้งชนิดดั้งเดิมและชนิดกลายพันธุ์ และยังพบว่าคอนฟอร์เมชันของสารยับยั้งอีฟาวิเร็นซ์ที่ได้จากการคำนวณนี้ สอดคล้องกับคอนฟอร์เมชันของสารยับยั้งอีฟาวิเร็นซ์ในโพรงการจับของเอนไซม์การถ่ายแบบเอชไอวี-1 ที่ได้จากการคำนวณโมเลคูลาร์ด็อกกิ้ง นอกจากนี้ในการศึกษานี้ได้ทำการศึกษาอันตรกิริยาระหว่างสารอนุพันธ์อีฟาวิเร็นซ์และโพรงการจับของเอนไซม์การถ่ายแบบเอชไอวี-1 ทั้งชนิดดั้งเดิมและชนิดกลายพันธุ์โดยการคำนวณโมเลคูลาร์ด็อกกิ้ง ด้วยโปรแกรม Autodock 3.05 จากการศึกษาพบว่าการคำนวณโมเลคูลาร์ด็อกกิ้งมีความสามารถในการทำนายตำแหน่งการจัดวางตัวของสารยับยั้งอีฟาวิเร็นซ์ ในโพรงการจับของเอนไซม์การถ่ายแบบเอชไอวี-1 ทั้งชนิดดั้งเดิมและชนิดกลายพันธุ์ได้สอดคล้องกับผลที่ได้จากการศึกษาโครงสร้างผลึกทางเอ็กซ์เรย์โดยให้ค่า root mean square deviation น้อยกว่า 1.0 อังสตรอม ดังนั้นการคำนวณ

โมเลคูลาร์ด็อกกิ้งจึงมีความเหมาะสมที่จะนำไปใช้ในการทำนายตำแหน่ง และการจัดวางตัวของสารอนุพันธ์อีฟาวิเร็นซ์ในโพรงการจับของเอนไซม์การถ่ายแบบเอชไอวี-1 ที่ยังไม่มีการศึกษาข้อมูลทางโครงสร้างผลึกทางเอ็กซ์เรย์มาก่อน และผลที่ได้จากการคำนวณโมเลคูลาร์ด็อกกิ้งนี้สามารถอธิบายถึงอันตรกิริยาที่สำคัญของสารยับยั้งอีฟาวิเร็นซ์ และสารอนุพันธ์อีฟาวิเร็นซ์ในการยับยั้งเอนไซม์การถ่ายแบบเอชไอวี-1 ทั้งชนิดดั้งเดิมและชนิดกลายพันธุ์ได้ นอกจากนี้ความสัมพันธ์ระหว่างอันตรกิริยาที่ได้จากการคำนวณโมเลคูลาร์ด็อกกิ้ง และค่ากัมมันตภาพในการยับยั้งที่ได้จากการทดลองสามารถทำให้เข้าใจถึงอันตรกิริยาที่สำคัญของตัวยับยั้งเอนไซม์การถ่ายแบบเอชไอวี-1 นอกจากนี้เมื่อทำการศึกษาความสัมพันธ์ระหว่างโครงสร้าง และค่ากัมมันตภาพในเชิงสามมิติของสารอนุพันธ์อีฟาวิเร็นซ์ในการยับยั้งเอนไซม์การถ่ายแบบเอชไอวี-1 ด้วยระเบียบวิธีการวิเคราะห์เชิงเปรียบเทียบสนามของโมเลกุลและวิธีวิเคราะห์เปรียบเทียบดัชนีความเหมือนเชิงโมเลกุล โดยใช้การวางซ้อนทับกันของโมเลกุลที่ได้จากการคำนวณโมเลคูลาร์ด็อกกิ้ง พบว่าแบบจำลองที่ได้จากทั้งสองวิธีสามารถทำนายกัมมันตภาพในการยับยั้งที่สอดคล้องกับค่าที่ได้จากการทดลอง นอกจากนี้แผนภาพคอนทัวร์ที่ได้จากวิธีการวิเคราะห์เชิงเปรียบเทียบสนามของโมเลกุล และวิธีวิเคราะห์เปรียบเทียบดัชนีความเหมือนเชิงโมเลกุล สามารถชี้ให้เห็นถึงความต้องการทางโครงสร้างของตัวยับยั้งเอนไซม์การถ่ายแบบเอชไอวี-1 ทั้งชนิดดั้งเดิมและชนิดกลายพันธุ์ได้ เมื่อพิจารณาผลการศึกษาทั้งหมดที่ได้จากวิธีการคำนวณทางเคมีควอนตัม การคำนวณโมเลคูลาร์ด็อกกิ้ง และการศึกษาความสัมพันธ์ระหว่างโครงสร้างและค่ากัมมันตภาพในเชิงสามมิติ สามารถชี้แนะถึงความต้องการทางโครงสร้างที่สำคัญของตัวยับยั้งเอนไซม์การถ่ายแบบเอชไอวี-1 ในกลุ่มของสารอนุพันธ์อีฟาวิเร็นซ์ และสามารถออกแบบโมเลกุลของตัวยับยั้งในกลุ่มของสารอนุพันธ์อีฟาวิเร็นซ์ให้มีประสิทธิภาพสูงในการยับยั้งเอนไซม์การถ่ายแบบเอชไอวี-1 ได้ ซึ่งนับว่าเป็นประโยชน์อย่างยิ่งต่อการพัฒนาตัวยับยั้งเพื่อใช้เป็นยาต้านโรคเอดส์ต่อไป

ABSTRACT

TITLE : THEORETICAL INVESTIGATION OF HIGHLY POTENT HIV-1 RT INHIBITORS IN THE CLASS OF EFAVIRENZ DERIVATIVES, BASED ON QUANTUM CHEMICAL CALCULATIONS AND MOLECULAR MODELING

BY : AURADEE PUNKVANG

DEGREE : MASTER OF SCIENCE

MAJOR : CHEMISTRY

CHAIR : ASSOC.PROF.SUPA HANNONGBUA, Ph.D.

KEYWORDS : HIV-1 RT INHIBITORS / EFAVIRENZ / MOLECULAR DOCKING / 3D-QSAR / CONFORMATIONAL ANALYSIS

Conformational analysis of HIV-1 reverse transcriptase inhibitor (s)–6-chloro–4-(cyclopropylethynyl)-1,4–dihydro-4-(trifluoromethyl)-2H-3, 1-benzoxazin-2-one (efavirenz) and selected derivatives were investigated based on various methods of quantum chemical calculations. The 2D PES and 3D PES for these compounds were examined. The results show that the conformational analysis based on high theory of calculations could provide beneficial information concerning the preferred conformation. Moreover, the conformation analysis results are accurate enough to predict the binding mode of compounds comparable to docking calculations. Consecutively, molecular docking and 3D-QSAR analyses were performed to understand the interaction between a series of efavirenz derivatives with WT and K103N HIV-1 RT. To model the potential binding modes of efavirenz derivatives in the binding pocket of WT and K103N HIV-1 RT, molecular docking approach by using Autodock 3.05 program was carried out. The results show that the obtained docking results reveal a good ability to reproduce the X-ray bound conformation with rmsd less than 1.0 Å for both WT and mutant enzymes. The docking calculations of all efavirenz derivatives in the data set were, then, carried out to elucidate their orientations in the binding pockets. The results derived from docking analysis give additional information and further probes the inhibitor-enzyme interactions. The correlation of the

results obtained from docking models and the inhibitory activities validate each other and lead to better understanding of the structural requirements for the activity. Therefore, these results are informative to improve the development of more efficient HIV-1 RT inhibitors, especially, active against the mutant enzyme. Based on the molecular alignment of conformations obtained from molecular docking procedures, the high predictive 3D-QSAR models were produced by using CoMFA and CoMSIA approaches. The CoMFA models reveal the importance of steric and electrostatic interactions through contour maps. The resulting CoMSIA models enhance the understanding of steric, electrostatic, hydrophobic, electron donor and acceptor requirements for ligands binding to the K103N HIV-1 RT. Accordingly, the results obtained from quantum chemical calculations, structure-based and ligand-based design approaches can be combined to identify the structural requirements of HIV-1 RT inhibitors in the class of efavirenz compounds. The principle derived from the present study provides a gainful guideline to design and predict novel and highly potent compounds for WT and K103N HIV-1 RT inhibitions.

CONTENTS

LIST OF TABLES

LIST OF TABLES (CONTINUED)

LIST OF TABLES (CONTINUED)

LIST OF FIGURES

LIST OF FIGURES (CONTINUED)

LIST OF FIGURES (CONTINUED)

LIST OF FIGURES (CONTINUED)

LIST OF FIGURES (CONTINUED)

ABBREVIATIONS

AIDS	=	Acquired Immunodeficiency Syndrome
AM1	=	Austin Model 1
CoMFA	=	Comparative Molecular Field Analysis
CoMSIA	=	Comparative Molecular Similarity Index Analysis
cv	=	Cross-validation
DFT	=	Density functional theory
ddI	=	2',3' -dideoxyinosine
ddC	=	2',3' -dideoxycytidine
F	=	F-test Value
GIAO	=	Gauge-including atomic orbitals
GTO	=	Gaussian Type Orbital
HEPT	=	1-[(2-Hydroxyethoxy)methyl]-6-(phenylthio)thymine
HF	=	Hartree-Fock Theory
His	=	Histidine
HIV-1	=	Human Immunodeficiency Virus Type 1
LCAO-MO	=	Linear Combination of Atomic Orbitals to Molecular Orbitals
Leu	=	Leucine
log (1/C)	=	Logarithms of Reciprocal Molar Concentrations
Log P	=	Log of the Octanol-water Partition Coefficient
LGA	=	Lamarckian Genetic Algorithm
Lys	=	Lysine
MLR	=	Multiple Linear Regression
MT	=	Mutant Type
noc	=	Number of Component
NRTI	=	Nucleoside Reverse Transcriptase Inhibitor
NNRTI	=	Non-Nucleoside Reverse Transcriptase Inhibitor
Phe	=	Phenylalanine
PLS	=	Partial Least-Suqares

ABBREVIATIONS (CONTINUED)

PM3	=	Modified Neglect of Diatomic overlap, Parametric Method Number 3
PRESS	=	Prediction Error Sum of Squares
Pro	=	Proline
r^2_{cv}	=	Predictive Ability
QSAR	=	Quantitative Structure-Activity Relationships
2D PES	=	The two-dimensional potential energy surface
3D PES	=	The three-dimensional potential energy surface
3D-QSAR	=	Three dimensional quantitative structure activity relation ships
r^2	=	Squared correlation coefficient
RT	=	Reverse Transcriptase
RMS	=	Root mean square
SAR	=	Structure-activity Relationships
SCF	=	Self-Consistent Field
SD	=	Standard deviation
S_{PRESS}	=	The Standard of Error of Prediction
SSY	=	Sum of Squares of Deviation between the Affinities of the Fitted Set and Their Mean Affinity
STO	=	Slater Type Orbital
TIBO	=	Tetrahydroimidazo [4,5,1-jk]benzo diazepine-2(1H)-thione
Trp	=	Tryptophan
Tyr	=	Tyrosine
Val	=	Valine
WT	=	Wild Type

CHAPTER 1

INTRODUCTION

AIDS (Acquired Immunodeficiency Syndrome) is a worldwide pandemic caused by an infection with HIV. Already, more than twenty-five million people around the world have died of AIDS-related diseases [http://www.avert.org/aroundworld.html]. At time AIDS still remains an incompletely treatment. Therefore, the treatment for AIDS has been the most challenging worldwide medical problem. HIV is a retrovirus, which replicates in a human host cell. In the life cycle of HIV, the reverse transcriptase (RT) is a key multifunctional enzyme that constitutes an important target for the development of new antiviral agents. HIV-1 RT copies the RNA genome of HIV-1 into DNA, which is subsequently integrated into the host cell's genome [Tummino *et al.*, 1995].

The crystal structure of HIV-1 RT had been solved [Kohlstaedt *et al.*, 1992]. The HIV-1 RT is a heterodimer, composed of a 66 kDa subunit and its truncated N-coterminal 51 kDa define as p66 and p51, respectively. The crystal structure of HIV-1 RT resembles a human right hand and it reveals that both subunits each contain four common subdomains, termed the finger, palm, thumb and connection (Figure 1). The overall folding of the subdomians is similar in p66 and p51 but their spatial arrangements differ markedly. The p66 subunit has a large nucleic acid-binding cleft formed by the finger, palm and thumb. The polymerase active site of the enzyme resides within the p66 palm domain as show in Figure 1.

HIV-1 RT inhibitors have been developed and classified into two main categories: nucleoside and non-nucleoside analogues. The nucleoside RT inhibitors (NRTIs) such as AZT, ddC and ddI, shown in Figure 2, have been widely used to treat AIDS patients. NRTIs are attractive drug candidates in that their binding site is unique to the reverse transcriptase of HIV-1. Thus these derivatives are high cellular toxicity and several side effects result from the disruption of normal DNA polymerase activity. The other class of HIV-1 RT inhibitors is the non-nucleosides RT inhibitors (NNRTIs). The NNRTIs are highly specific for HIV-1 reverse transcriptase by binding an allosteric site in a noncompetitive manner with respect to the substrate

and displacing the polymerase active site catalytic residues [Evans *et al*, 1991]. The NNRTIs have been classified into first and second generation NNRTIs. The first generation NNRTIs such as 1-[(2-Hydroxyethoxy)-methyl]-6-(phenylthio) thymine (HEPT), tetrahydroimidazo [4,5,1-jk]benzo diazepine-2(1H)-thione (TIBO) and dipyridodiazepinone (nevirapine), shown in Figure 3, are much less toxic than the NRTIs. Nevertheless, the emergence of drug-resistant viral strains has limited the therapeutic efficacy of NNRTIs [Tantillo *et al*, 1994]. Therefore, the second generation NNRTIs such as efavirenz, capravirine and dapivirine, shown in Figure 4, are identified and discovered for high binding affinity in both absence and presence of specific mutations.

Efavirenz, (-)-6-chloro-4-cyclopropylethynyl-4-trifluoromethyl-1, 4-dihydro-2*H*-3, 1-benzoxazin-2-one, was selected in this study. Efavirenz (SUSTIVA) is the second generation NNRTI which has been approved for the treatment of the acquired immunodeficiency syndrome at Merck research laboratories [Young *et al*, 1995]. However, efavirenz encounters with the rapid drug resistance. The mutations at K103N, L100I, and Y188L have been observed [Young *et al*, 1995]. Among the mutations, K103N is most frequently observed (>90%) in patients failing therapy, either alone or in combination with additional mutations [Miller *et al.*, 1998; Torti *et al*, 2001; Conway *et al.*, 2001; Bacheler *et al.*, 2001]. Due to the observation of breakthrough mutations of the reverse transcriptase enzyme during efavirenz therapy, the development processes of an optimized efavirenz derivatives are still required.

Developments of compound with the high ability to inhibit both wild type and mutant type HIV-1 RT need to understand the inhibitory molecular mechanic, three dimensional structure and structural requirements of inhibitors. Computer aided molecular design has developed into useful tools in facilitating new drug discovery. By the use of this method, the biological activity of the candidate molecules can be estimated before experimental trials. Thus, they are simple and non-expensive and expedite to design molecules with desirable biological activity. Quantitative structure-activity relationship (QSAR) and docking procedure are two mostly used computational methods in drug design. In QSAR methodologies, a mathematical relationship, relating the biological activity to some molecular descriptors is obtained. Docking studies were used to study the binding mode of the candidate inhibitors to an enzyme with known structure. Through docking procedures, not only new biological active compound is introduced,

but also the chemistry of the inhibitor–enzyme interaction is well recognized.

In the present study, to investigate highly potent HIV-1 RT inhibitors in class of efavirenz derivatives the following objects were performed;

(1) Conformational analysis was used to search the possible conformation of efavirenz and its derivatives based on quantum chemical calculation.

(2) Molecular docking calculation was used to investigate interaction and binding mode of efavirenz derivatives in WT and K103N HIV-1 RT binding pocket.

(3) CoMFA and CoMSIA were used to better understand the relation between structure and activity of efavirenz derivative.

(4) The obtained results were used to design new potent inhibitors in the class of efavirenz derivatives for against WT and K103N HIV-1 RT.

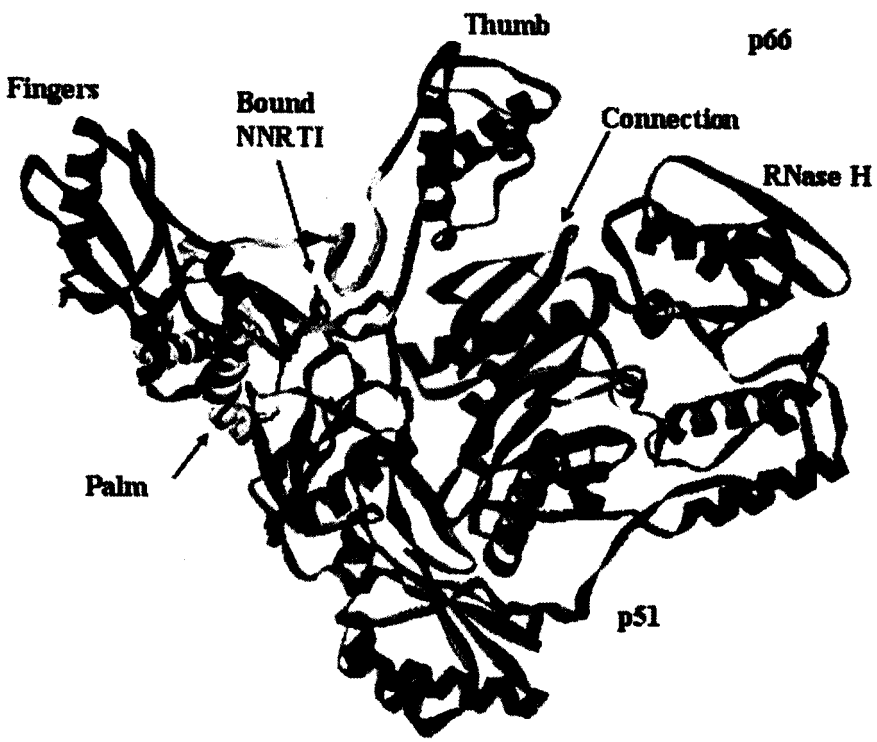

Figure 1 Structure of the HIV-1 RT in complex with the non-nucleoside inhibitor efavirenz (coordinates are from PDB entry 1FK9)

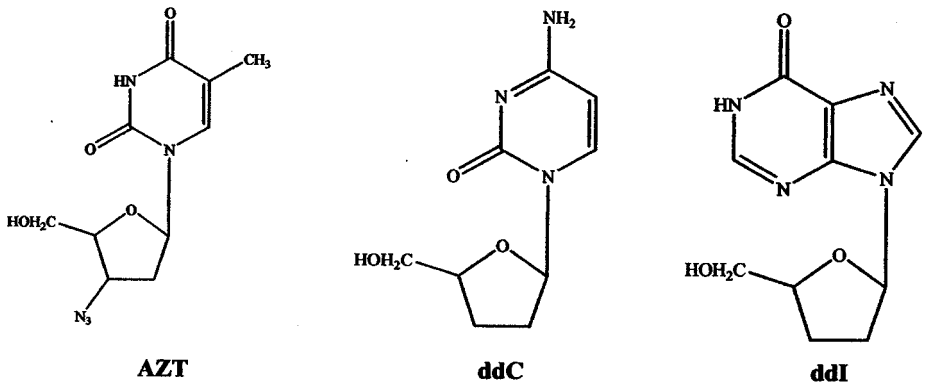

Figure 2 The nucleoside RT inhibitors (NRTIs); AZT, ddC and ddI

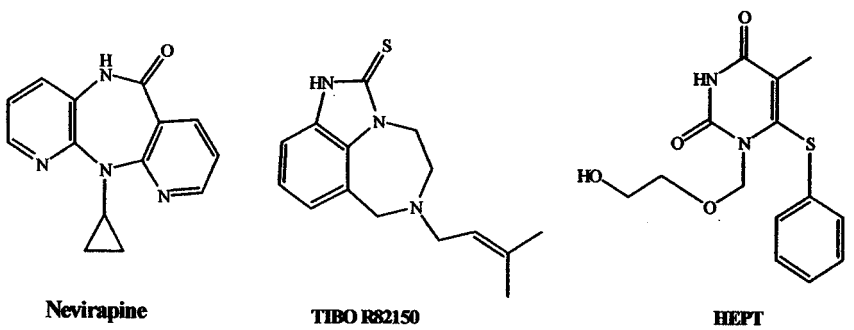

Figure 3 The first generation NNRTIs; HEPT, TIBO and nevirapine

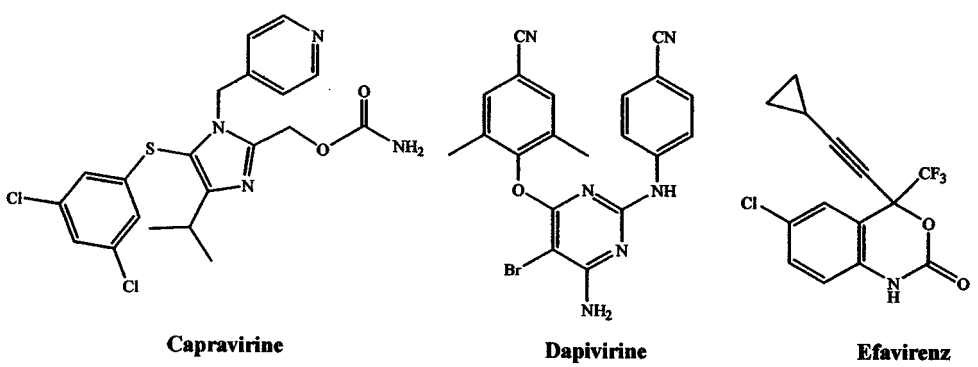

Figure 4 The second generation NNRTIs; dapivirine, capravirine and efavirenz

CHAPTER 2

LITERATURE REVIEW

Smith *et al.* (1995) investigated three nonnucleoside inhibitors (nevirapine, a-APA, TIBO) complexe with human immunodeficiency virus type 1 (HIV-1) reverse transcriptase (RT) by using computer modeling. Results from the minimizations of solvated complexes of three nonnucleoside inhibitors show that all three inhibitors maintaain very similar conformational shape, roughly overlay each other in the binding pocket.

Young *et al.* (1995) developed a new class of NNRTIs, the 1,4-dihydro-2*H*-3, 1-benzoxazin-2-ones. L-743,726 (DMP-266). Result, the compound was a potent inhibitor of the wild-type HIV-1 RT (K_i = 2.93 nM) and exhibited a 95% inhibitory concentration of 1.5 nM for the inhibition of HIV-1 replicative spread in cell culture. In addition, L-743,726 was found to be capable of inhibiting a single mutant RT amino acid. Derivation of virus with notably reduced susceptibility to the inhibitor required prolonged cell culture selection and was mediated by a combination of at least two RT amino acid substitutions. Studies of L-743,726 in rats, monkeys, and a chimpanzee demonstrated the compound's potential for good oral bioavailability and pharmacokinetics in humans.

Hopkins *et al.* (1996) investigated crystal structures of HIV-1 RT complex with inhibitors of the HEPT Series. These structures reveal that conformational changes which correlate with changes in potency, suggest that a major determinant of increased potency in the analogues of HEPT is an improved interaction between residue Tyr181 in the protein and the 6-benzyl ring of the inhibitors which stabilizes the structure of the complex.

Font *et al.* (1997) investigated the relationship between the chemical structure and the HIV-1 RT inhibitory activity for a series of quinoline derivatives. Two methods were used: a standard QSAR analysis, by combining the methods of Hansch and Free-Wilson, and an analysis using quantum chemistry indices as descriptor parameters, by the semiempirical method AM1. The result show that the activity of the compounds increases, mainly, with the presence of electron-withdrawing substituents in position 6 of the quinoline ring that cause a decrease in the

energy from the molecular orbital LUMO.

Vig *et al.* (1998) have been synthesized and designed a series of novel phenethylthiazolylthiourea (PETT) derivatives targeting the nonnucleoside inhibitor (NNI) binding site of HIV reverse transcriptase (RT) based on structure-based design. The results show that these novel PETT derivatives were more active than AZT or trovirdine and showed potent anti-HIV activity with IC50[p24] values of <1 nM and selectivity indices of >100,000.

Sudbeck *et al.* (1998) designed two highly potent dihydroalkoxybenzyloxopyrimidine (DABO) derivatives targeting the nonnucleoside inhibitor (NNI) binding site of human immunodeficiency virus (HIV) reverse transcriptase (RT) based on the structure-based design and tested for anti-HIV activity. DABO derivative, 5-isopropyl-2-[(methylthiomethyl)thio]-6-(benzyl)-pyrimidin-4-(1*H*)-one, elicited potent inhibitory activity against purified recombinant HIV RT at nanomolar concentrations (50% inhibitory concentration, <1 nM) but showed no detectable cytotoxicity at concentrations as high as 100 mM.

Hsiou *et al.* (1998) determined the structure of HBY 097 complexed with wild-type and mutant type (Tyr188Leu) HIV-1 RT at 3.1 Å and 3.3 Å resolution, respectively. The results present that both complex structure reveal an overall inhibitor geometry and binding mode differing significantly from RT/NNRTI structures reported earlier, in that HBY 097 does not adopt the usual butterfy-like shape. Moreover, the results could suggest that inhibitor flexibility can help to minimize drug resistance.

Barreca *et al.* (1999) analyzed the reverse transcriptase (RT) inhibitory activity of TIBO derivatives by comparative molecular field analysis (CoMFA). Besides conventional steric and electrostatic fields, molecular lipophilicity potential (MLP) was also used as a third field in CoMFA. An informative and statistically significant model (q^2=0.70, r^2=0.90, s=0.46) was obtained by taking into account the three field types together. The results show good predictions and suggesting a similar binding mode for TIBO and TBZ derivatives. Flexible docking experiments on TBZ, TIBO and other NNIs conformed common binding characteristics, as found out also by CoMFA, and moreover a good correlation between calculated binding energies and inhibitory potency was found.

Lawtrakul *et al.* (1999) calculated the conformations of the HIV-1 reverse transcriptase inhibitor 1-[(2-hydroxyethoxy)methyl]-6-(phenylthio)thymine (HEPT) by

semiempirical and mainly by *ab initio* methods in order to estimate the potential for the rotation around the carbon sulfur single bond. The conformational analysis of HEPT shows two energy minima with respect to the orientation of both aromatic systems. The NMR spectra of two local minima are calculated to obtain some information about its structure in solution. The structure of HEPT in the complex is analysed to study the intermolecular interactions between the inhibitor and the surrounding protein, which determine the geometry of the inhibition complex.

Hannongbua *et al.* (1999) applied quantitative structure-activity relationships (QSAR) and comparative molecular field analysis (CoMFA) to explain the structural requirements of HIV-1 reverse transcriptase (HIV-1 RT) inhibitory activity of TIBO derivative on the MT-4 cells. The results indicate the importance of electronic contributions toward the HIV-1 RT inhibition of this class of compounds. However, it could not reveal any hydrophobic influence because of high collinearity between C2 and log P variables. The obtained CoMFA model shows high predictive ability, $r_{cv}^2 = 0.771$, and clearly demonstrates its potential in the steric feature of the molecular through contour maps, explaining a majority (81.8%) of the variance in the data. Consequently, these results can be useful in identifying the structural requirements of TIBO derivatives and helpful for better understanding the HIV-1 RT inhibition. Eventually, they provide a beneficial basis to design new and more potent inhibitors of HIV-1 RT.

Patel *et al.* (1999) designed and synthesized efavirenz (SUSTIVA") is a potent non-nucleoside reverse transcriptase inhibitor. The result shows that two substitution patterns on the aromatic ring that give rise to benzoxazinones that are equipotent to efavirenz, they are the 6-methoxy (4m) and the 5,6-difluoro (4f) substituted compounds. The potential metabolic liability of the methoxy group precluded further consideration and as a result only the 5,6-difluoro substitution pattern will be incorporated in the second generation series.

Patel *et al.* (1999) prepared and evaluated two series of benzoxazinones differing in the aromatic substitution pattern were as HIV-1 reverse transcriptase inhibitors. The 5-fluoro and 6-nitro substituted compounds are the lead structure of the series. This report discovered that both the 5-fluoro and 6-nitro substituted benzoxazinones have activity comparable or better than efavirenz, and as a result, will be considered for incorporation in the second generation series.

Corbett *et al.* (2000) synthesized a series of 4-alkenyl and 4-alkynyl-3,4-dihydro-4-(trifluoromethyl)-2-(1*H*)-quinazolinones were as potent non-nucleoside reverse transcriptase

inhibitors (NNRTIs) of human immunodeficiency virus type-1 (HIV-1). From this study, were found quinazolinones derivatives show low nanomolar potency to exhibit wild-type RF virus and various single and many multiple amino acid substituted HIV-1 mutant viruses.

Patel *et al.* (2000) prepared and evaluated a series of 3,3-disubstituted quinoxalinones as HIV-1 reverse transcriptase inhibitors. This report show the N-allyl, N-cyclopropylmethyl and N-carboalkoxy substituted compounds displayed activity comparable or better than efavirenz and GW420867X.

Pungpo and Hannongbua (2000) applied a three-dimensional quantitative structure activity relationships (3D QSAR) method, Comparative Molecular Field Analysis (CoMFA) to a set of dipyridodiazepinone (nevirapine) derivative active against wild-type (WT) and mutant-type (Y181C) HIV-1 reverse transcriptase. The result, CoMFA models yield satisfactory predictive ability regarding WT and Y181C inhibitions, with r_2^{cv} = 0.624 and 0.726, respectively. CoMFA contour maps reveal that steric and electrostatic interactions corresponding to the WT inhibition are 58.5% and 41.5%, respectively, while steric and electrostatic effects have equal contributions for the explanation of inhibitory activities against Y181C. The results obtained provide information for a better understanding of the inhibitor-receptor interactions of dipyridodiazepinone analogs.

Ren *et al.* (2000) determined crystal structures of efavirenz and nevirapine with wild type RT and the clinically important K103N mutant. The results, efavirenz molecule within the non-nucleoside inhibitor binding pocket of RT are significant rearrangements of the drug binding site within the mutant RT compared with the wild-type enzyme. These changes, which lead to the repositioning of the inhibitor, are not seen in the interaction with the first-generation drug nevirapine. Therefore, repositioning of efavirenz within the drug binding pocket of the mutant RT could represent a general mechanism whereby certain second-generation non-nucleoside inhibitors are able to reduce the effect of drug-resistance mutations on binding potency.

Markwalder *et al.* (2001) synthesized metabolites of efavirenz to confirm their structure and to evaluate their activity as antivirals. The results, all of compounds disclosed are significantly weaker inhibitors of reverse transcriptase and poorer antivirals than efavirenz.

Cocuzza *et al.* (2001) synthesized a series of 4,1-benzoxazepinone analogues of efavirenz (Sustiva™) as potent non-nucleoside reverse transcriptase inhibitor. The results show

the cis-3-alkylbenzoxazepinones are more potent then the trans isomers and can be synthesized preferentially by a novel stereoselective cyclization. The best compounds could be exhibit of both wild type HIV-1 and K103N mutant virus, but are highly protein-bound in human plasma.

Cocuzza *et al.* (2001) have been developed two series of efavirenz analogues: one in which the cyclopropane ring has been replaced by small heterocycles and another in which the entire acetylenic side chain has been replaced by alkyloxy groups. Several members of both series show equivalent potency to efavirenz against both wild-type virus and the key K103N mutant.

Hannongbua *et al.* (2001) applied comparative molecular field analysis (CoMFA) to a large set of 1-[(2-hydroxyethoxy)-methyl]-6-(phenylthio)thymine (HEPT) analogues. Results, the best CoMFA model is satisfactory in both statistical significance and predictive ability. It shows excellent, high predictive ability as r^2_{cv} = 0.858. The derived model indicates the importance of steric contributions (64.4%) as well as electrostatic interactions for the HIV-1 RT inhibition. In addition, steric and electrostatic contour maps concluded that a moderately sized group at C5 enhances contact with Tyr181 enough to push it into a position which renders the protein nonfunctional, but a smaller group has insufficient steric requirements to do this and a larger group renders the ligand too large for the cavity.

Corbett *et al.* (2001) synthesized a series of unique 3,3a-dihydropyrano[4,3,2-de]quinazolin-2(1H)-ones and a 2a,5-dihydro-2H-thieno[4,3,2-de]quinazo-line-4(3H)-thione as HIV-1 non-nucleoside reverse transcriptase inhibitors. One of these compounds, as the racemate, possessed an IC_{90}=4.6 nM against wild-type virus in a whole cell antiviral assay and had an IC_{90}=76 and 897 nM against the clinically significant K103N and K103N/L100I mutant viruses, respectively.

Hannongbua *et al.* (2001) used the Cornell et al. force field through ab initio and semiempirical methods in the conformational analysis for TIBO R82913, TIBO R79882, and nevirapine. Various conformational search protocols were tested and the pseudosystematic method SUMM led to the best results. A better understanding of the distribution of conformers was obtained through clustering techniques in the data reduction stages. It was possible to reproduce various experimental data such as the crystallographic structures of the isolated or reverse transcriptase-complexed (RT) molecules. The proton-proton coupling constants obtained for TIBO through NMR were also reproduced. Cremer and Pople puckering parameters enabled

a precise description of both the conformation of the seven-membered rings and the relative position of the substituents on them. These parameters also demonstrated the efficiency and precision of the two-stage clustering method.

Hannongbua *et al.* (2001) investigated the structure and the conformational behavior of 11-cyclopropyl-5,11dihydro-4-methyl-6H-dipyrido[3,2-b2',3'-e][1,4]diazepin-6-one (nevirapine) by semiempirical (MNDO, AMI and PM3) method, *ab initio* at the HF/3-21G and HF/6-31G** levels and density functional theory at the B3LYP/6-31G** level. Results, a similar geometrical minimum is obtained from all methods which show an almost identical structure to the geometry of the molecule in the complex structure with HIV-1 reverse transcriptase. The calculated ^{1}H-NMR and ^{13}C-NMR spectra for the energy minimum geometry agree well with the experimental results, which indicated that the geometry of nevirapine in solution is very similar to that of the molecule in the inhibition complex.

Chen *et al.* (2003) investigated the intermolecular interaction between two types of non nucleoside reverse transcriptase inhibitors (NNRTIs), HEPT and TIBO, and HIV reverse transcriptase receptor by the docking study and three 3D-QSAR models. The result, docking study show that two types of NNRTIs presents similar interaction mechanism with HIVRT. The most active compound of every type of inhibitors could form one hydrogen bond with the residue Lys101 and has hydrophobic interaction with residues Tyr181, Tyr188 and Tyr318, etc. Three 3D-QSAR models including two partial correlation models (one for each family of HEPT and TIBO) and a mixed model gathering two families were constructed. Comparative study of these models indicated that the mixed model offered the strongest prediction ability. For this model, the cross-validated q^2 values were 0.720 and 0.675, non-cross-validated r^2 values were 0.940 and 0.920 for CoMFA and CoMSIA, respectively.

Saen-oon *et al.* (2003) investigated the conformational of (+)-(s)-4,5,6,7-tetrahydro-9-chloro-5-methyl-6-(3-methyl-2-butenyl)imidazol[4,5,1-*jk*][1,4]benzodiazepin-2(1*H*)-thione or 9-Cl *TIBO* using high level of calculations, *ab initio* and DFT theory. The results show that the eight pronounced local minima were found to exist within an energy difference of less 10 kJ/mol. The energy barriers between the different local minima are lower 15 kJ/mol. The some calculated conformers with correlate the bound conformer in the X-ray structure. The calculated ^{1}H NMR and ^{13}C NMR chemical shifts for the lowest energetic conformer give the greatest correspondence

with the experimental results.

Pungpo *et al.* (2003) applied hologram quantitative structure-activity relationships (HQSAR) to three different data sets, 70 TIBO, 101 HEPT and 125 dipyridodiazepinone derivatives. The results show that all derived HQSAR models produce satisfying predictive ability and yield r^2_{cv} values ranging from 0.62-0.84. The obtained HQSAR results indicate the similarity of the interactions of these three different NNRTIs with the inhibition pocket of the enzyme. Comparisons of different QSAR methods on these NNRTIs data sets, the predictive ability of the models derived from dipyridodiazepinone analogues was significantly improved and apparently revealed differentiating structural requirements between WT and Y181C HIV RT inhibition.

Medina-Franco *et al.* (2004) applied CoMFA and CoMSIA to a set of pyridinone derivative based on docking method. The 3D-QSAR models produce satisfying predictive ability r^2_{pred} values of 0.720 and 0.750 for CoMFA and CoMSIA, respectively. The CoMFA, CoMSIA and docking results help to understand the type of interactions that occur between pyridinone derivatives with the nonnucleoside reverse transcriptase inhibitor binding pocket, and explain the viral resistance to pyridinone derivative upon mutation of amino acids Tyr181 and Tyr188.

Ragno *et al.* (2004) synthesized four new DABO derivatives (5-alkyl-2-cyclopentylamino-6-[1-(2,6-difluorophenyl)alkyl]-3,4-dihydropyrimidin-4(3*H*)-ones, F2-*NH*-DABOs) and used the computer-aided design to investigate the binding mode of these compounds. Docking result show binding mode resembles that reported for F2-*S*-DABOs, with the difference that the NH moiety at the C-2 position represents a new anchor site for ligand/enzyme complexation. The F2-*NH*-DABOs were shown to be highly active in both anti-RT and anti-HIV biological assays with IC_{50} and EC_{50}.

Zhou and Madura (2004) used 3D-QSAR (CoMFA and CoMSIA) based on Docking conformation and alignment on TIBO derivatives. The 3D-QSAR models demonstrate a good ability to predict the activity of studied compounds (r^2 = 0.972, 0.944, q^2 = 0.704, 0.776). The steric and electrostatic properties predicted by CoMFA contours can be related to the binding structure of the complex. The results demonstrate that the combination of ligand-based and receptor-based modeling is a powerful approach to build 3D-QSAR models.

Medina-Franco *et al.* (2004) investigated the interaction of the pyridinone derivative in nine NNRTIs binding pockets of HIV-1 reverse transcriptase (RT) structures. The docking results indicate that pyridinone analogues adopt a butterfly conformation and share the same binding mode as the crystal inhibitors in the pocket geometries of nevirapine, 1051U91, 9-Cl-TIBO, Cl-a-APA, efavirenz, UC-781 and S-1153. The results aid in the understanding of the biological response of published hybrid pyridinone molecules and design further pyridinone derivatives active against RT containing mutations.

Kalyan *et al.* (2004) investigated the binding mode of the non-nucleoside reverse transcriptase inhibitor (NNRTI); TMC125-R165335 (etravirine) and diarylpyrimidine (DAPY) analogues by molecular docking. The results show that TMC125-R165335 and DAPY analogues can adapt to changes in the NNRTI-binding pocket in multiple conformations and thereby escape the effects of drug-resistance mutations. This result suggests that the conformational flexibility inhibitor (such as torsional flexibility about strategically located chemical bonds) can be a powerful drug design concept, especially for designing drugs that will be effective against rapidly mutating targets.

Rodriguez-Barrios *et al.* (2005) applied molecular dynamics simulations to assess the effect of the common Lys103Asn mutation in HIV-1 reverse transcriptase (RT) has on the binding of three representative non-nucleoside RT inhibitors (NNRTI), nevirapine, efavirenz, and etravirine. The results show that the extra Asn103-Tyr188 hydrogen is seen to affect each NNRTI differently. The ability disrupts this interaction increasing in the order etravirine, efavirenz, nevirapine. This strongly suggests that attempts to overcome resistance through structure-based drug design may be considerably more successful if dynamic structural aspects of the type studied here are considered, particularly in cases where binding energy-based structure-activity relationship methods are unable to provide the required information.

Mei *et al.* (2005) investigated the binding of efavirenz (EFZ) to HIV-1 reverse transcriptase (RT) and its K103N and Y181C mutants using the MFCC (molecular fractionation with conjugate caps) method. The binding interaction energies between EFZ and each protein fragment are calculated using a combination of HF/3-21G, B3LYP/6-31G* and MP2/6-31G* *ab initio* levels. The present computation shows that efavirenz binds to HIV-1 RT predominantly through strong electrostatic interaction with the Lys101 residue. The small losses of binding to

K103N mutant by efavirenz result form a slightly weakened interaction between the drug and Lys101 due to a conformational change of mutation. The small loss of binding to Y181C mutant by efavirenz can be attributed to the Glu698 residue moving closer to EFZ due to conformational change, which results in an increase of repulsive energy relative to the wild type (WT).

Chen *et al.* (2005) used molecular docking and molecular dynamics simulation to determine the binding mode of 3',4'-di-O-(S)-camphanoyl-(+)-cis-khellactone (DCK) analogs anti-HIV inhibitors with HIV-1 RT. The results reveal that the strong hydrogen bond could form between DCK O16 and NH of Lys101, and that DCK analogues might act similarly as other types of HIV-1 RT inhibitors. The investigation about drug resistance for DCK shows no remarkable influence on the most frequently observed mutation K103N of HIV-1 RT. Based on the proposed mechanism, some new structures were designed and predicted by a SVM model. All compounds exhibited potent inhibitory activities against HIV (EC_{50}) values lower than 1.95 microM.

Heeres *et al.* (2005) synthesized a series of novel pyrazinones as non-nucleoside reverse transcriptase inhibitors (NNRTIs and investigated the structure-activity relationship (SAR). The results show that the activity decreases when the 4-position was substituted with a fluorine atom or a CF_3 group. Modeling studies reveal that the hydrogen in position 4 can undergo a favorable electrostatic interaction with the backbone carbonyl of H235 of the RT enzyme, whereas the corresponding fluorine compound undergoes an unfavorable electrostatic interaction with the same carbonyl, explaining the lower activity.

Ragno *et al.* (2005) used three-dimensional quantitative structure-activity relationship (3D-QSAR) studies and docking simulations on indolyl aryl sulfones (IASs) highly active against wild type and some mutant (Y181C, K103N-Y181C, K103R-V179D-P225H, highly resistant to efavirenz). Result, the derived 3D-QSAR models show r^2 and q^2 values ranging from 0.79 to 0.93 and from 0.59 to 0.84, respectively. From the synthesis of six designed derivatives (prediction set) of new IASs, these compound show high anti-HIV-1 activities.

Weinzinger *et al.* (2005) evaluated the properties of efavirenz (SUSTIVA) and a set of its derivatives (benzoxazinones) in the nonnucleoside analogue binding site of the enzyme by molecular docking. Then the resulting geometries were used for a molecular dynamics simulation and binding energy calculations. Based on MD simulations, the obtained results indicate that the ligand bind to the HIV-1 RT binding pocket based on hydrogen bonding between efavirenz's N1

and the oxygen of the backbone of Lys 101, with an estimated average distance of 1.88 Å. Moreover, electrostatic interaction could be observed by two amino acid residues in the binding site; Lys 101 and His 235. MD simulations open the possibility to study the reaction of the flexible enzyme to those substances as well as the overall affinity.

Martino *et al.* (2005) synthesized 1-[2-(Diarylmethoxy)ethyl]-2-methyl-5-nitroimidazoles (DAMNIs) derivative and investigated the binding mode by docking calculations. The results show that the replacement of one phenyl ring of nitroimidazole derivative with heterocyclic rings, such as 2-thienyl or 3-pyridinyl, led to novel DAMNIs with increased activity is a novel family of HIV-1 NNRTIs active at submicromolar concentration. Moreover, some compound was found more active than efavirenz to against the K103N mutation, suggesting for these compounds a potential use in efavirenz based anti-AIDS regimens.

Ranise *et al.* (2005) described our structure-based ligand design, synthetic strategy, and structureactivity relationship (SAR) studies that led to the identification of thiocarbamates (TCs), a novel class of NNRTIs. Results, the para-substituted TCs were active against wild type HIV-1 at nanomolar concentrations (EC_{50} range: 0.04-0.01 M). The most potent bears a methyl group at position 4 of the phthalimide moiety and a nitro group at the para position of the *N*-phenyl ring. Most of the TCs showed good selectivity indices, since no cytotoxic effect was detected at concentrations as high as 100 M. TCs significantly reduced the Y181C mutant, but they were inactive against K103R and K103N + Y181C mutants. The docking model predictions were consistent with biological activity of the anti-HIV-1 of the TCs and related compounds synthesized.

Saparpakorn *et al.* (2006) designed novel nevirapine analogues insensitive to the K103N and Y181C HIV-1 RT. Result, 360 nevirapine derivatives were designed using a combinatorial library design approach and these compounds were docked into the binding pocket of mutant HIV-1 RT enzyme structures, using the GOLD program. 124 Compounds having a GoldScore higher than that of nevirapine (55.00 and 52.00 for K103N and Y181C mutants, respectively) were first retrieved and submitted to a topological analysis with the SILVER program. Consequently, 31 compounds presenting a significant percentage of the surfaces buried upon binding (>80%) and exhibiting hydrogen bonds to either N103 or C181 residues of the HIV-RT were selected. To ensure that these compounds had hydrogen bonding

either N103 or C181 residues, their interaction energies were estimated by quantum chemical calculations (QCCs). Finally, QCCs represent an alternative method for performing post docking procedure.

Zhang *et al.* (2006) applied molecular docking and 3D-QSAR approaches based on their binding conformations to dual functional of efavirenz (SUSTIVA) against both wild type (WT) and K103N mutant reverse transcriptases (RTs) of HIV-1. The 3D-QSAR models show r^2_{cv} values ranging from 0.656 to 0.834 for CoMFA and CoMSIA, respectively. CoMFA models were found to be well matched with the binding sites of both WT and K103N RTs. On the basis of both the 3D-QSAR and pharmacophore models reveal the structural requirement of potent dual functional drug.

Pungpo *et al.* (2006) applied 3D-QSAR (CoMSIA, CoMFA) and molecular docking (GOLD and FlexX programs) to a series of 74 efavirenz compounds effectively inhibiting wild type (WT) and mutant type (K103N) HIV-1 reverse transcriptase (RT). Result reliable QSAR models for WT and K103N inhibitions show high predictive abilities. CoMFA models with r^2_{cv} = 0.651 and 0.678 and CoMSIA models with r^2_{cv} = 0.662 and 0.743, respectively. The interpretation obtained from the models highlights different structural requirements for inhibition of WT and K103N HIV-1 RT. The results derived from docking analysis give additional information and further probe the inhibitor-enzyme interactions. The correlation of the results obtained from 3D QSAR and docking models validate each other and lead to better understanding of the structural requirements for the activity.

Rawal *et al.* (2007) performed flexible docking simulations on two series of 4-thiazolidinones as HIV-1 reverse transcriptase (HIV-1 RT) inhibitors. A good correlation between the predicted binding free energies and the experimentally observed inhibitory activities (EC_{50}) suggest that the identified binding conformations of these inhibitors are reliable. The results of docking studies provide an insight into the pharmacophoric structural requirements for the HIV-1 RT inhibitory activity of this class of molecules.

CHAPTER 3

MATERIAL AND METHODS

3.1 Biological activity data

The biological activity data (Table 1) of efavirenz derivatives (56 molecules) were taken from the same laboratory to ensure that all experimental data were determined under consistent assay condition [Corbett *et al.*, 2000, Cocuzza *et al.*, 2001; Corbett *et al.*, 2001]. The inhibition activity has been expressed as log (1/C), where C is the ability of the compound to inhibit wild-type and K103N strain of HIV-1 RT (IC_{90}).

3.2 Molecular structures and optimization

The structures of the 56 efavirenz derivatives reported in Table 1 were constructed using the ALCHEMY 2000 program [Tripos Associates Inc., 1998]. The geometries of these efavirenz derivatives were fully optimized by the GAUSSIAN 03 program [Frisch *et al.*, 2004] based on *ab-initio* molecular orbital method at HF/3-21G level. The structure of HIV-1 RT in complex with efavirenz was obtained from Protein Data Bank (PDB codes 1fk9 and 1fko for the efavirenz/WT HIV-1 RT complex and the efavirenz/K103N complex, respectively).

3.3 Conformational analysis

Conformational analysis of efavirenz compound and selected derivatives (the highest activity compound against WT and K103N HIV-1 RT) were investigated based on various methods of quantum chemical calculations, AM1, PM3, HF/3-21G, HF/6-31G* and B3LYP/6-31G*. The starting geometry of efavirenz compound was taken from the complex X-ray crystal structure of the HIV-1 RT and efavirenz inhibitor (pdb code 1FK9 and 1FKO). The derivatives were constructed by ALCHEMY 2000 program and then, fully optimized by HF/3-21G method. The potential energy surfaces of these compounds were calculated by using the GAUSSIAN 03 program. The calculated conformations were then compared to the results of

the X-ray investigation on efavirenz associated with HIV-1 RT and the docked conformation obtained from molecular docking calculations based on AUTODOCK 3.05 program [Morris *et al.*, 2000].

3.4 Docking simulation

Docking calculations were performed by using Autodock 3.05, a program combining a rapid energy evaluation through precalculated grids of affinity potentials. This program keeps the macromolecule rigid, while allows torsional flexibility for the ligand. Docking to macromolecule was carried out using Lamarckian Genetic Algorithm (LGA), with an initial population of 50 randomly placed individuals. Fifty independent docking runs were carried out for each ligand. Results differing by less than 1.0 Å in positional root-mean-square deviation (rmsd) were clustered together and represented by the result with the most favorable free energy of binding. The docking procedure was carried out using two different X-ray structures of efavirenz complex with WT and K103N HIV-1 RT. Before performing docking experiment the structure of the original ligand was removed from each complex. Solvation parameters were added to the final macromolecule structure using Addsol utility of Autodock. The grid maps representing the protein in the actual docking process were calculated with Autogrid. The grids (one for each atom type in the ligand, plus one for electrostatic interactions) were chosen to be sufficiently large to include the posed original inhibitor. The dimensions of the grids were thus 60×50×30, with a spacing of 0.375 Å between the grid points and the center close to the ligand. After that, efavirenz was docked back into the corresponding binding pocket to validate the docking method. Then 56 efavirenz derivatives were docked into WT and K103N HIV-1 RT binding pockets to investigate the binding modes of all efavirenz derivatives. The binding mode with the lowest binding free energy of efavirenz derivatives compound obtained from molecular docking method was used for structural alignment of 3D-QSAR analyses.

3.5 3D-QSAR analysis

To investigate the relationships between the structures and the biological activity of HIV-1 RT inhibitors, CoMFA and CoMSIA based on the docked structural alignment were

applied to 56 efavirenz derivative compounds. 49 compounds were used as training set and 7 compounds were use as test set (Table1). The test set compounds were selected manually from each subgroup of the training set such that structural diversity and broad range of activity in the data set were included. In the CoMFA method, the two fields (steric and electrostatic) are calculated by using Lennard-Jones and Coulombic potentials, respectively. For calculation of both the steric and electrostatic energy terms, a sp^3 carbon atom with +1 charge served as the probe atom to generate both field. The grid spacing with 2 Å was used to generate a cubic lattice around the aligned molecules. The probe atom was placed at each grid point and steric and electrostatic interactions with each atom in the molecule were all calculated with CoMFA standard scaling and then put into a CoMFA QSAR table. The minimum sigma and energy cutoff values were set to 2.0 and 30 kcal/mol, respectively, for both steric and electrostatic fields. In CoMSIA, similarity is expressed in terms of five physicochemical properties: steric, electrostatic, hydrophobic, H-bond donor and H-bond acceptor fields. These fields were calculated using the same lattice box as used for the CoMFA calculation, with a grid spacing of 2 using a common C probe atom of 1 radius and +1.0 charge. For field calculation, singularities were avoided at atomic position because the Gaussian equations were adopted, thus no cutoffs were required. The default value of 0.3 was used as the attenuation factor probe atom with a radius of 1.0 Å placed at a regular grid spacing. The optimum number of components and the predictive ability (q^2) were determined by selecting the lowest PRESS. The final non-cross validated prediction model was derived with the number of components obtained from the cross validation analysis. The results were interpreted graphically by field contribution maps.

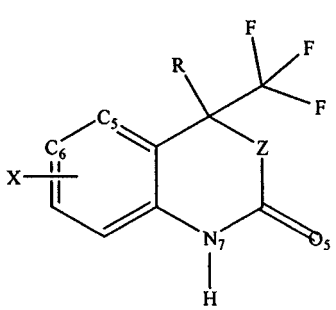

Figure 5 The template structure of efavirenz derivatives and the symbol of substituent position, used in this study

Table 1 The structures and biological activity for against WT and K103N HIV-1 RT of the 56 efavirenz derivatives

Cpds No.	X	R	Z	log(1/C)	
				WT	K103N
01[a]	6-Cl	CC-cyclopropyl	O	8.77	7.19
02[a]	6-Cl	CC-2-pyridyl	O	8.27	5.96
03[b]	6-Cl	CC-3-pyridyl	O	8.40	6.94
04[a]	6-Cl	CC-2-furanyl	O	8.42	6.82
05[a]	6-Cl	CC-3-furanyl	O	8.42	6.49
06[a]	5,6-diF	CC-3-pyridyl	O	8.65	7.23
07[a]	6-F	CC-3-furanyl	O	8.60	6.43
08[a]	6-F	CC-3-pyridyl	O	8.59	6.48
09[b]	5,6-diF	CC-3-furanyl	O	8.49	6.55
10[a]	5,6-diF	CC-2-thienyl	O	8.65	6.81
11[a]	5,6-diF	CC-3-thienyl	O	8.63	6.86
12[a]	6-Cl	$OCH_2CH_2CH_2CH_3$	O	7.99	6.00
13[a]	6-Cl	$OCH_2CH_2CH(CH_3)_2$	O	8.00	6.54
14[a]	6-Cl	$OCH_2CHCH(CH_3)$cis	O	8.36	6.63
15[a]	6-Cl	$OCH_2CHCH(CH_3)$tran	O	8.25	6.39
16[a]	6-Cl	$OCH_2CHC(CH_3)_3$	O	8.57	7.08
17[a]	6-Cl	OCH_2CCCH_3	O	8.50	6.51
18[a]	6-Cl	OCH_2CHCCl_2	O	8.02	6.62
19[a]	6-F	$OCH_2CHC(CH_3)_2$	O	8.53	6.97
20[a]	6-F	$OCH_2CHCH(CH_3)$tran	O	8.05	5.94
21[a]	5,6-diF	$OCH_2CHC(CH_3)_2$	O	8.81	7.19
22[b]	5,6-diF	OCH_2CHCH_2	O	8.19	5.79
23[a]	5,6-diF	OCH_2CHCCl_2	O	8.20	6.74
24[a]	5,6-diF	CC-ethyl	NH	8.82	7.85
25[a]	5-F	CC-cyclopropyl	NH	8.85	7.05
26[a]	5-Cl,6-F	CC-isopropyl	NH	8.52	7.82
27[a]	5-Cl	CC-cyclopropyl	NH	8.60	7.2
28[a]	5,6-diF	CC-cyclopropyl	NH	8.68	7.89
29[a]	5,6-diF	CC-isopropyl	NH	8.68	7.85
30[a]	6-F	CC-cyclopropyl	NH	8.70	7.32

Table 1 The structures and biological activity for against WT and K103N HIV-1 RT of the 56 efavirenz derivatives (continued)

Cpds No.	X	R	Z	log(1/C)	
				WT	K103N
31[a]	5,6-diF	CC-2-pyridyl	NH	8.70	6.96
32[a]	6-F	CC-ethyl	NH	8.60	7.15
33[a]	5-Cl,6-F	CC-cyclopropyl	NH	8.57	7.74
34[a]	6-MeO	CC-cyclopropyl	NH	8.54	7.4
35[a]	6-F	CC-2-pyridyl	NH	8.30	6.32
36[a]	5-F,6-Cl	CC-cyclopropyl	NH	8.32	7.74
37[b]	5-Cl,6-F	CC-2-pyridyl	NH	8.64	7.14
38[a]	6-Cl	CC-cyclopropyl	NH	8.57	7.66
39[b]	6-MeO	CC-isopropyl	NH	8.42	7.25
40[a]	6-MeO	CC-phenyl	NH	8.49	6.55
41[a]	5,6-diF	CC-phenyl	NH	8.21	6.72
42[b]	6-F	CC-phenyl	NH	8.18	6.49
43[a]	6-Cl	CC-2-pyridyl	NH	8.47	6.8
44[a]	6-Cl	CC-ethyl	NH	8.48	7.59
45[a]	6-Cl	CC-phenyl	NH	8.15	6.6
46[a]	6-F	CC-isopropyl	NH	8.59	7.57
47[b]	5,6-diCl	CC-cyclopropyl	NH	8.10	7.74
48[a]	6-Cl	CC-isopropyl	NH	8.52	7.66
49[a]	6-MeO	CC-2-pyridyl	NH	8.09	6.47
50[a]	5-MeO,6-Cl	CC-cyclopropyl	NH	8.46	8.12
51[a]	5-MeO,6-Cl	CC-phenyl	NH	8.10	6.95
52[a]	5-MeO,6-Cl	CC-3-pyridyl	NH	8.15	6.86
53[a]	5-OH,6-Cl	CC-cyclopropyl	NH	8.44	7.55
54[a]	6-Cl	CHCO-cyclopropyl	NH	8.44	7.12
55[a]	6-Cl	CHCO-phenyl	NH	8.09	7.34
56[a]	6-Cl	CHCO-3-pyridyl	NH	8.34	7.12

[a] The training set for CoMFA and CoMSIA model

[b] The test set for CoMFA and CoMSIA model

3.6 Theoretical background in quantum chemistry

3.6.1 Molecular orbital theory

Molecular orbital calculation is the important method in quantum chemistry for approximate structures and dynamics of molecular system. This approach provides a great promise in calculating electronic structures and predicting properties of drug molecules. Until now, molecular orbital investigations have been introduced into drug research to study mechanisms of action and to guide the design of more potent agents.

The quantum chemical methods are based on finding solutions to the Schrodinger wave equation on molecular orbital theory

$$H\Psi = E\Psi \quad (1)$$

Where H is the Hamiltonian operator which gives the kinetic and potential energies of the system

$$H = -\frac{\hbar^2}{2m}\nabla^2 + V \quad (2)$$

Then, rewrite equation (1) is;

$$\left\{-\frac{\hbar^2}{2m}\nabla^2 + V\right\}\Psi = E\Psi \quad (3)$$

where

$$\nabla^2 = \frac{\partial^2}{\partial x^2} + \frac{\partial^2}{\partial y^2} + \frac{\partial^2}{\partial z^2} \quad (4)$$

ħ is Plank's constant divided by 2π. Ψ is the wave function which characterizes the particle's properties. E is the energy of the particle.

3.6.2 The LCAO-MO approximation

The most common formalism for building molecular orbitals is the Linear Combination of Atomic Orbitals (LCAO) method. The molecular orbitals (Ψ_i) can be composed of a set of atomic functions (θ_μ) centered on each nucleus.

$$\Psi_i = \sum_k c_{\mu i}\theta_\mu \tag{5}$$

Where $C_{\mu i}$ are the coefficients and θ_μ are real atomic functions. The requirement that the orbitals are orthonormal is

$$\sum_{\mu\nu} c^*_{\mu i} c_{\nu i} S_{\mu\nu} = \delta_{ij} \tag{6}$$

Where δ_{ij} is the Kronecker delta and S_μ is overlap integral for atomic functions ϕ_μ and ϕ_ν

$$S_{\mu\nu} = \int \phi_\mu(1)\phi_\nu(1)d\tau \tag{7}$$

3.6.3 Solving for the molecular orbital: LCAO-MO-SCF

Introducing Eq. (6) into Eq. (1), the equation takes the final form generally known as the Roothaan equations as

$$\sum_\nu \left(F_{\mu\nu} - \varepsilon_i S_{\mu\nu}\right) c_{\nu i} = 0 \tag{8}$$

The elements of the matrix representation of the Hartree-Fock Hamiltonian operator F are

$$F_{\mu\nu} = H_{\mu\nu} + \sum P_{\lambda\sigma}\left[(\mu\nu/\lambda\sigma) - \tfrac{1}{2}(\mu\lambda/\nu\sigma)\right] \tag{9}$$

and density matrix defined as

$$P_{\mu\nu} = 2\sum_{i} c_{\mu i}^{*} c_{\nu i} \tag{10}$$

$$(\mu\nu/\lambda\sigma) = \iint \phi_{\mu}(1)\phi_{\nu}(1)\frac{1}{r_{12}}\phi_{\lambda}(2)\phi_{\sigma}(2)d\tau_1 d\tau_2 \tag{11}$$

and one-electron orbital energy is

$$\varepsilon_i = H_i^{(1)} + \sum_{j} 2J_{ij} - K_{ij} \tag{12}$$

where

Coulomb integral, $$J_{ij} = \sum_{\mu\nu\lambda\sigma} c_{\mu i}^{*} c_{\lambda j}^{*} c_{\nu i} c_{\sigma j} (\mu\nu/\lambda\sigma) \tag{13}$$

Exchange integral, $$K_{ij} = \sum_{\mu\nu\lambda\sigma} c_{\mu i}^{*} c_{\lambda i}^{*} c_{\nu i} c_{\sigma i} (\mu\lambda/\nu\sigma) \tag{14}$$

The total electronic energy is

$$\varepsilon = \sum_{i} \left(\varepsilon_i + H_{ii}^{(1)}\right) \tag{15}$$

Therefore, Eq. (8) can be written in matrix form as

$$FC = SCE \tag{16}$$

Where E is the diagonal matrix of the ε_i and the elements of a matrix C are the coefficients in the expansion LCAO.

Hartree-Fock or self-consistent field method introduces some elegant approximations to solve a one electron eigenvalue problem, and must be solved iteratively. Solving the Eq. (16) for the coefficient C describing the LCAO expansion of the orbital ψ_i and orbital energies ε_i which require a matrix diagonalized. Note that F depends on the coefficient C.

They may be usefully transformed by defining new matrices

$$F^{\tau} = S^{\frac{1}{2}} F S^{\frac{1}{2}} \tag{17}$$

$$C^{\tau} = S^{\frac{1}{2}} C \tag{18}$$

then obtain

$$F^{\tau} C^{\tau} = C^{\tau} E \tag{19}$$

matrix equation (19) can be solved using standard methods. The basis function coefficients can be obtained from using $C = S^{1/2} C^{\tau}$. The matrix element of the Hartree-Fock Hamiltonian operator are dependent of the orbitals through the elements $P_{\mu\nu}$ and the Roothaan equations are solved by first assumimg an initial set of linear expansion coefficients. The whole process is then repeated until the coefficients no longer change within a given tolerance on repeated iteration. The solution is then said to be self-consistent and the method is then referred to as the SCF method.

3.7 The Basis Set

A basis set is a set of functions used to create the molecular orbitals, which are expanded as a linear combination of such functions with the weights or coefficients to be determined. Usually these functions are atomic orbitals. The molecular orbital is depended on the quality and the number of atomic orbital. The basis functions should describe as closely as possible the correct distribution of electrons in the vicinity of nuclei and yet be simple enough that the integrations can actually be carried out efficiently. According to equation

$$\Psi_i = \sum_{k}^{M} c_{ik} \phi_k \tag{20}$$

where Ψ_i = the unknown Hartree-Fock orbitals

ϕ_k = known basis functions

c_{ik} .= and expansion coefficients

The basis functions given as a Slater Type Orbital (STO) equation.

$$STO=\frac{\xi^3}{\pi^{0.5}} e^{(-\xi r)} \tag{21}$$

Now it is important to remember that STO is a very difficult calculation. Therefore, the Gaussian Type Orbital (GTO) equation was developed.

$$GTO=\frac{2\chi}{\pi^{0.75}} e^{(-\chi r^2)} \tag{22}$$

Notice that the difference between the STO and GTO is in the r. The GTO squares the r so that the product of the gaussian primitives (original gaussian equations) is another gaussian. By doing this, the equation is much easier. However, this equation is loss of accuracy. To compensate for this loss, combine the more gaussian equations are more accurate basis function. There are two general categories of basis sets.

3.7.1 Minimal basis sets

The minimal basis set is one basis function for every atomic orbital that is required to describe the free atom. A common naming convention for minimal basis sets is STO-XG, where X is an integer. This X value represents the number of gaussian primitive functions comprising a single basis function. Several minimal basis sets are in common used STO-2G, STO-3G and STO-6G. The most common of these is STO-3G, where a linear combination of three GTOs are fitted to an STO, i.e, the STO-3G basis set for methane consists of a total of 9 contracted functions built from 27 primitive functions.

3.7.2 Extended basis sets

The extended basis sets are the ones that consider the higher orbitals of the molecule and account for size and shape of molecular charge distributions. There are several types of extended basis sets: Double-Zeta, Triple-Zeta, Quadruple-Zeta, Split-Valence, Polarized Sets and Diffuse Sets.

3.7.2.1 Double-Zeta, Triple-Zeta, Quadruple-Zeta

The minimal basis sets approximated all orbitals to be of the same shape, which this is not true. The double-zeta basis set is important to treat each orbital separately when conduct the Hartree-Fock calculation. This gives a more accurate representation of each orbital. In order to do this, each atomic orbital is expressed as the sum of two Slater-type orbitals (STOs). The two equations are the same except for the value of ξ (zeta). In this case, each STO represents a different sized orbital because the zetas are different. The triple and quadruple-zeta basis sets work the same way, except use three and four Slater equations instead of two.

3.7.2.2 Split-Valence

Often it takes too much effort to calculate a double-zeta for every orbital. Instead, many scientists simplify matters by calculating a double-zeta only for the valence orbital. Since the inner-shell electrons aren't as vital to the calculation, they are described with a single Slater Orbital. This method is called a split-valence basis set. A few examples of common split-valence basis sets are 3-21G, 4-31G, and 6-31G.

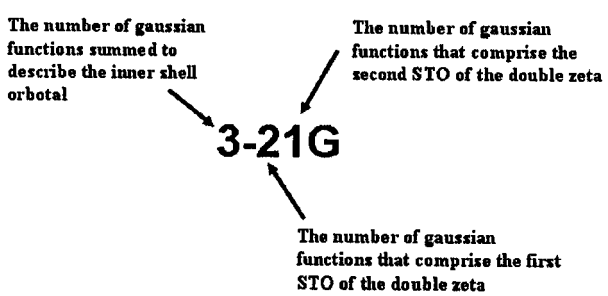

i.e using a 3-21G basis set to calculate a carbon atom. This means summing 3 gaussians for the inner shell orbital, two gaussians for the first STO of the valence orbital and 1 gaussian for the second STO. Hydrogen atoms are not considered to have a core so only the split valence part of the designation applies to H.

3.7.2.3 Polarized Sets

In the previous basis sets treated atomic orbitals as existing only as s, p, d, f etc. Although those basis sets are good approximations, a better approximation is to acknowledge and account for the fact that sometimes orbitals share qualities of s and p orbitals or p and d, etc. and not necessarily have characteristics of only one or the other. As atoms are

brought close together, their charge distribution causes a polarization effect which distorts the shape of the atomic orbitals. In this case, s orbitals begin to have a little of the p flavor and p orbitals begin to have a little of the d flavor. Therefore, the polarization has been taken into them. The most common polarization functions is add polarisation functions to the 6-31G basis set as follows:

6-31G* (6-31G (d)) adds a set of d functions to the atoms in the first and second rows (Li-Cl).

6-31G** (6-31G (d,p)) adds a set of d functions to the atoms in the first and second rows (Li-Cl) and a set of p functions to hydrogen.

3.7.2.4 Diffuse Sets

In some cases the normal basis functions are not adequate. This is particularly the case in excited states and in anions where the electronic density is more spread out over the molecule. To model this correctly have to use some basis functions which themselves are more spread out. These additional basis functions are called diffuse functions. Diffuse basis sets are represented by the + signs. One + means that are accounting for the p orbitals, while ++ signals that we are looking at both p and s orbitals. The most common used is 6-31+G adds a set of diffuse s and p orbitals to the atoms in the first and second rows (Li - Cl) and 6-31++G adds a set of diffuse s and p orbitals to the atoms in the first and second rows (Li- Cl) and a set of diffuse functions to hydrogen.

3.8 Semi empirical calculations

Semi-empirical calculations are based on the Hartree-Fock formalism, but make many approximations and obtain some parameters from empirical data. They are very important in computational chemistry for treating large molecules where the full Hartree-Fock method without the approximations is too expensive. The use of empirical parameters appears to allow some inclusion of electron correlation effects into the methods. Within the framework of Hartree-Fock calculations, some pieces of information (such as two-elecron integrals) are sometimes approximated or completely omitted. In order to correct for this loss for semi-empirical methods.

Semi-empirical calculations are much faster than their *ab initio* method. Their results, however, can be very wrong if the molecule being computed is not similar enough to the molecules in the database used to parametrize the method. Semi-empirical calculations have been

most successful in the description of organic chemistry, where only a few elements are used extensively and molecules are of moderate size. The most frequently used methods are MNDO, AM1 and PM3.

3.9 *Ab initio* calculation

Ab initio quantum chemistry methods are computational chemistry methods based on quantum chemistry. The simplest type of *ab initio* electronic structure calculation is the Hartree-Fock (HF) scheme, in which the Coulombic electron-electron repulsion is not specifically taken into account. Only its average effect is included in the calculation. This is a variational procedure used to approximate energies, which energies are always equal or greater than the exact energy and tend to a limiting value called the Hartree-Fock limit as the size of the basis is increased. Many types of calculations begin with a Hartree-Fock calculation and subsequently correct for electron-electron repulsion, referred to also as electronic correlation. Møller-Plesset perturbation theory (MP*n*) and coupled cluster theory (CC) are examples of these post-Hartree-Fock methods. In some cases, particularly for bond breaking processes, the Hartree-Fock method is inadequate and this single-determinant reference function is not a good basis for post-Hartree-Fock methods. It is then necessary to start with a wave function that includes more than one determinant such as Multi-configurational self-consistent field and methods have been developed that use these multi-determinant references for improvements.

3.10 Density functional calculation

Density functional theory (DFT) is a quantum mechanical method used in physics and chemistry to investigate the electronic structure of many-body systems. DFT methods are often considered to be *ab initio* methods for determining the molecular electronic structure, even though many of the most common functionals use parameters derived from empirical data, or from more complex calculations. This means that they could also be called semi-empirical methods. It is best to treat them as a class on their own. In DFT, the total energy is expressed in terms of the total electron density rather than the wave function. In this type of calculation, there is an approximate Hamiltonian and an approximate expression for the total electron density. DFT

methods can be very accurate for little computational cost. The drawback is, that unlike *ab initio* methods, there is no systematic way to improve the methods by improving the form of the functional.

3.11 Molecular docking

The molecular docking is a research technique for predicting the low energy binding modes of a small molecule or ligand based on the lock and key mechanism, within the active site of a macromolecule, or receptor, whose structure is known. It plays an important role in drug design. To perform a docking, the first requirement is a structure of the protein of interest. Usually the structure has been determined in the lab using a biophysical technique such as X-ray crystallography, or less often, NMR spectroscopy. This protein structure and a database of potential ligands serve as inputs to a docking program. The success of a docking program depends on two components: the search algorithm and the scoring function.

AutoDock program was used in this study. AutoDock is a docking program that uses a genetic algorithm for docking of ligands into binding sites on proteins. It has been widely used and there are many examples of its successful applications. It is very fast, provides high quality predictions of ligand conformations, and good correlations between predicted inhibition constants and experimental ones. AutoDock actually consists of two main programs: AutoDock performs the docking of the ligand to a set of grids describing the target protein; AutoGrid pre-calculates these grids. In addition to using them for docking, the atomic affinity grids can be visualised. This can help, for example, to guide organic synthetic chemists design better binders.

3.12 Three dimentional quantitative structure activity relationships analysis (3D-QSAR)

Three dimensional quantitative structure-activity relations produce quantitatively correlation between three-dimensional properties of molecules and the biological activity of these compounds. The 3D-QSAR method is ligand-based manners, which it is useful for a fine 3D structure of experimentally unavailable target proteins. In the present study, CoMFA and CoMSIA techniques were selected as appropriate tools to study the QSAR of efavirenz analogues active against WT and K103N HIV-1 RT.

3.12.1 The QSAR Table

The QSAR tables (molecular spreadsheets) comprise horizontal row that corresponds to a molecular model in a SYBYL database and column that corresponds to a property of a compound (Figure 6). The QSAR analysis techniques may also be applied to spreadsheets which each row corresponds to a molecular conformation and each column to a conformation property. Whatever the data source, study of the differences in the data values within a molecular spreadsheet (MSS) graphically or by multivariate analysis frequently leads to new scientific insights.

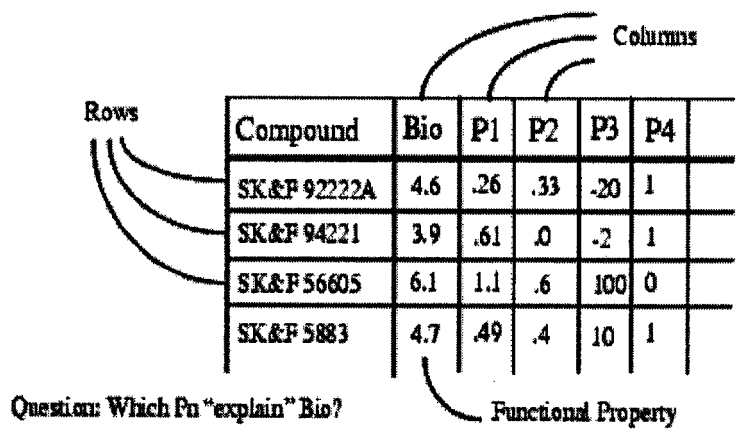

Figure 6 A QSAR table

3.12.2 Comparative Molecular Field Analysis (CoMFA)

Comparative Molecular Field Analysis (CoMFA) is a QSAR approach whose models have shown unprecedented accuracy in prediction. The idea of CoMFA is that differences in a target property are often related to differences in the shapes of the non-covalent fields surrounding the tested molecules. In CoMFA, molecules are represented and compared by their steric and electrostatic fields sampled at the intersections of one or more lattices (or grids, or boxes) spanning a three-dimensional region. Thus each CoMFA descriptor column of a QSAR MSS contains the magnitudes of either the steric or electrostatic field exerted by the atoms in the tabulated molecules on a probe atom located at a point in Cartesian space. Figure 7 illustrates the construction and analysis of a CoMFA QSAR MSS.

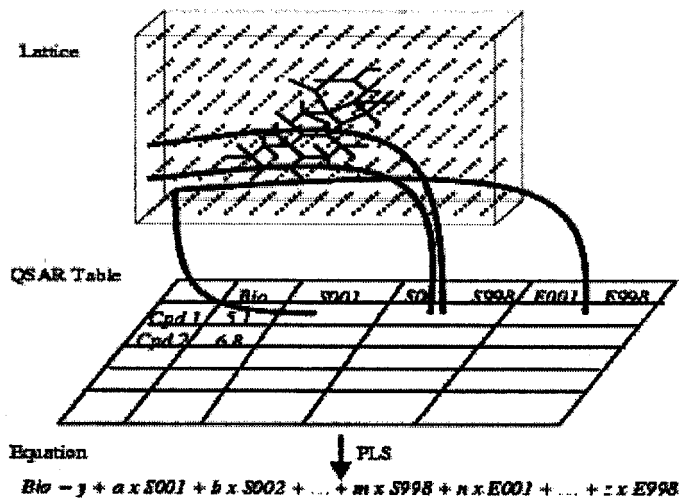

Figure 7 The CoMFA process

3.12.3 The three major phases of CoMFA process

3.12.3.1 CoMFA set up

1) The alignment rule

In CoMFA or other 3D-QSAR studies, the molecule alignment is so important because of the relative interaction energies depend strongly on relative molecular positions. In most cases a bound efavirenz derivatives/RT complex is not available. Therefore, a computation method has to be deployed to determine conformations and alignment of a set of molecules. Several strategies have been used to determine conformation and align molecules. In this study, docking method was used to determine of the binding mode of each molecule and the molecular alignment for CoMFA.

2) Calculations of interaction energy

CoMFA cubic lattice was generated around these molecules based on the molecular volume of the structures. In this investigation, three different atoms, sp^3 carbon atom with +1 charge (default probe atom in SYBYL), sp^3 oxygen atom with –1 charge and H atom with +1 charge, served as probe atoms. The probe atom was placed at each lattice point and their interactions of the steric and electrostatic fields with each atom in molecule were all calculated with CoMFA standard scaling and then put in a CoMFA QSAR table. In order to speed up the analysis and reduce the amount of noise, the minimum sigma value was set to 2.0 kcal/mol and energy cutoff values of 30 kcal/mol were selected for both electrostatic and steric fields.

- Steric Field

All atoms exhibit a short range interaction. This is generally referred to as the Van der waals interaction. The best known of the Van der waals potential functions is the Lenard-Jones 12-6 function, which can be described in the form below

$$E = \sum_i \sum_j \frac{A_{ij}}{r_{ij}^6} + \frac{B_{ij}}{r_{ij}^{12}} \quad (23)$$

Where

A_{ij} = the coefficient depicting repulsive heteroatomic interaction with hydrogen $((A_iA_j)^{1/2})$

B_{ij} = the coefficient depicting attractive heteroatomic interaction with hydrogen $((B_iB_j)^{1/2})$

r_{ij} = the distance between atom *i* from drug molecule and probe atom *j* (Å)

- Electrostatic Fields

Electrostatic interactions are usually calculated from coulomb potential using a charge probe atom. Electrostatic properties of molecules are typically described by point charges at the center of atoms. In SYBYL, the electrostatic energies are usually calculated with H^+ probe atom coulombic interaction. The general form of electrostatic interaction between two molecules is given by

$$E = \sum_i \sum_j \frac{q_i q_j}{r_{ij}} \quad (24)$$

Where

q_I, q_j = the atomic net charges of atom i from drug molecule and of Probe atom *j*, respectively.

r_{ij} = the distance between atom *i* from drug molecule and probe atom atom *j* (Å).

3.12.3.2 Partial least-squares (PLS)

A typical CoMFA data table usually contains hundreds or thousands of columns of interaction energy values and the number of compounds included in the study is relatively much smaller than the number of the energy columns. Thus, a mathematical difficulty arises because a large number of descriptor variables is used to describe the biological activity of a much smaller number of compounds. For this reason, the multiple linear regression technique

cannot be used directly without the danger of chance correlation. More statistic details were described in statistical analysis for QSAR analysis section.

3.12.3.3 Interpretation of CoMFA results

The results of CoMFA are an equation showing the contribution of energy field at each lattice point. In order to facilitate their interpretation of the results, they are also displayed as coefficient (or standard deviation time coefficient or stdev*coeff) contour plot showing the regions in space where specific molecular properties increase or decrease the potency. The coloring is standardized as followings:

a) The contours are colored in green and yellow for positive and negative steric effect, respectively. Positive steric contours show the regions where substituents increase the biological potency if occupied and the negative steric contours show the area where substituents decrease the potency.

b) The contours are colored in blue and red for positive and negative electrostatic effect, respectively. The positive electrostatic contours indicate the region where positive charge increases the potency, whereas the negative electrostatic contours display the region where negative charges increase the potency.

3.12.4 Comparative Molecular Similarity Indices Analysis (CoMSIA)

Comparative Molecular Similarity Indices Analysis (CoMSIA) is a method for comparing molecular structures among a group of structures brought into a common alignment. This technique is most commonly used in drug discovery, to find the common features that are important in binding to the biologically relevant receptor. CoMSIA is an extension of the CoMFA methodology. Both are based on the assumption that changes in binding affinities of ligands are related to changes in molecular properties, represented by fields. They differ only in the implementation of the fields.

3.12.4.1 CoMSIA field descriptions

In both CoMFA and CoMSIA, a group of structurally aligned molecules are represented in terms of fields around the molecule. These molecular property fields are evaluated between a probe atom and each molecule, at regularly spaced intervals on a grid. The value displayed in the MSS for each CoMSIA column is the RMS deviation of the points that constitute the field.

CoMFA calculates steric fields using a Lennard-Jones potential, and electrostatic fields using a Coulombic potential. While this approach has been widely accepted and exceptionally valuable, it is not without problems. In particular, both potential functions are very steep near the Van der waals surface of the molecule, causing rapid changes in surface descriptions, and requiring the use of cut-off values so calculations are not done inside the molecular surface. In addition, a scaling factor is applied to the steric field, so both fields can be used in the same PLS analysis. Finally, changes in orientation of the superimposed molecule set, relative to the calculation grid, can cause significant changes in CoMFA results, again probably due to strict cut-off values.

In CoMSIA, five different similarity fields are calculated: steric, electrostatic, hydrophobic, hydrogen bond donor and hydrogen bond acceptor. These fields were selected to cover the major contributions to ligand binding. Similarity indices are calculated at regularly spaced grid points for the pre-aligned molecules. A comparison of the relative shapes of CoMSIA and CoMFA fields is shown in Figure 8.

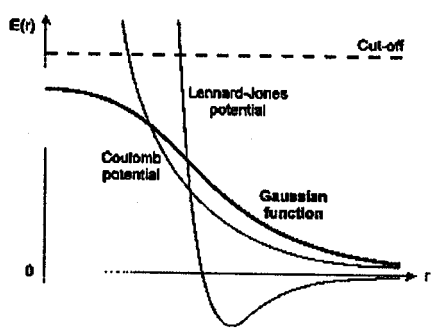

Figure 8 Shapes of various functions

For the distance dependence between the probe atom and the molecule atoms a Gaussian function is used. Because of the different shape of the Gaussian function, the similarity indices can be calculated at all grid points, both inside and outside the molecular surface. The equation used to calculate the similarity indices is as follows:

$$A_{F,k}^{q}(j) = \sum_{i} w_{probe,k} w_{ik} e^{-\alpha r_{iq}^{2}} \qquad (25)$$

where:

A = Similarity index at grid point q, summed over all atoms i of the molecule j under investigation.

$w_{probe, k}$ = Probe atom with radius 1 Å, charge +1, hydrophobicity +1, hydrogen bond donating +1, hydrogen bond accepting +1.

w_{ik} = Actual value of the physicochemical property k of atom i.

r_{iq} = Mutual distance between the probe atom at grid point q and atom i of the test molecule.

α = Attenuation factor, with a default value of 0.3, and an optimal value normally between 0.2 and 0.4.

Larger vales result in a steeper Gaussian function, and a strong attenuation of the distance-dependent effects of molecular similarity. Global molecular features become less important, and there is little averaging of local features. With an α of 0.3, each property value of a given atom is felt by 74.1% at 1 Å from the atom, by 30.1% at 2 Å, and by 6.7% at 3 Å.

CHAPTER 4

RESULTS AND DISCUSSION

4.1 Conformational analysis

4.1.1 Conformational analysis of efavirenz compound

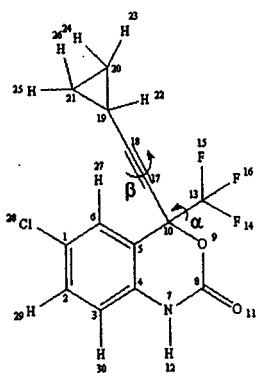

Figure 9 Structure, numbering and defined dihedral angle of efavirenz compound used in this study

4.1.1.1 The two-dimensional potential energy surface (2D PES)

The conformational analysis was performed for two different starting geometry of efavirenz, obtained from WT and K103N HIV-1 RT binding pockets. Form this study, the conformational analysis of two different starting geometry show highly correspondent results. Therefore, only one result of conformational analysis of efavirenz obtained from WT HIV-1 RT binding pocket was described as following.

The structure of efavirenz is shown in Figure 9. Two interesting sidechains were selected for conformational analysis, the cyclopropyl sidechain (β dihedral angle, C20-C19-C10-O9) and the CF_3 group (α dihedral angle, F15-C13-C10-C5). Conformational analysis of efavirenz was calculated by using various calculations, semiempirical (AM1, PM3), Hartree-Fock (HF/3-21G, 6-31G*) and DFT (B3LYP/6-31G*). The α dihedral angle shows the

symmetric rotational potential energy profile (Figure 10a). All methods show the same three local minima at 60, 180 and 300 degree for α dihedral angle. For 2D PES of the β dihedral angle, all methods show the relative energy less than 1.0 kcal/mol (Figure 10b). These results indicate that the cyclopropyl group is a high flexible sidechain. The enlarge scale of the 2D PES of the β dihedral angle based on HF and B3LYP calculations clearly show two pronounced energetic local minima at 120 and 330 degree (Figure 10c). The energy difference between these two minima obtained from HF/3-21G, HF/6-31G* and B3LYP/6-31G* are 0.211, 0.202 and 0.156 kcal/mol, respectively. The energy barrier between the local minima is very small, ranging from 0.3-0.7 kcal/mol. On the other hand, AM1 and PM3 calculations seem to be not accurate enough to search all conformations of this molecule.

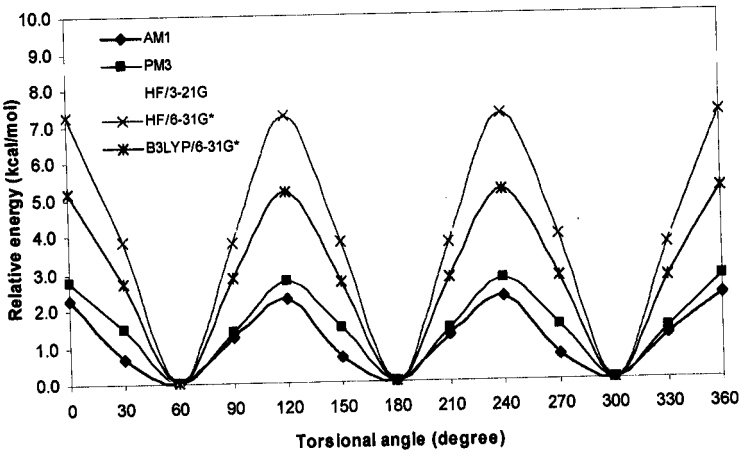

(a)

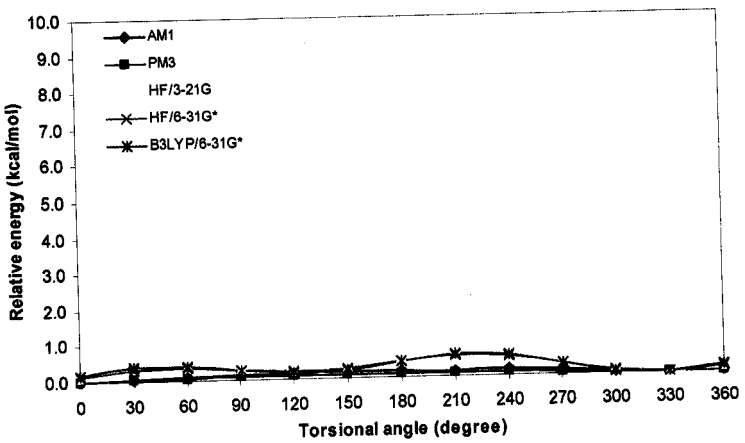

(b)

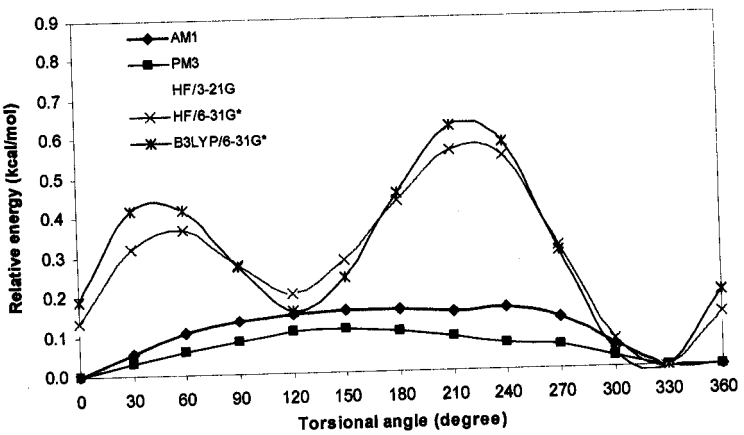

(c)

Figure 10 The 2D PES of α dihedral angle (a) The 2D PES of β dihedral angle (b) of efavirenz The scale enlargement of the 2D PES of β dihedral angle of efavirenz (c)

4.1.1.2 The three-dimensional potential energy surface (3D PES)

The potential energy surface (3D PES) of efavirenz compound obtained from varying two dihedral angles of CF_3 group (α dihedral angle) and cylopropyl group (β dihedral angle) is shown in Figure 11. The symmetric PES was obtained because of the influence of the symmetric CF_3 group. The range of the relative energy is approximately 0-5.5 kcal/mol calculated at the B3LYP/6-31G* level. Three pronounced local minima for the energy less than 0.50 kcal/mol exist at α dihedral angle 50-65, 165-185 and 285-305 with the consistent β dihedral angle from 0 to 360 degree. This result reveals that the α dihedral angle is restricted to three pronounced local minima with rather large energy barrier (5.5 kcal/mol). Nevertheless, the effect of the symmetric CF_3 group brings three pronounced local minima of α dihedral angle show the same conformation of CF_3 group. On the other hand, the β dihedral angle shows the smooth energy hypersurface and low energy barrier (0.50 kcal/mol). The results present the high flexibility of the cyclopropyl group.

The results from 3D PES agree well with 2D PES of β dihedral angle and α dihedral angle. The CF_3 group is restricted to three pronounced local minima, whereas, the cyclopropyl group shows the high flexibility. However, the 2D PES could provide the obvious local minima conformer of the cyclopropyl group more than the 3D PES.

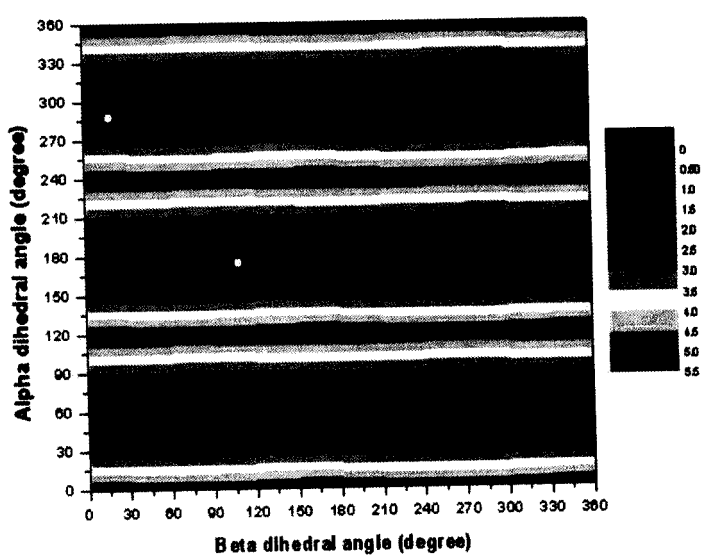

Figure 11 The 3D PES of the efavirenz calculated at the B3LYP/6-31G* level as a function of varying α and β dihedral angles

4.1.1.3 The full optimization of the local minima conformation

Based on 2D PES results, all local minima of the β dihedral angle and the global minimum of α dihedral angle were selected. The global minimum of the α dihedral angle from HF/3-21G, HF/6-31G* and B3LYP/6-31G* methods was defined as C1. For the β dihedral angle, the first local minima (120 degree) for HF/3-21G, HF/6-31G* and B3LYP/6-31G* methods were defined as C2, whereas, the second local minima (330 degree) were defined as C3. The full optimization was performed for each individual local minimum by using respective methods for each local minimum. The absolute geometry and relative energies obtained from each method are present in Figure 12 and Table 2. As show in Table 2, the C3 absolute conformation obtained from each method is the lowest energy conformer, while the C1 and C2 conformations show equal relative energy. Figure 12 presents that C1 and C2 for all methods are the same conformation. The results reveal that efavirenz shows two lower energetically favorable conformations. The orientation of the cyclopropyl group (β dihedral angle) is only different for two conformers. The β dihedral angle is about 120 for first conformer (C1 and C2) and β dihedral angle is about 330 for second conformer (C3).

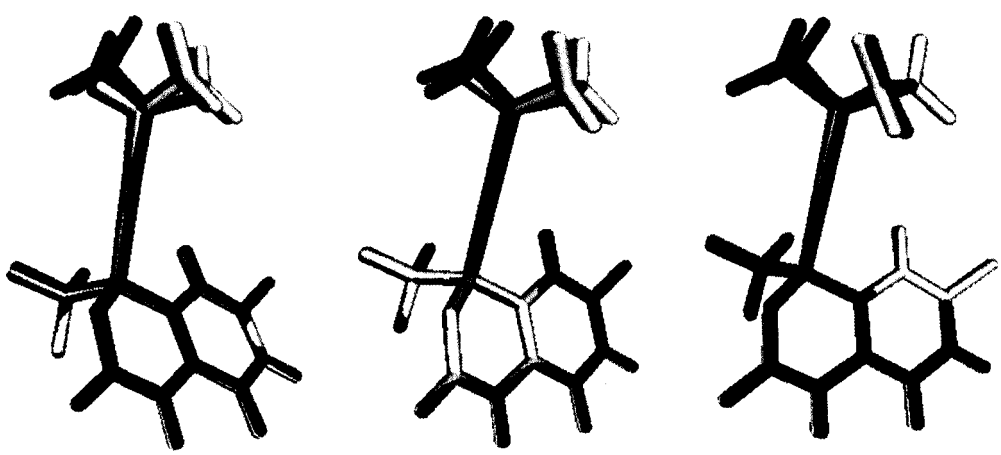

Figure 12 The optimized structure of C1 (green), C2 (yellow) and C3 (red) obtained from HF/3-21G (a), HF/6-31G*(b) and B3LYP/6-31G*(c)

Table 2 Relative energy of the optimized local conformers of efavirenz

Local minima	Relative energy (kcal/mol)
HF/3-21G	
C1	0.21
C2	0.21
C3	0.00
HF/6-31G*	
C1	0.21
C2	0.21
C3	0.00
B3LYP/6-31G*	
C1	0.17
C2	0.17
C3	0.00

4.1.1.4 Comparison of the optimized local conformer with the X-ray structure of efavirenz in WT HIV-1 RT binding pocket

Figure 13 shows that the first conformer is very similar to the X-ray structure more than the second conformer, which is lowest energetic conformer. This shows that the orientation of the cyclopropyl group of the X-ray structure differs from the lowest energetic conformer more than 150 degree. However, the conformation of efavirenz in the binding pocket corresponds to the lower energetic conformation. The deviation of cyclopropyl group from the lowest energetic conformer in the binding pocket clearly demonstrates in Table 3 and Figure 14. The cyclopropyl group of the lowest energetic conformer could encounter with the aromatic sidechain of Tyr181 amino acid residue, whereas, the X-ray crystal structure could not be found. Therefore, the deviation of the sidechain from energetically favorable conformer resulted from reducing the repulsion with the aromatic sidechain of Tyr181 amino acid.

To compare the ability to reproduce the binding mode of efavirenz in binding pocket of conformational analysis and docking method, the first conformer, which is

similar to the X-ray structure, was selected. Some dihedral angles of the first conformer obtained from conformational analysis method (HF/3-21G, HF/6-31G* and B3LYP/6-31G*) and docked conformer were compared with the X-ray (Table 4). The docked conformer shows that the standard deviation (SD) value is smaller than obtained from the first conformer. However, the first conformer based on the B3LYP/6-31G* method shows a good standard deviation more than those obtained from HF/3-21G and HF/6-31G* methods. The results indicate that the calculated conformer from B3LYP/6-31G* calculation lead to more accurate result than HF/3-21G and HF/6-31G*. Moreover, the conformer based on B3LYP/6-31G* calculation is not much different from the docked conformer as indicated by SD value (Table 3). These results reveal that conformational analysis conformer based on high level theory of calculations could be comparable with docking molecular method to predict binding mode of efavirenz in WT RT binding pocket.

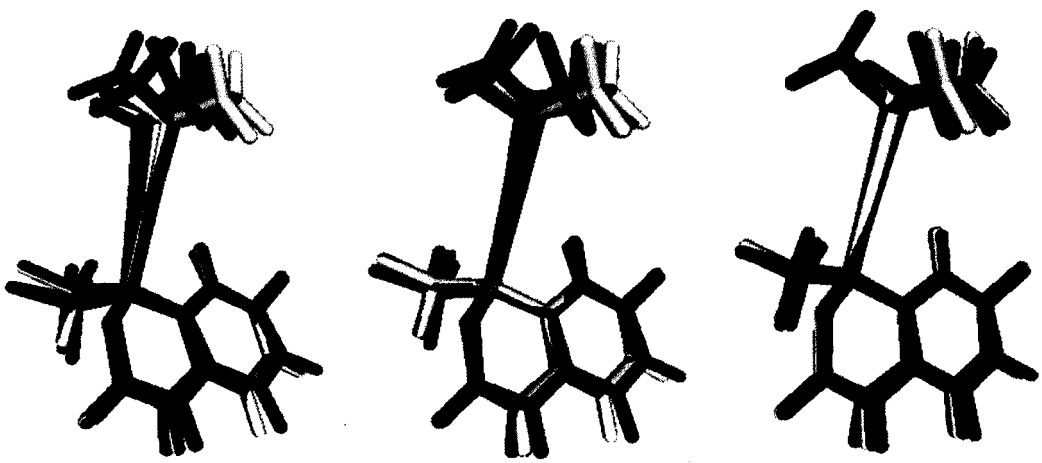

Figure 13 Superimposition of the X-ray structure (black), docked conformer (pink), first conformer (yellow) and second conformer (red) of efavirenz in WT RT binding pocket obtained from HF/3-21G (a), HF/6-31G*(b) and B3LYP/6-31G*(c)

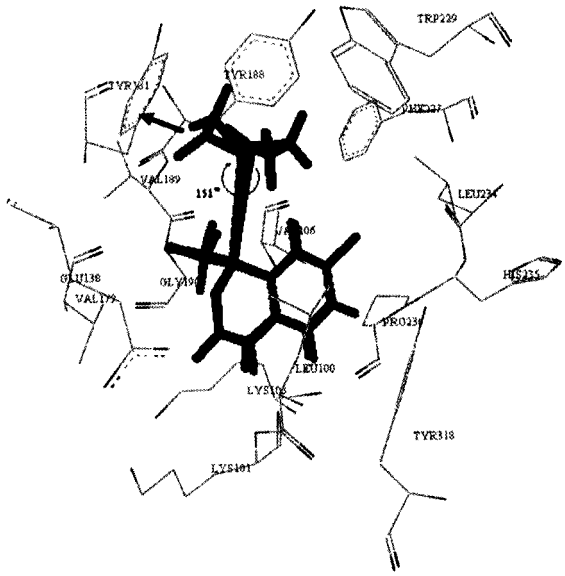

Figure 14 The X-ray crystal structure (black) and the lowest energetic conformer (red) of efavirenz in WT HIV-1 RT binding pocket

Table 3 Interatomic distance of the different conformers of efavirenz and atom of amino acid in WT HIV-1 RT binding pocket

Atom of compound and amino acid	Interatomic distance (Å)			
	X-ray	Dock	1st conformer	2nd conformer
C20				
CD1(Tyr181)	3.92	3.69	3.84	**2.49**
C19				
CD1(Tyr188)	3.93	4.02	4.04	4.02
CD2(Tyr188)	3.83	3.97	3.97	3.98
CG(Tyr188)	3.57	3.61	3.61	3.6
CD1(Tyr181)	3.49	3.54	3.54	3.52
CG(Tyr181)	3.75	3.66	3.66	3.66
C21				
CD1(Tyr188)	3.88	4.02	4.02	4.01
CD1(Tyr181)	4.47	4.35	4.35	**2.17**
CG(Tyr181)	4.88	4.04	4.04	**2.26**
CE1(Tyr181)	4.88	4.28	4.28	**2.39**

Table 4 Comparison of some selected dihedral angles of the X-ray of efavirenz in WT pocket, docked and the first conformer

Dihedral angle	HF/3-21G	HF/6-31G*	B3LYP/6-31G*	Dock	X-ray
O9-C10-C19-C21	52.6	50.6	50.2	44.2	46.2
β dihedral angle	121.1	120.0	119.4	112.6	111.1
C5-C10-C19-C21	357.2	356.8	355.9	348.7	348.1
C5-C10-C19-C20	288.6	287.4	286.7	280.3	283.2
SD	9.7	8.4	7.3	2.3	-

4.1.1.5 Comparison of the optimized local conformer with the X-ray structure of efavirenz in K103N HIV-1 RT binding pocket

Figure 15 shows the superimposition of the X-ray structure in K103N RT pocket, docked conformer in K103N RT pocket, the first and second conformers of efavirenz obtained from HF/3-21G, HF/6-31G* and B3LYP/6-31G* methods. The second conformer, which is the lowest energetic conformer, is similar to the X-ray structure more than the first conformer. Nevertheless, the orientation of the cyclopropyl group of the X-ray structure rather large differs from the second conformer (Table 5). Figure 16 could demonstrate the deviation of the cyclopropyl group of the X-ray crystal structure from two energetic conformers. The cyclopropyl group of two lower energetic conformers loses interaction with the aromatic sidechain of Tyr188 amino acid, whereas the cyclopropyl group on the configuration of the X-ray crystal structure could form the hydrophobic interaction with the aromatic sidechain of Tyr188 amino acid (Table 6). Therefore, more interaction with Tyr188 could change the conformation of the cyclopropyl group from the lower energetic conformer.

The second conformer, which is similar to the X-ray structure, was selected to compare the ability to reproduce the binding mode of efavirenz in binding pocket of conformational analysis and docking method. Some dihedral angles of the second conformer obtained from conformational analysis method (HF/3-21G, HF/6-31G* and B3LYP/6-31G*) and docked conformer were compared with the X-ray as show in Table 5. The docked conformer shows the SD value smaller than the second conformer. The second conformers obtained from HF/3-21G, HF/6-31G* and B3LYP/6-31G* methods show higher SD value.

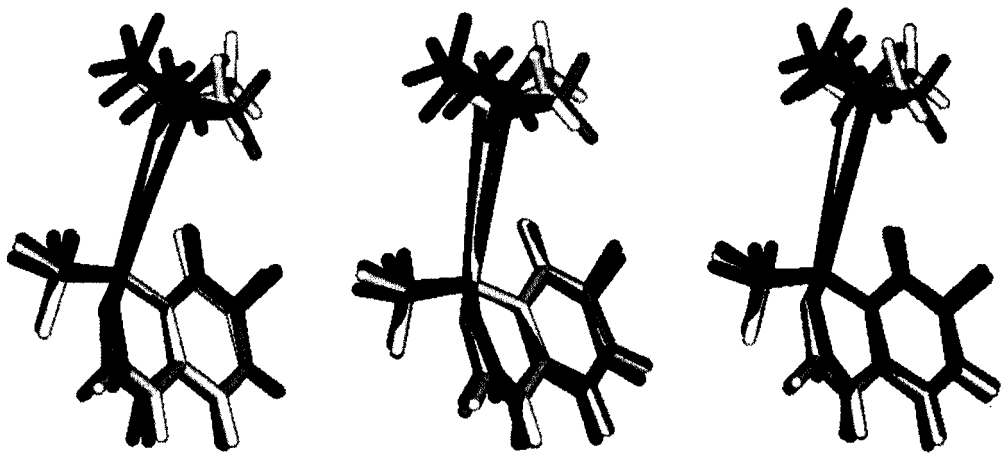

Figure 15 Superimposition of the X-ray structure (black), docked conformer (pink), the first conformer (yellow) and second conformer (red) of efavirenz in K103N RT pocket obtained from HF/3-21G (a), HF/6-31G*(b) and B3LYP/6-31G*(c)

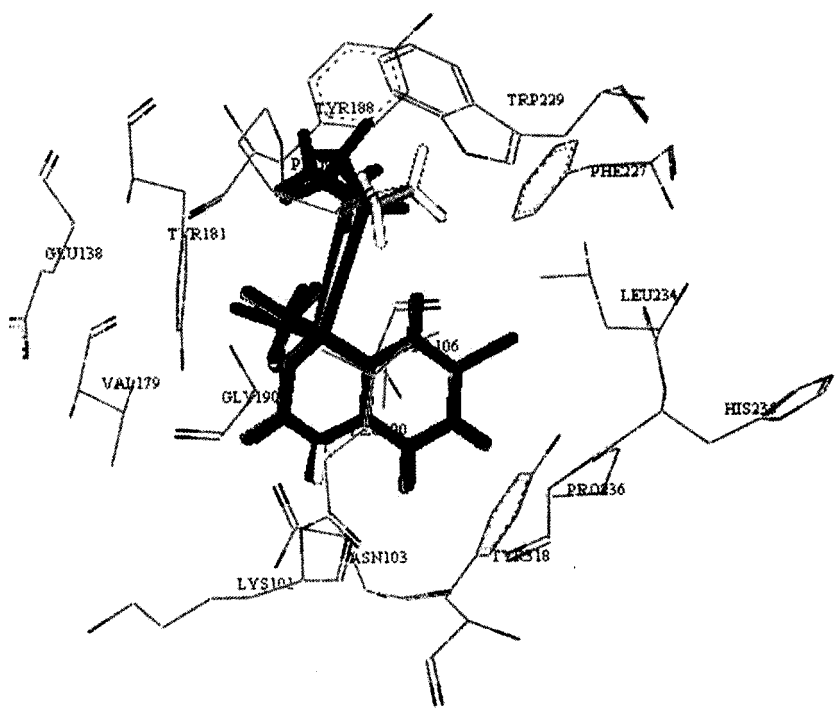

Figure 16 The X-ray crystal structure (black), the first conformer (yellow) and second conformer (red) of efavirenz in K103N HIV-1 RT binding pocket

Table 5 Comparison of some selected dihedral angles of the X-ray of efavirenz in K103N pocket, docked and the second conformers

Dihedral angle	HF		DFT	Dock	X-ray
	3-21G	6-31G*			
C6-C5-C10-C19	314.6	320.8	322.1	317.0	327.3
O9-C10-C19-C20	263.3	256.0	251.2	353.7	319.8
β dihedral angle	331.4	324.9	320.0	61.9	25.1
C5-C10-C19-C21	207.8	201.7	196.6	298.1	262.8
C5-C10-C19-C20	139.7	132.8	127.8	229.9	197.4
SD	162.3	160.8	158.9	35.0	-

Table 6 Interatomic distance of the different conformer of efavirenz and atom of amino acid in K103N HIV-1 RT binding pocket

Atom of efavirenz and amino acid	Interatomic distance (Å)			
	X-ray	Dock	1st conformer	2nd conformer
C21				
CD1(Tyr181)	3.93	3.53	**6.12**	**7.17**
CG(Tyr188)	3.84	4.80	**4.77**	**4.86**
CD2(Tyr188)	3.74	4.69	**4.95**	**5.16**
CE3(Trp229)	3.74	4.99	3.58	3.50
CD2(Trp229)	3.58	4.93	3.38	3.37
C20				
CD1(Tyr188)	3.84	4.22	**5.69**	**5.35**
CD2(Tyr188)	3.77	4.15	**5.54**	**5.95**
CG(Tyr188)	3.55	3.86	**5.51**	**5.59**
CB(Tyr188)	3.90	4.00	**5.87**	**6.00**
CD1(Leu100)	3.27	4.30	3.72	3.04

4.1.1.6 ^{1}H chemical shifts calculations of efavirenz

The conformation analysis of the efavirenz compound based on *ab initio* calculation reveals that efavirenz conformation is favorable to two lower energetic conformers (the first and second optimized conformers). To obtain the corresponding conformer to the conformational structure in solution, the NMR chemical shift calculation was performed. In this study the ^{1}H chemical shifts were calculated by the GIAO method at the B3LYP/6-311++G** level of theory on the optimized geometries of two local minimum structures by B3LYP/6-31G** and compared with the experimental results. The calculated ^{1}H NMR chemical shifts is summarized in Tables 7. The correlations between the experimental and the calculated chemical shifts are higher for the second conformers than the first conformer as shown by the SD and r^2 values reported in Table 7. The results indicate that the conformation of efavirenz in solution is favorable with the lowest energetic conformers (the second conformer).

Table 7 Calculated ^{1}H NMR chemical shifts of the first and second conformers of efavirenz compared with experimental value

H^1 NMR	Chemical shift		
	1st conformer	2nd conformer	Exp. conformer
H22	7.03	6.94	6.81
H23	7.03	6.98	7.37
H24	7.68	7.72	7.49
H25	7.86	7.99	8.71
H26	1.62	1.60	1.40
H28	0.99	1.04	0.94
H29	1.01	1.04	0.94
H30	0.83	0.97	0.85
H27	0.77	0.91	0.85
SD	0.35	0.32	-
R^2	0.99	0.99	-

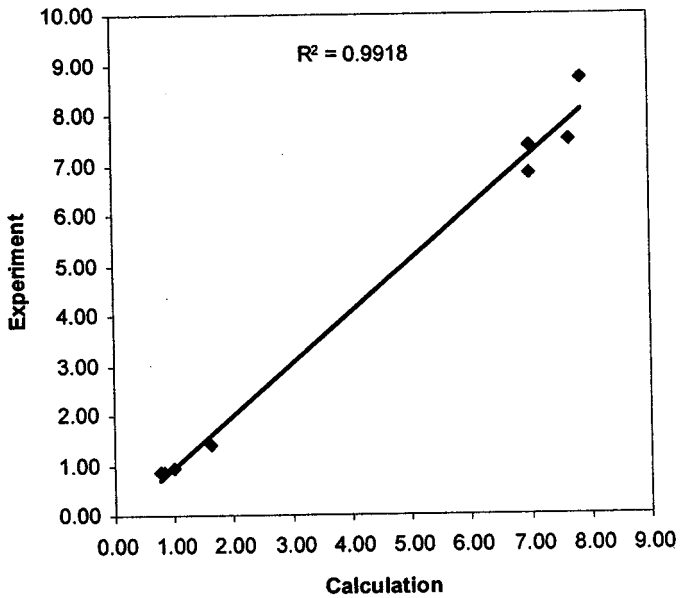

(a)

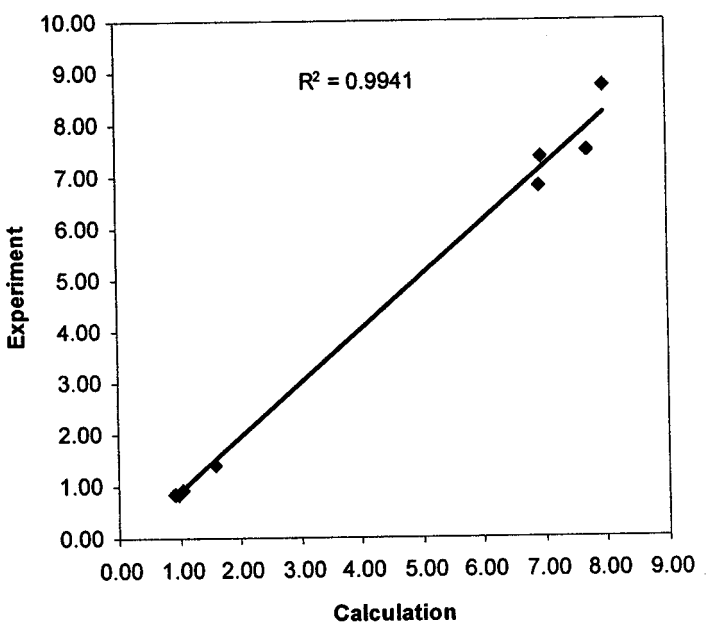

(b)

Figure 17 Correlation plot between calculated and experimental ^{1}H NMR chemical shifts for the first (a) and second (b) conformers of efavirenz

4.1.2 Conformational analysis of compound 25, the highest activity compound against WT HIV-1 RT

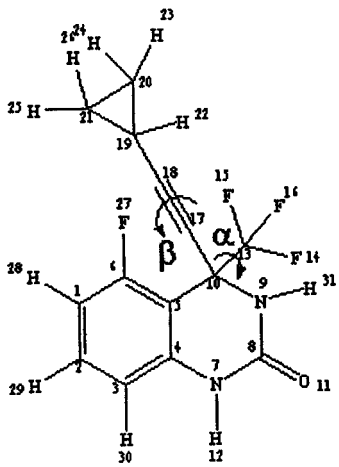

Figure 18 Structure of compound 25, the highest activity compound against WT HIV-1 RT

4.1.2.1 The two-dimensional potential energy surface

The structure of compound 25, the highest activity compound against WT HIV-1 RT, is shown in Figure 18. The rotational potential of the cyclopropyl sidechain (β dihedral angle, C20-C19-C10-N9) and the CF_3 group (α dihedral angle, F15-C13-C10-C5) were calculated by using various calculations, semiempirical (AM1, PM3), *ab initio* (HF/3-21G, HF/6-31G*), DFT calculations (B3LYP/6-31G*). The rotational potential energy profile of the α dihedral angle obtained from all methods show symmetric profile and same three local minima at 60, 180 and 300 degree (Figure 19a).

The rotational potential profile of the β dihedral angle is shown in Figure 19b. All methods show the relative energy of the rotational potential energy less than 1.0 kcal/mol (Figure 19b). These results reveal that the cyclopropyl group is a high flexible sidechain. The enlarge scale of the 2D PES of the β dihedral angle based HF and B3LYP calculations clearly show the global minimun at 150 degree (Figure 19c). AM1 and PM3 calculations seem to be not enough to search the possibility local conformation of compound 25.

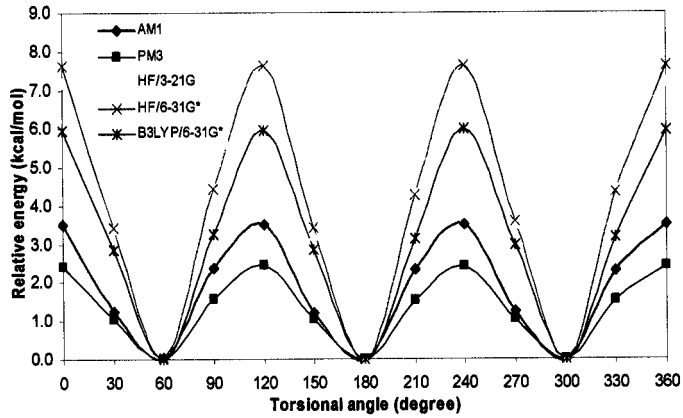

(a)

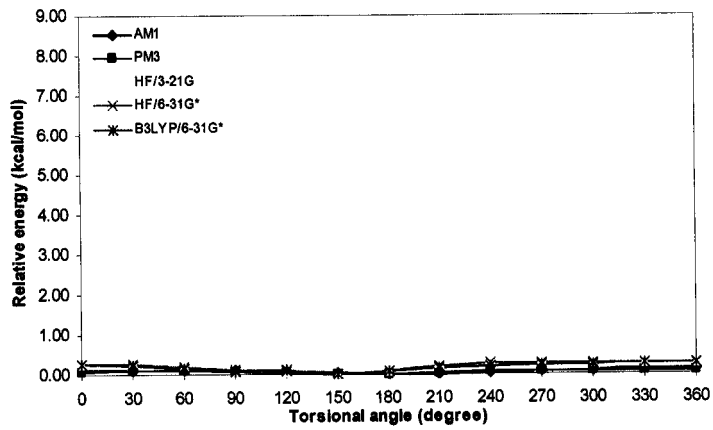

(b)

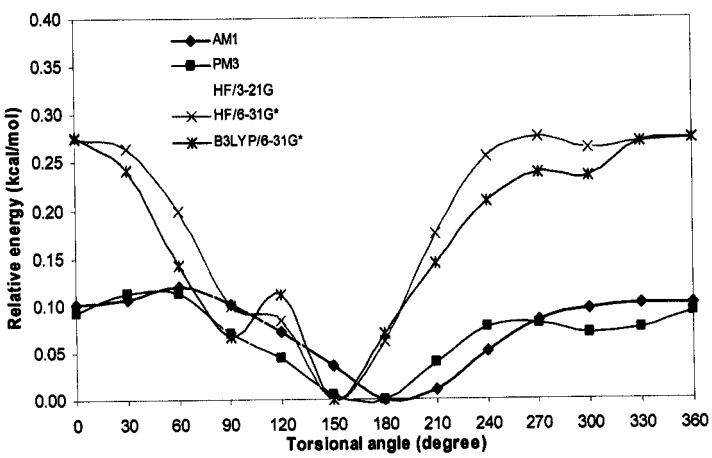

(c)

Figure 19 The 2D PES of α dihedral angle of compound 25 (a) The 2D PES of β dihedral angle of compound 25 (b) The scale enlargement of the 2D PES of β dihedral angle of compound 25 (c)

4.1.2.2 The three-dimensional potential energy surface

The potential energy surface of compound 25 obtained from varying two dihedral angles of cylopropyl group (β dihedral angle) and CF_3 group (α dihedral angle) is shown in Figure 20. The 3D PES of the highest activity compound against WT HIV-1 RT is similar to the 3D PES of efavirenz. The range of the relative energy is approximately 0-7.00 kcal/mol calculated at the B3LYP/6-31G* level. There are three pronounced local minima for the energy less than 0.875 kcal/mol existing at α dihedral angle about 50-65, 165-185 and 285-305 degree, respectively, with the consistent β dihedral angle from 0 to 360 degree. This result reveals that the α dihedral angle is restricted to three pronounced local minima, while the β dihedral angle shows high flexibility.

Comparison of the 3D PES and the 2D PES obviously shows that the 2D rotational potential of β dihedral angle provides more information to predict all possible local minima conformer of compound 25 than 3D PES.

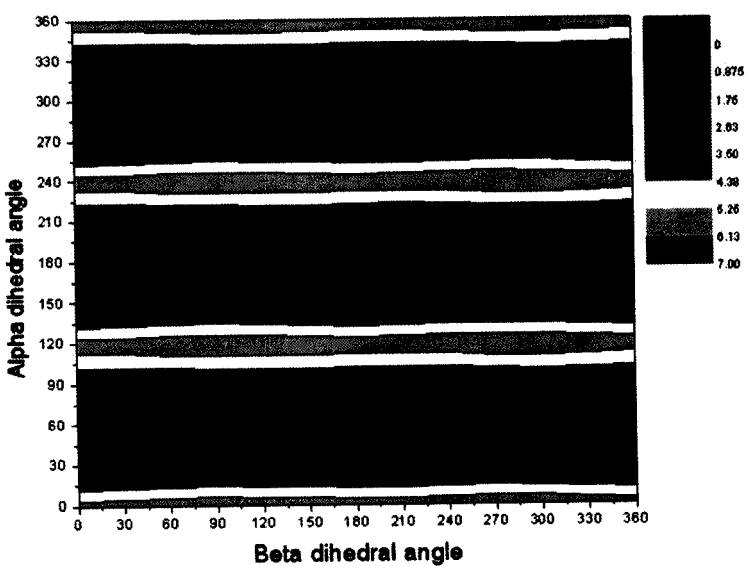

Figure 20 The 3D PES of compound 25 calculated at the B3LYP/6-31G* level as a function of varying α and β dihedral angles

4.1.2.3 The full optimization of local minima conformation

The global minimum from the 2D PES of α dihedral angle and two local minima from the 2D PES of β dihedral angles were selected. The global minimum of α dihedral angle of HF/3-21G, HF/6-31G* and B3LYP/6-31G* methods was defined as B1. For the rotational potential energy of β dihedral angle, the first local minima (90 degree) for HF/3-21G, HF/6-31G* and B3LYP/6-31G* methods was defined as B2, whereas, the second local minima (150 degree) was defined as B3. The optimized local geometry of each individual local minimum was obtained from the full optimization with respective to conformational analysis method for each local minimum. The optimized local conformation of the B3 obtained from each method is the lowest energy conformer, whereas the B1 and B2 show equal relative energy, reported in Table 8. The superimposition of all optimized local conformers obtained from HF/3-21G, HF/6-31G* and B3LYP/6-31G* calculations shows that the B1 and B2 conformers are identical conformation (Figure 21). These results reveal that the highest activity compound against WT HIV-1 RT pronounces two lower energetic conformers. The first conformer shows the orientation of the cyclopropyl group at β dihedral angle about 90 (B1 and B2) and the second conformer exists at β dihedral angle about 150 (B3).

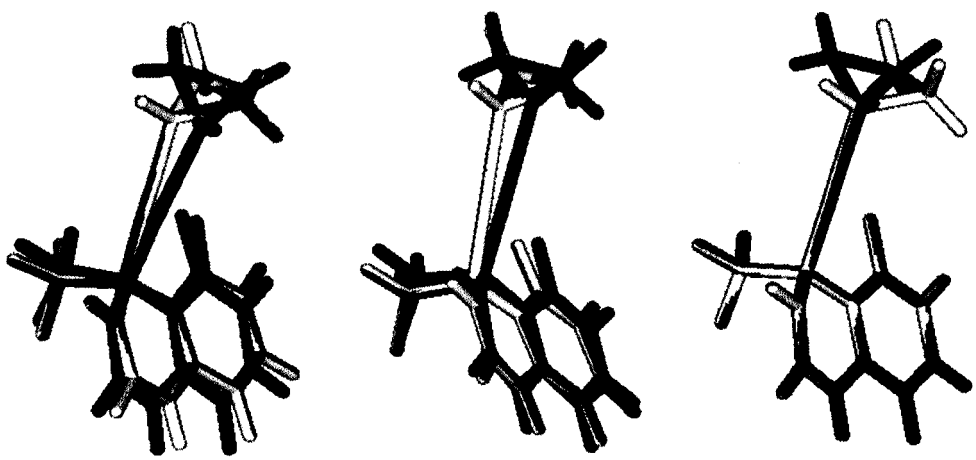

Figure 21. The optimized local structure of B1 (green), B2 (yellow) and B3 (red) obtained from HF/3-21G (a), HF/6-31G*(b) and B3LYP/6-31G*(c) methods

Table 8 Relative energy of all optimized local conformers of compound 25

Optimized local conformer	Relative energy (kcal/mol)
HF/3-21G	
B1	0.07
B2	0.07
B3	0.00
HF/6-31G	
B1	0.10
B2	0.10
B3	0.00
B3LYP/6-31G*	
B1	0.07
B2	0.07
B3	0.00

4.1.2.4 Comparison of the docked and optimized local conformer of compound 25

At the X-ray crystal of compound 25 complex with WT HIV-1 RT has not been investigated, the docked conformation of this compound in the WT HIV-1 RT binding pocket was compared with the results obtained from conformational analysis. Figure 22 shows that the first conformer of all methods is more similar to the docked conformation than the second conformer, which is lowest energetic conformer. However, the cyclopropyl group of the docked conformer differs from the both lower energetic conformer. Figure 23 and Table 9 could clearly demonstrate the deviation of the cyclopropyl group. The cyclopropyl group of docked conformation could form more interaction with the surrounding amino acid than other conformations (Table 9). The first conformer reveals poor interactions because the cyclopropyl group loses interaction with the sidechain of Pro95 and Tyr181. In contrast, the second conformer loses interaction because the cyclopropyl group encounters with the aromatic sidechain of Tyr188.

Therefore, the cyclopropyl group of inhibitor in the binding pocket differs from the energetically favorable conformer because of much interaction effect.

To validate the methods used for searching binding conformation of compound 25 in binding pocket, the dihedral angle of the first conformer from each method were compared with the docked structure as show in Table 10. The calculated conformer based on DFT calculation shows high correspondence to the docked conformation.

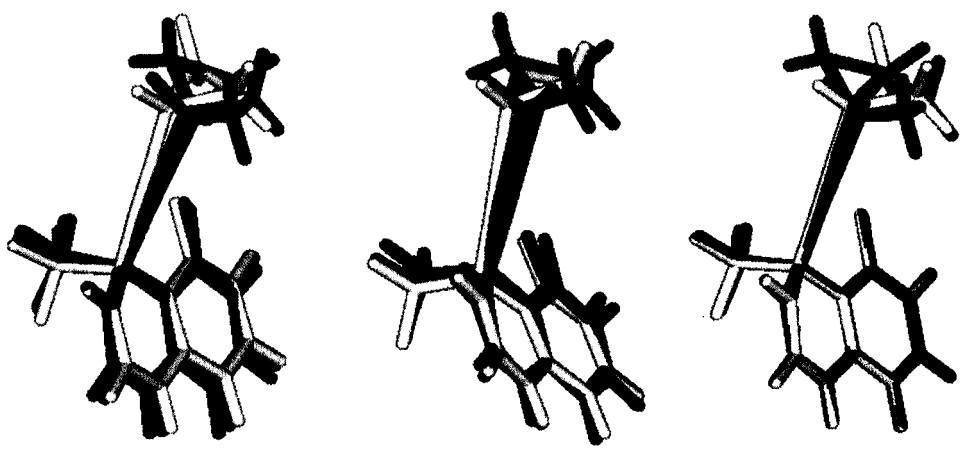

Figure 22 The superimposition of docked conformation (black), first optimized local conformer (yellow) and second optimized local conformer (red) obtained from HF/3-21G (a), HF/6-31G* (b) and B3LYP/6-31G* (c), respectively

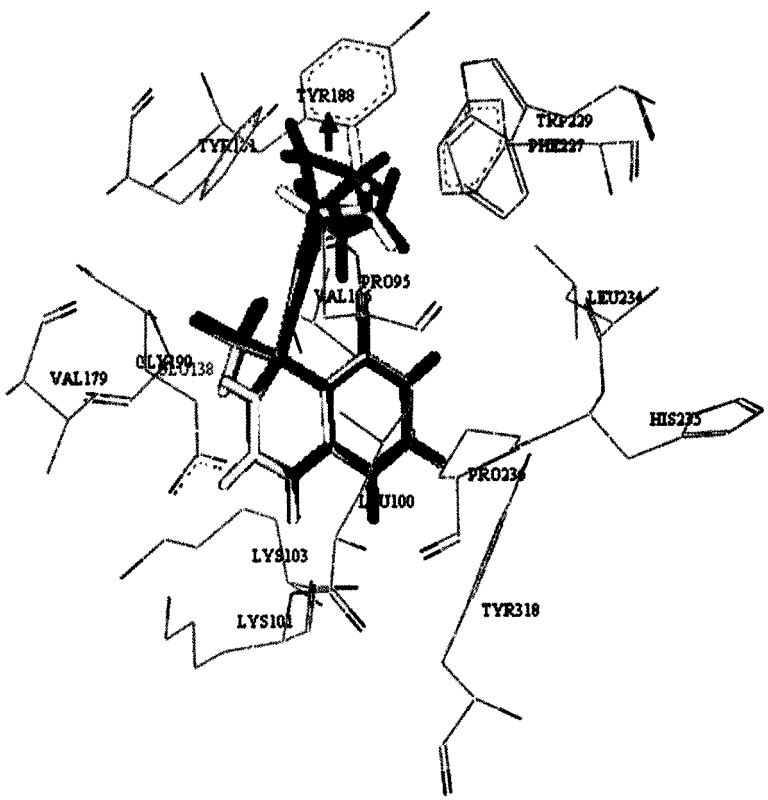

Figure 23 The docked conformer (black), the first conformer (yellow) and the second conformer (red) of compound 25 obtained from which method in WT HIV-1 RT binding pocket

Table 9 Interatomic distance of the different conformation of compound 25 and atom of amino acid in WT HIV-1 RT binding pocket

Atom of inhibitor and amino acid residues	Interatomic distance (Å)		
	Dock	**1st conformer**	**2nd conformer**
C20			
CG(Pro95)	3.82	**4.83**	6.15
CG(Tyr181)	3.77	**4.41**	4.74
C17			
CD1(Tyr188)	3.91	3.71	3.75
CD2(Tyr188)	3.90	3.63	3.66
CG(Tyr188)	3.51	3.25	3.29
CD1(Tyr181)	3.65	3.46	3.46
CG(Tyr181)	3.77	3.63	3.63
CG(Pro95)	3.82	**5.41**	5.37
CB(Tyr188)	3.64	3.61	3.41
C21			
CG(Tyr188)	4.08	2.64	**1.97**
CB(Tyr188)	4.65	3.39	**2.42**
CD2(Tyr188)	4.36	2.98	**2.15**

Table 10 Comparison of some selected dihedral angles of the docked and the first conformer of compound 25

Dihedral angle	HF/3-21G	HF/6-31G*	DFT	Dock
N9-C10-C19-C20	96.3	99.9	86.4	42.3
β dihedral angle	164.2	169.2	155.0	109.7
C5-C10-C19-C20	333.60	338.9	325.3	279.7
SD	66.3	72.0	55.1	-

4.1.2.5 Calculated ^{1}H chemical shifts

The conformational analysis of compound 25 based on *ab initio* calculations shows that there are two lower energetic local conformers (β dihedral angle about 90 and 150 degree). To obtain the conformer corresponds to the conformational in solution, the NMR chemical shift calculation was performed. The calculated ^{1}H NMR chemical shifts is summarized in Tables 11. The result shows the calculated chemical shifts derived from the second conformer (β dihedral angle about 150) highly correlate with the experimental data than the first conformer (β dihedral angle about 90). As indicated by high correspondence of the calculated and experimental ^{1}H NMR data, it reveals that the conformation analysis based on which method is reliable for prediction of inhibitor conformation.

Table 11 Calculated ^{1}H NMR chemical shifts of two lower energetic local conformers and experimental value

H^1 NMR	chemical shift		
	1st conformer	2nd conformer	Exp. conformer
H1	7.17	7.19	9.20
H23	7.01	6.96	7.57
H24	7.84	7.76	7.42
H22	7.02	6.91	6.84
H31	5.48	5.54	5.48
H25	1.55	1.47	1.41
H 28	0.98	0.95	0.88
H 27	0.94	0.93	0.88
H26	0.67	0.85	0.67
H29	0.81	0.82	0.72
SD	0.72	0.71	-
$\mathbf{R^2}$	0.96	0.97	-

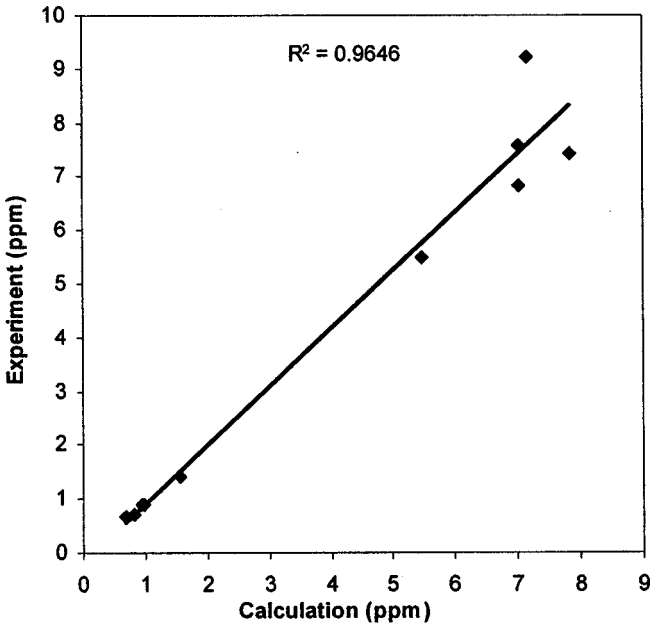

(a)

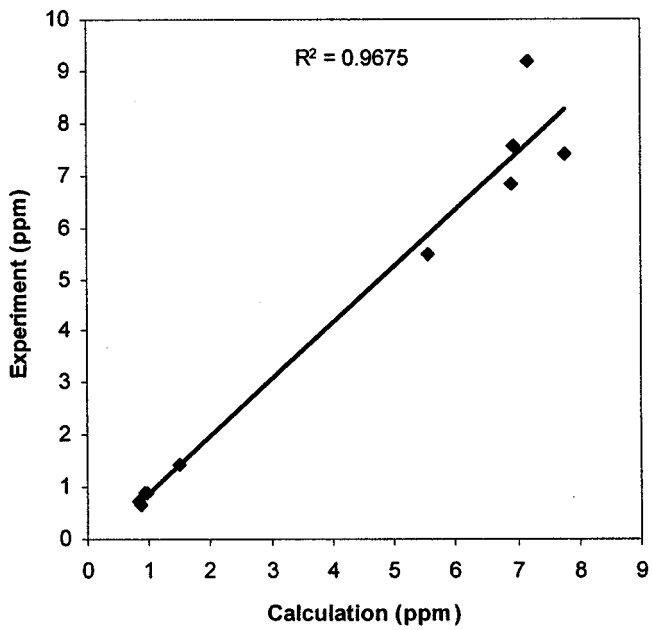

(b)

Figure 24 Correlation plot between calculated and experimental ^{1}H NMR chemical shifts for the first (a) and second (b) conformers of compound 25

4.1.3 Conformational analysis of compound 50, the highest activity compound against K103N HIV-1 RT

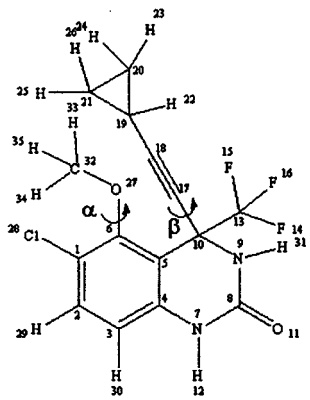

Figure 25 Structure of compound 50, the highest activity compound against K103N HIV-1 RT

4.1.3.1 The two-dimensional potential energy surface

Figure 25 shows the structure of compound 50, the highest activity compound against K103N HIV-1 RT. The rotational potential of the cyclopropyl sidechain (β dihedral angle, C20-C19-C10-N9) and the methoxy group (α dihedral angle, C32-O27-C6-C1) of the inhibitor were calculated by using HF/3-21G, HF/6-31G* and B3LYP/6-31G* methods. The rotational potential energy profile of the α dihedral angles is shown in Figure 26a. Two pronounced energetic local minima conformer of the α dihedral angle were found at 60 and 300 degree for HF/6-31G* and B3LYP/6-31G* method, and the α dihedral angle at 60 and 270 degree were found for HF/3-21G method. The energy barrier between the local minima of the α dihedral angle is very large, ranging from 10-16 kcal/mol. On the other hand, the energy barrier of the β dihedral angle shows a small energy barrier (Figure 26b). The results indicate that the cyclopropyl group could change the conformation easier more than the methoxy group. For the enlarge scale of the 2D PES of the β dihedral angle is shown in Figure 26c. Two pronounced energetic local minima conformer of β dihedral angle were found at 60 and 270 degree were obtained from HF/6-31G* and B3LYP/6-31G* methods, respectively, and at 60 and 300 degree were obtained from HF/3-21G method.

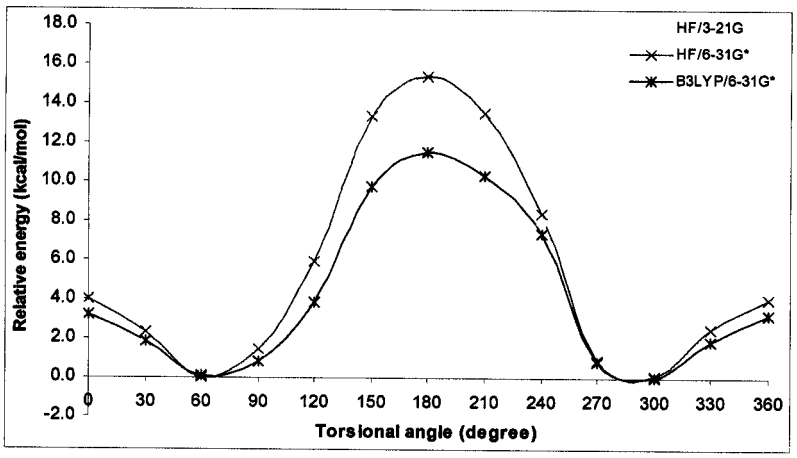

(a)

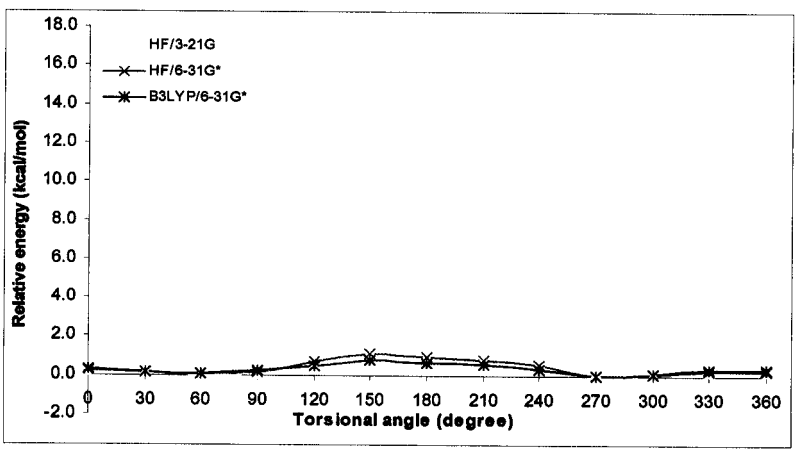

(b)

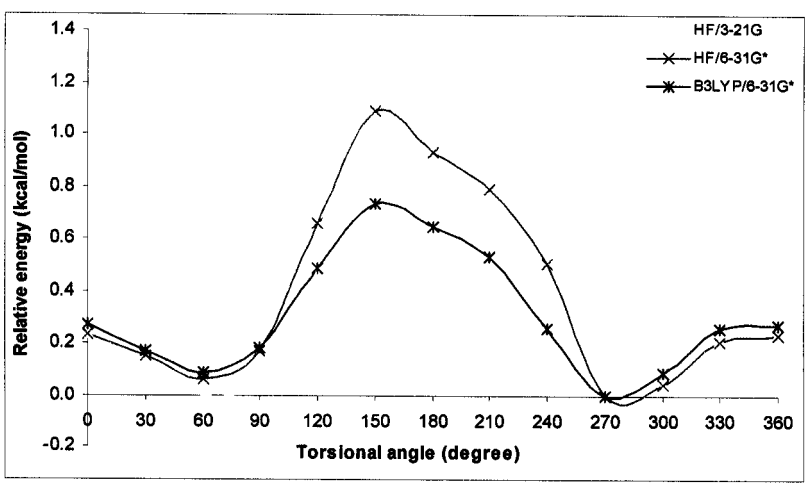

(c)

Figure 26 The 2D PES of α dihedral angle of compound 50 (a) The 2D PES of β dihedral angle of compound 50 (b) The scale enlargement of the 2D PES of β dihedral angle of compound 50 (c)

4.1.3.2 The three-dimensional potential energy surface

The three-dimensional potential energy surface of compound 50 obtained by varying two dihedral angles of the methoxy group (α dihedral angle) and the cylopropyl group (β dihedral angle) is shown in Figure 27. There are some regions of low and high relative energy due to steric interaction of the cyclopropyl group with the methoxy group. The large region of lower energetic surface shows at α dihedral angle between 180 and 210 within the complete range of the β dihedral angle. The results indicate the high flexibility of the cyclopropyl group. Another low energy region is shown for α dihedral angle at 45-60 degree and β dihedral angle at 180-360 degree.

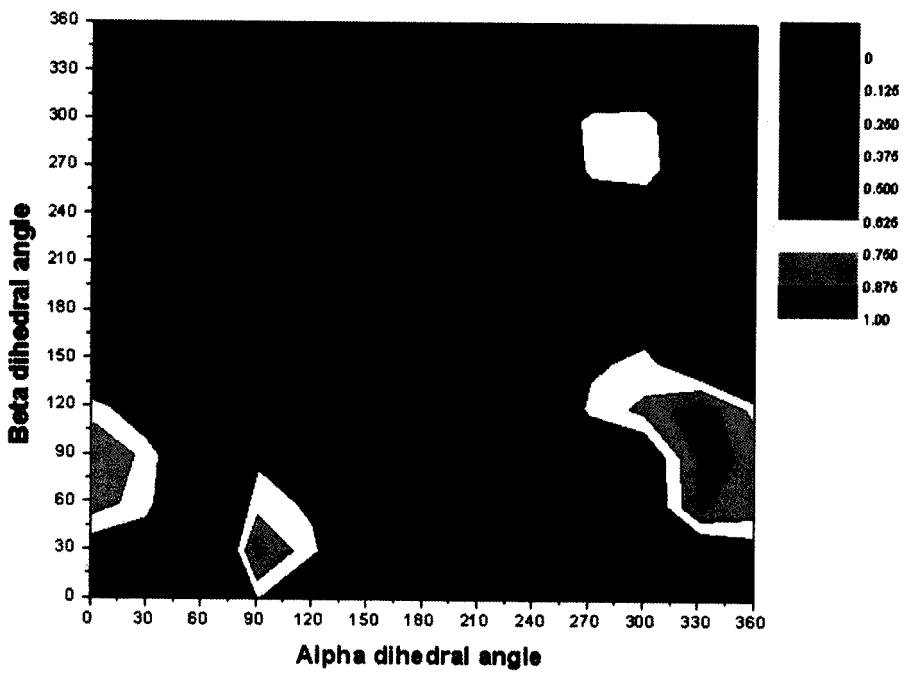

Figure 27 The 3D PES of compound 50 calculated at the B3LYP/6-31G* level as a function of varying α and β dihedral angles

4.1.3.3 The full optimization of local minima conformation

Two local minima from 2D PES of α dihedral angle for HF/3-21G, HF/6-31G* and B3LYP/6-31G* methods were selected and defined as BM1 and BM2, whereas, two local minima of β dihedral angle were defined as BM3 and BM4. The absolute conformation of each individual local minimum was performed by full optimization with respective to conformer analysis method for each local minimum. The optimized conformations and relative energies obtained from each method are present in Figure 28 and Table 12, respectively. The optimized conformation of BM4 from HF/6-31G* and B3LYP/6-31G* calculations show the lowest energy conformer, while the HF/3-21G results show that BM1 is the lowest energy conformer. For the cycloproply group, four different conformations were found, while the methoxy group is restricted to two conformers (α dihedral angle equal 60 and 300 degree).

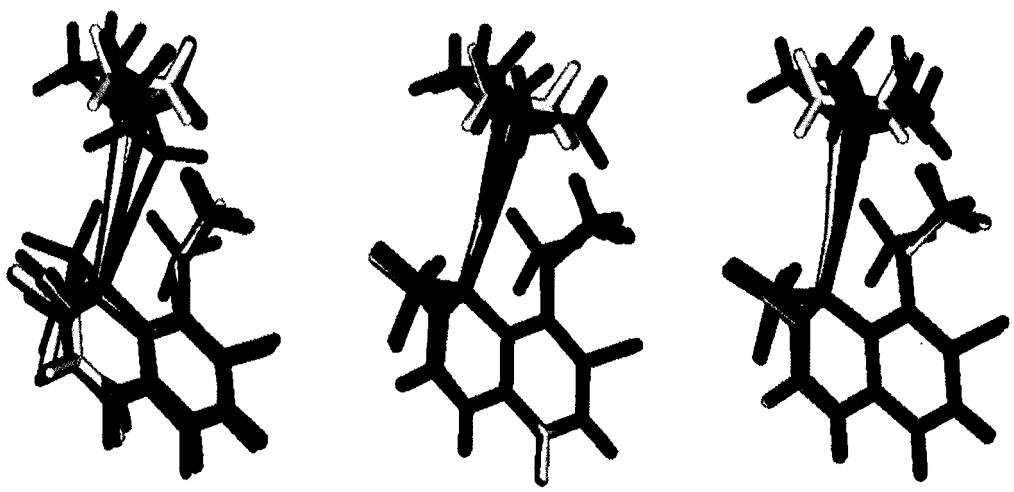

Figure 28 Superimposition of docked (black), BM1 (pink) and BM2 (cyan), BM3 (yellow) and BM4 (red) conformations obtained from HF/3-21G (a), HF/6-31G* (b) and B3LYP/6-31G* (c)

Table 12 Relative energy of all optimized local conformer of compound 50

Local minima	Relative energy (kcal/mol)
HF/3-21G	
BM1	0.00
BM2	1.78
BM3	1.17
BM4	1.19
HF/6-31G*	
BM1	0.32
BM2	0.09
BM3	0.09
BM4	0.00
B3LYP/6-31G*	
BM1	0.12
BM2	0.35
BM3	0.08
BM4	0.00

4.1.3.4 Comparison of the docked and optimized local conformer

The superimposition of the docked and all optimized local conformers shows the BM2 obtained from HF/6-31G* and B3LYP/6-31G* calculations are the most similar to the docked conformer. On the other hand, HF/3-21G shows BM3. This result shows that the binding mode of the highest activity compound in K103N HIV-1 RT binding pocket is unfavorable to the lowest energetic conformer (BM4). Figure 29 and Table 13 could clearly demonstrate the deviation of the cyclopropyl group. The cyclopropyl group of the lowest energetic conformer conflicts with the aromatic sidechain of Tyr188 and losses the interaction with the sidechain of Trp229, whereas, the docked conformation shows the possibility to form the hydrophobic interaction with two amino acid sidechains. Therefore, the reduced repulsion with Tyr181 and more interaction with Trp229 are the main cause of the deviation of cyclopropyl group.

To validate method for searching binding conformation of compound 50 in binding pocket, the dihedral angle of the similar docked conformer (BM2 for HF/6-31G* and B3LYP/6-31G* and BM3 for HF/3-21G) obtained from each method were compared with the docked structure as shown in Table 14. The B3LYP/6-31G* and HF/6-31G* methods show less standard deviation compared to HF/3-21G method. This reveals that the calculated conformer based on B3LYP/6-31G* and HF/6-31G* methods are high correspondence to the docked conformation.

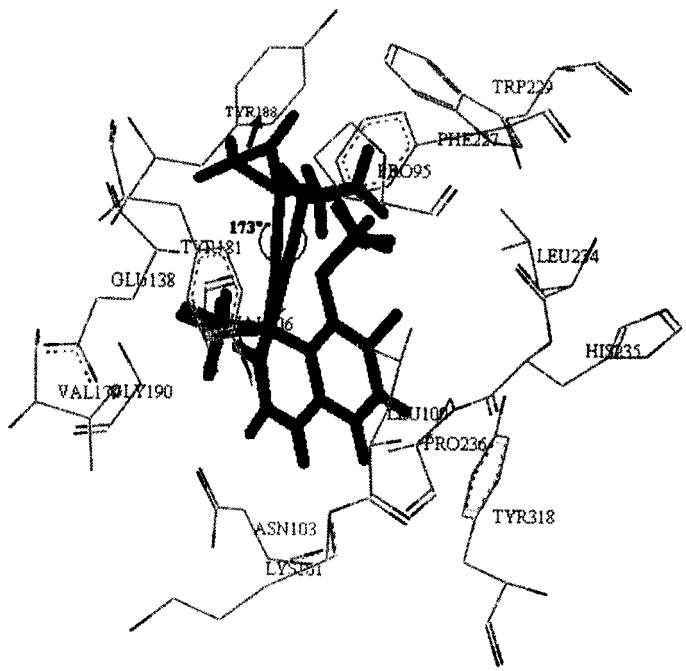

Figure 29 The docked (black) and lowest energetic conformers (red) of compound 50 in K103N HIV-1 RT binding pocket

Table 13 Interatomic distance of the different conformation of compound 50 and atom of amino acid in K103N HIV-1 RT binding pocket

Atom of compound and amino acid residues	Interatomic distance (Å)		
	Dock	**BM2**	**BM4**
C19			
CB(Tyr188)	3.82	3.42	3.19
CG(Tyr188)	3.73	3.39	3.23
CD2(Tyr188)	3.96	3.62	3.19
CB(Tyr181)	3.77	3.44	3.22
CG(Tyr181)	3.98	3.79	3.64
C20			
CB(Tyr181)	3.84	3.23	**2.39**
CG(Tyr188)	4.98	4.60	**1.90**
CD1(Tyr188)	5.54	3.97	2.65
CD2(Tyr188)	4.91	4.46	**2.02**
C21			
CZ2(Trp229)	3.86	3.85	**5.98**
CD2(Trp229)	3.84	4.12	**6.57**
CE2(Trp229)	3.75	3.96	**6.51**

Table 14 Comparison of some selected dihedral angles of the docked and similar docked conformers of compound 50

Dihedral angle	Dock	Similar docked conformers		
		HF/3-21G	HF/6-31G*	B3LYP/6-31G*
C6-C5-C10-C19	310.6	310.6	314.5	315.3
β dihedral angle	91.2	84.0	71.8	78.5
C5-C10-C19-C21	329.0	321.9	311.0	318.1
C5-C10-C19-C20	260.5	297.3	241.9	249.0
α dihedral angle	294.7	297.3	287.9	295.8
SD	-	22.1	16.6	16.3

4.2 Docking analysis

4.2.1 Validation of the docking method

To investigate the binding modes of several efavirenz derivatives in the WT and K103N HIV-1 RT binding pockets, the inhibitors were docked into both binding pockets. Firstly, to ensure that the ligand orientation and the position obtained from the docking studies are similar to the binding modes of the crystal structure, the AUTODOCK docking parameters has to be validated for the crystal structures of efavirenz in the WT (1fk9) and K103N (1fko) RT binding pockets. The conformation efavirenz found in the both crystal structure, was extracted and docked back into the corresponding binding pocket. The results show that AUTODOCK determine the docked orientation of the efavirenz close to the original orientation found in both X-ray crystal structures (Figure 30). The root mean square deviations (RMSD) between the docked and crystal ligand coordinates are 0.353 Å and 0.533 Å for the WT and K103N RT binding pockets, respectively. This indicates the good alignment of the experimental and calculated positions. Therefore, the docking approach should be acceptable for searching binding conformations of the other inhibitors.

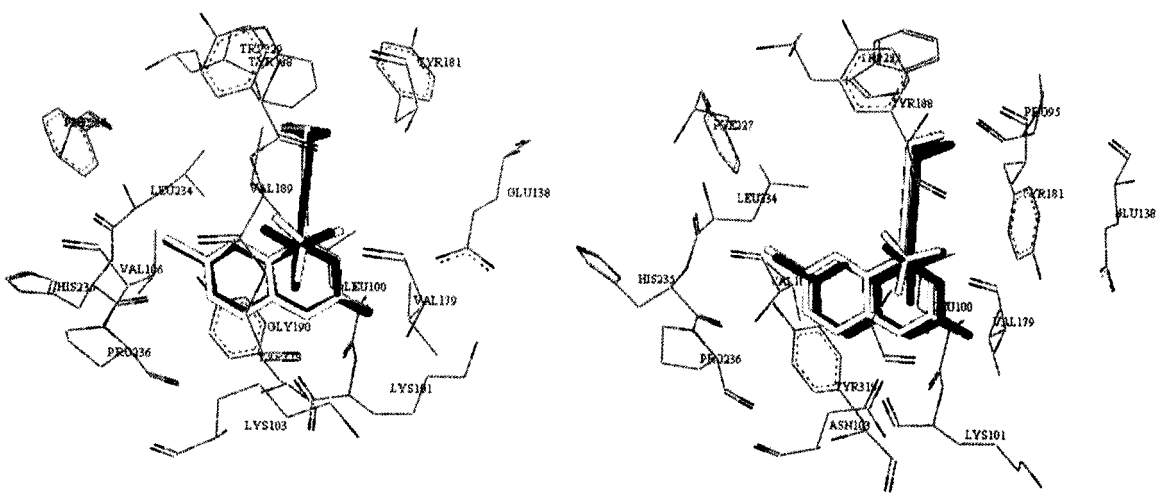

Figure 30 (a) Superimposition of the docked efavirenz (green) and the X-ray efavirenz (yellow) in the WT HIV-1 RT binding pocket

(b) Superimposition of the docked efavirenz (green) and the X-ray efavirenz (yellow) and K103N HIV-1 RT binding pocket

4.2.2 The X-ray crystal structures of efavirenz in complex with the WT and K103N RT

The position of efavirenz in the WT and K103N HIV-1 RT binding pockets obtained from the X-ray crystal structures are shown in Figure 31. Efavirenz shows the similar interaction of two hydrogen bond interaction with both binding pockets, NH of Lys101 with carbonyl oxygen of the benzoxazin-2-one ring and the main chain carbonyl oxygen of Lys101 and NH of the benzoxazin-2-one ring. The Van der waals interaction between 6-Cl of the ring and Val106 could be formed. However, the K103N mutation brings to Van der waals interaction loss of C9 and C8 with Lys103. Also the interaction between C9 and C10 with the main chain carbonyl oxygen of Pro236 was diminished in Table 15. Obviously, the hydrophobic surface of the cyclopropyl group matchs more complementally to the binding pocket of WT RT than K103N RT pocket (Figure 32). These reasons are the main cause for the lower activity of efavirenz in K103N HIV-1 RT binding pocket.

The superimposition of the X-ray crystal structure of efavirenz in the WT and K103N HIV-1 RT binding pockets is shown in Figure 33. The mutated side chain at 103 from lysine to asparagines turn makes the aromatic sidechain of Tyr181 flip to down orientation (red arrow) in K103N RT binding pocket. This reason brings the hydrophobic binding pocket of K103N RT to be obvious change. The cyclopropyl groups show high the difference orientation in both HIV-1 RT binding pockets (85 degree).

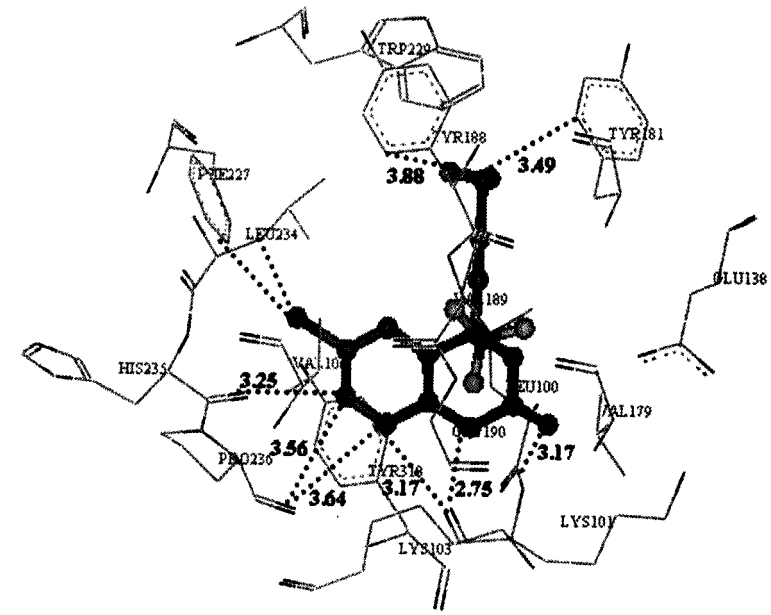

(a)

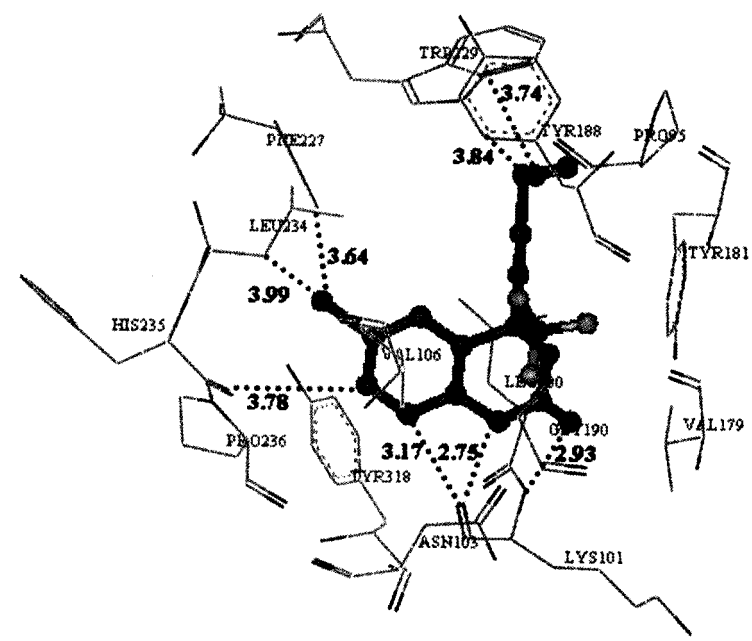

(b)

Figure 31 The X-ray structure of efavirenz in the WT (a) and K103N (b) HIV-1 RT binding pockets

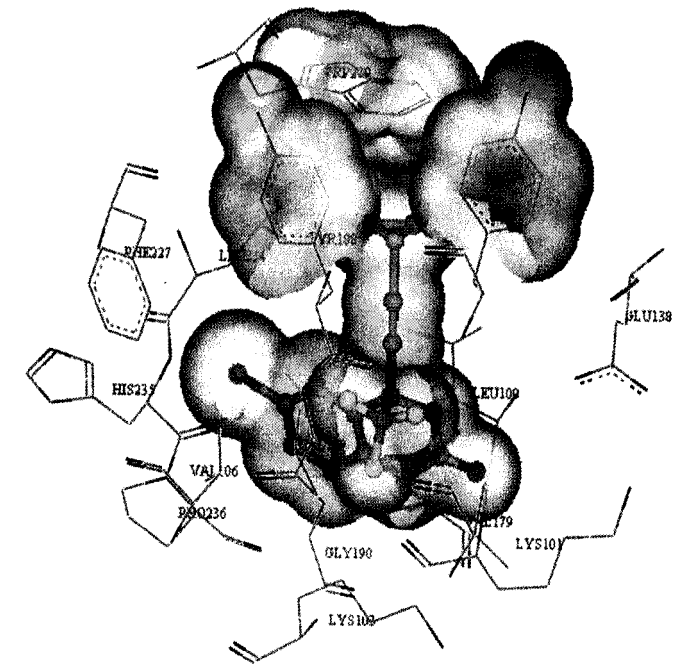

(a)

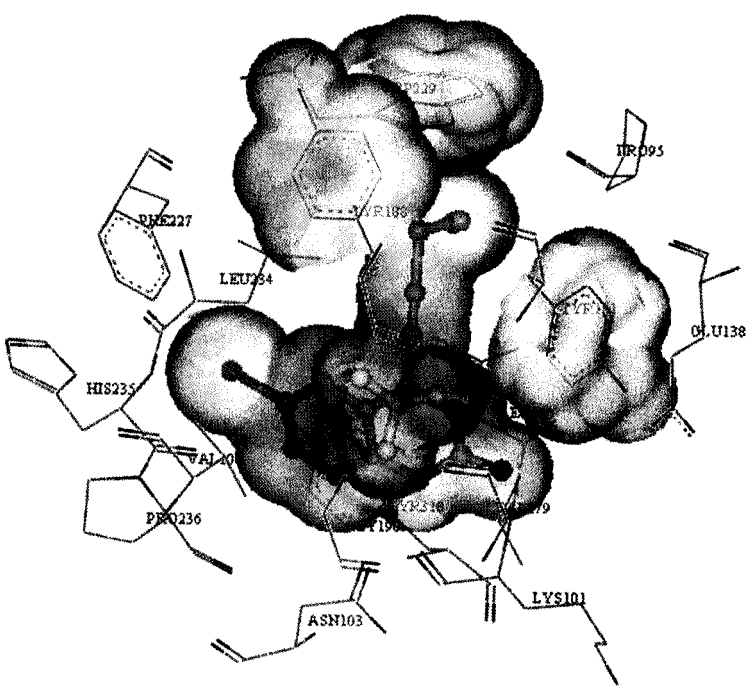

(b)

Figure 32 (a) Hydrophobic interaction of the X-ray structure of efavirenz in the WT HIV-1 RT binding pocket

(b) Hydrophobic interaction of the X-ray structure of efavirenz in the K103N HIV-1 RT binding pocket

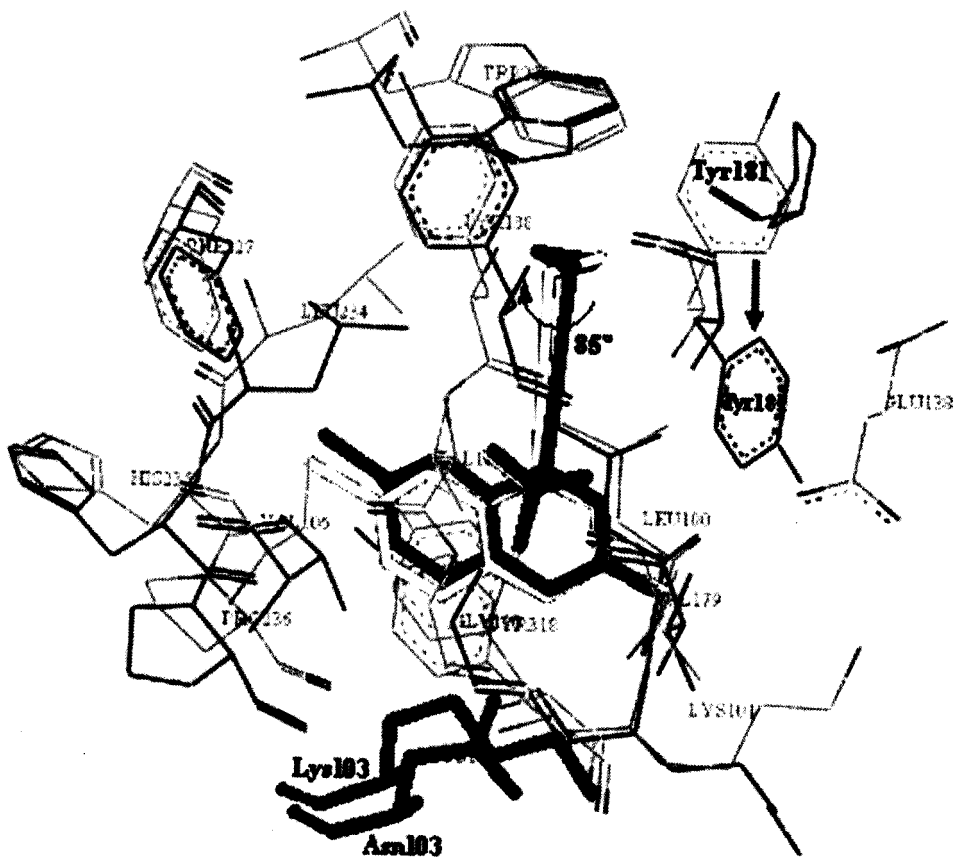

Figure 33 Superimposition of the crystal structures of efavirenz in the WT (red) and K103N (yellow) of HIV-1 RT binding pockets

Table 15 Interatomic distances of the X-ray structure of efavirenz and atom of amino acid in the WT and K103N HIV-1 RT binding pockets

Atom of efavirenz and amino acid	Interatomic distance (Å)	
	WT pocket	**K103N pocket**
C10		
O(His235)	3.25	3.78
O(Pro236)	3.56	**4.05**
CE2(Tyr318)	3.77	3.55
OH(Tyr318)	3.82	3.55
C9		
O(Pro236)	3.64	**4.25**
O(Lys101)	3.17	3.17
CG(Lys103)	3.72	**4.47**
C8		
CG(Lys103)	3.79	**4.51**
N7 (hydrogen bond)		
O(Lys101)	2.75	2.75
CG(Lys103)	3.59	**4.14**
O5 (hydrogen bond)		
NH(Lys101)	3.17	2.93
Cl1		
O(His235)	3.27	3.85
O(Leu234)	3.81	3.54
CB(Leu234)	3.75	3.99
CD2(Phe227)	3.82	3.64
CG1(Val106)	3.73	**4.87**
CG2(Val106)	4.00	3.88
C18		
CD1(Tyr181)	3.92	3.93

Table 15 Interatomic distances of the X-ray structure of efavirenz and atom of amino acid in the WT and K103N HIV-1 RT binding pockets (continued)

Atom of efavirenz and amino acid	Interatomic distance (Å)	
	WT pocket	K103N pocket
CG(Tyr188)	**4.73**	3.84
CD2(Tyr188)	**4.88**	3.74
C17		
CD1(Tyr188)	3.93	3.84
CD2(Tyr188)	3.83	3.77
CG(Tyr188)	3.57	3.55
CD1(Tyr181)	3.49	**4.92**
CG(Tyr181)	3.75	**4.65**
C19		
CD1(Tyr188)	3.88	**5.04**
CG(Tyr188)	3.94	3.55
CD1(Tyr181)	3.88	**4.92**
CZ2(Trp229)	4.26	3.89
CE2(Trp229)	4.08	4.00

4.2.3 Comparison of the docked conformation and the X-ray structure of efavirenz in the WT and K103N HIV-1 RT binding pockets

The docked conformation and the X-ray structure of efavirenz in WT binding pocket are shown in Figure 34. The binding mode of the docked efavirenz shows a very similar interaction with the X-ray crystallographic structure. The NH and carbonyl oxygen of the benzoxazin-2-one ring form two hydrogen bonds with the mainchain carbonyl oxygen and NH of Lys101 amino acid residue. There is hydrophobic interaction of the cyclopropyl group with the hydrophobic pocket of Tyr181, Tyr188 and Trp229. Moreover, the Van der waals interaction between 6-Cl and the sidechain of Val106 could be found. In the contrast, the docked structure of

efavirenz not shows Van der waals interaction between C9 with the CG carbon of the sidechain of Lys103 (Table 16).

In K103N binding pocket, the docked structure of efavirenz shows important interactions corresponding to the X-ray structure (Figure 35). The cyclopropyl group forms the hydrophobic interaction with the sidechain of Tyr188 and Trp229. The N7 and carbonyl oxygen (O5) of the benzoxazin-2-one ring form two hydrogen bonds with the mainchain carbonyl oxygen and NH of Lys101. There is the Van der waals interaction between 6-Cl and the sidechain of Val106 (Table 16).

The results indicate that the interactions of efavirenz in both binding pockets obtained from molecular docking study correspond well with the interaction observed in the X-ray structure of efavirenz. It reveals that the docking approach should be acceptable for describing interaction of the efavirenz derivatives in the HIV-1 RT binding pocket.

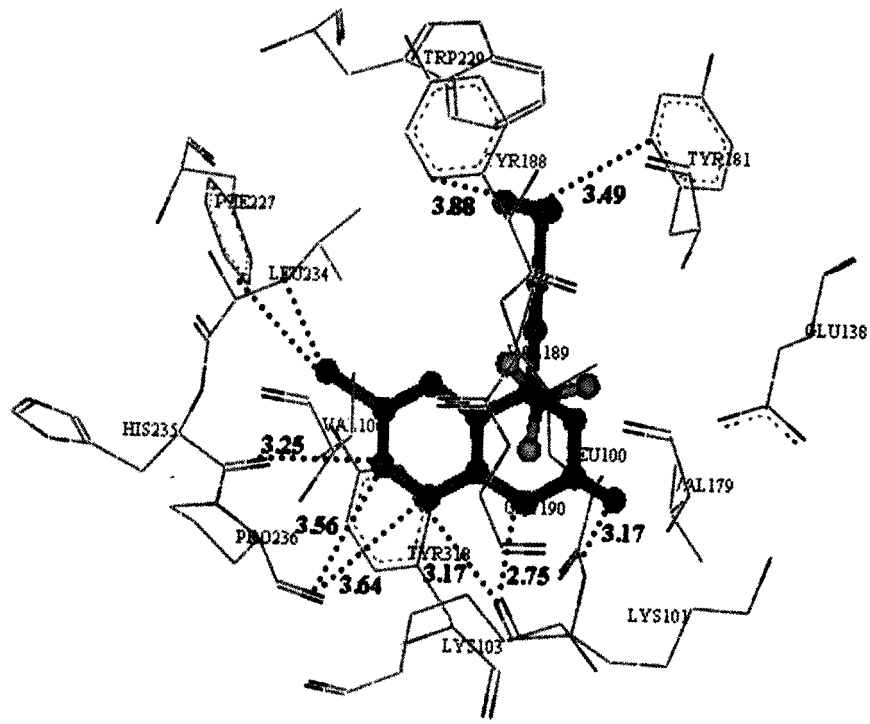

(a)

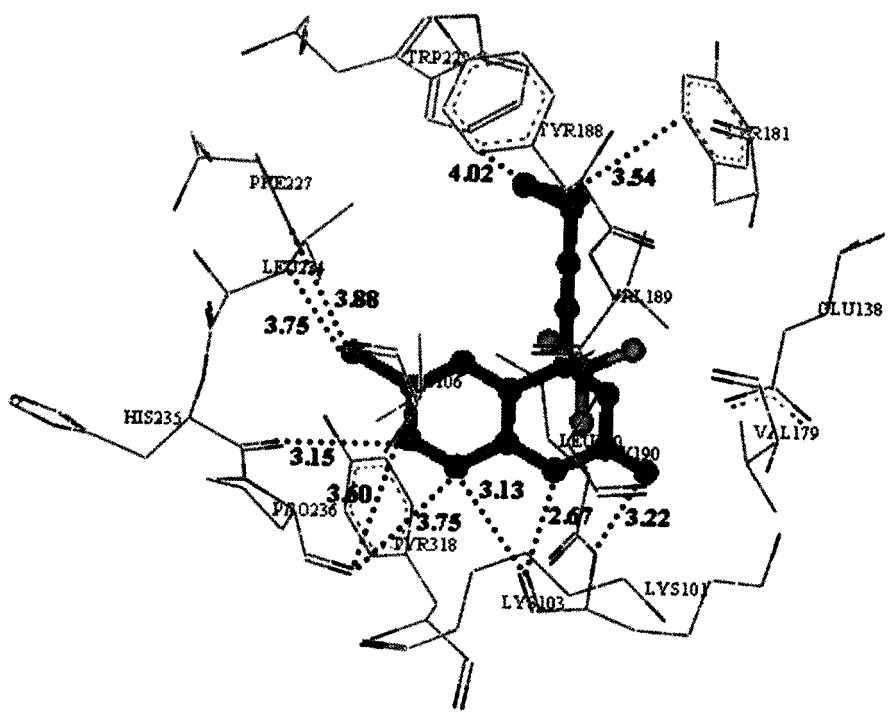

(b)

Figure 34 The X-ray structure (a) and the docked conformation (b) in the WT HIV-1 RT binding pocket

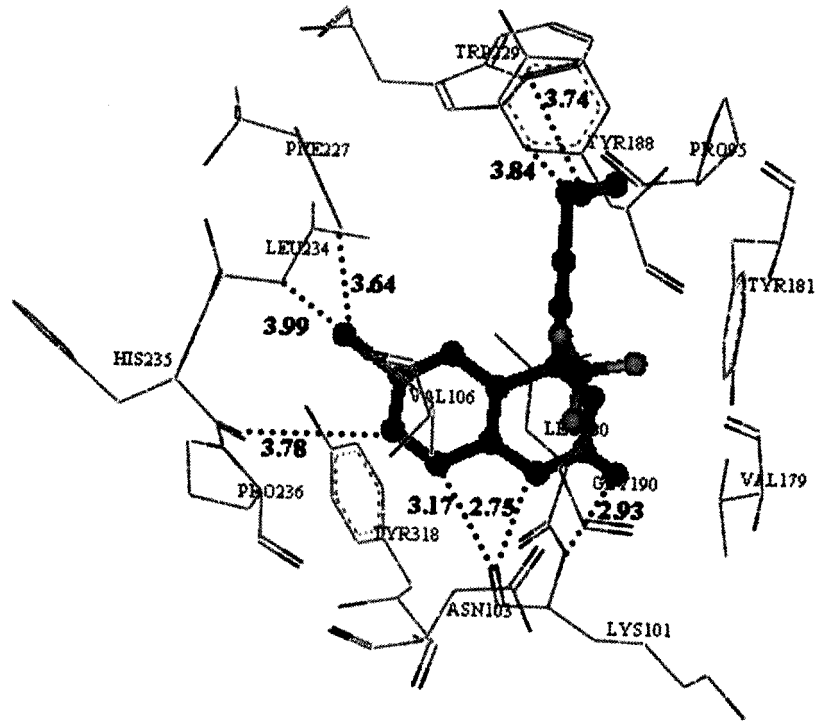

(a)

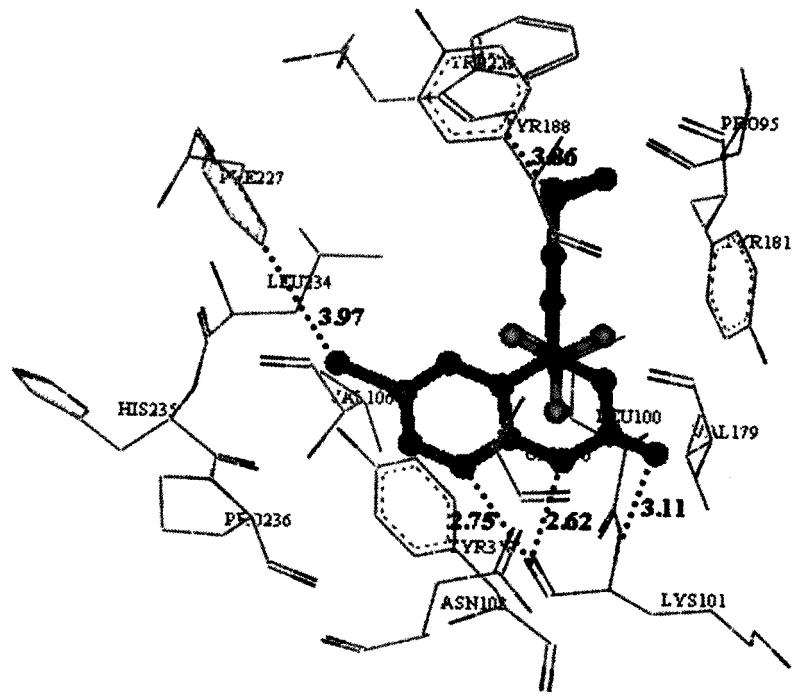

(b)

Figure 35 The X-ray structure (a) and the docked conformation (b) in K103N HIV-1 RT binding pocket

Table 16 Interatomic distances between the docked conformation and the X-ray structure of efavirenz with atom of amino acid in the WT and K103N HIV-1 RT binding pockets

Atom of efavirenz and amino acid	Interatomic distance (Å)			
	WT X-ray	WT dock	MT X-ray	MT dock
C10				
O(His235)	3.25	3.15	3.78	**4.08**
O(Pro236)	3.56	3.60	**4.05**	**4.14**
CE2(Tyr318)	3.77	3.48	3.55	3.37
OH(Tyr318)	3.82	3.51	3.55	3.58
C9				
O(Pro236)	3.64	3.75	**4.25**	**4.56**
O(Lys101)	3.17	3.13	3.17	2.75
CG(Lys103)	3.72	**4.12**	**4.47**	**4.57**
C8				
CG(Lys103)	3.79	4.00	**4.51**	**4.63**
N7 (hydrogen bond)				
O(Lys101)	2.75	2.67	2.75	2.62
CG(Lys103)	3.59	3.89	**4.14**	**4.54**
O5 (hydrogen bond)				
NH(Lys101)	3.17	3.22	2.93	3.11
Cl1				
O(His235)	3.27	3.16	3.85	3.92
O(Leu234)	3.81	3.78	3.54	4.03
CB(Leu234)	3.75	3.75	3.99	4.32
CD2(Phe227)	3.82	3.88	3.64	3.97
CG1(Val106)	3.73	3.72	4.87	4.47
CG2(Val106)	**4.00**	**4.05**	3.88	3.69
C18				
CD1(Tyr181)	3.92	3.69	3.93	3.53

Table 16 Interatomic distances between the docked conformation and the X-ray structure of efavirenz with atom of amino acid in the WT and K103N HIV-1 RT binding pockets (continued)

Atom of efavirenz and amino acid	Interatomic distance (Å)			
	WT X-ray	WT dock	MT X-ray	MT dock
CG(Tyr188)	4.73	4.91	3.84	4.80
CD2(Tyr188)	4.88	5.01	3.74	4.69
C17				
CD1(Tyr188)	3.93	4.02	3.84	4.22
CD2(Tyr188)	3.83	3.97	3.77	4.15
CG(Tyr188)	3.57	3.61	3.55	3.86
CD1(Tyr181)	3.49	3.54	**4.92**	**4.49**
CG(Tyr181)	3.75	3.66	**4.65**	**4.23**
C19				
CD1(Tyr188)	3.88	4.02	**5.04**	**5.35**
CG(Tyr188)	3.94	4.04	3.55	5.14
CD1(Tyr181)	3.88	4.35	**4.92**	**4.83**
CZ2(Trp229)	4.26	4.13	3.89	3.84
CE2(Trp229)	4.08	4.00	4.00	3.74

4.2.4 Docking analysis of efavirenz derivatives for against the WT HIV-1 RT

4.2.4.1 The highest activity efavirenz compound against the WT HIV-1 RT

Compound 25 is the highest activity compound against the WT HIV-1 RT. Figure 36a shows the docked conformation of compound 25 in the WT HIV-1 RT. The conformation reveals that the compound 25 could form the hydrophobic interaction between the cyclopropyl group and the hydrophobic pocket of Tyr181, Tyr188 and Trp229 (Table 17). The hydrogen bond between the 6-H position of the benzoxazin-2-one ring with carbonyl group of backbone His235 could be possibly formed. Moreover, there is possibility for the Van der waals interaction between 5-F of the ring and Val106.

Figure 36b shows the docked conformation of compound 25 in the K103N HIV-1 RT. The conformation reveals that the intermolecular hydrogen bond of hydrogen atom with His235 was eliminated. Moreover, the hydrophobic interaction between the cyclopropyl group with the Tyr181, Tyr188 and Trp229 was lost. This information obtained from docking conformations is in agreement with the experimental results that compound 25, showing the highest potency for the WT HIV-1 RT inhibition, has significantly diminished activity against K103N HIV-1 RT.

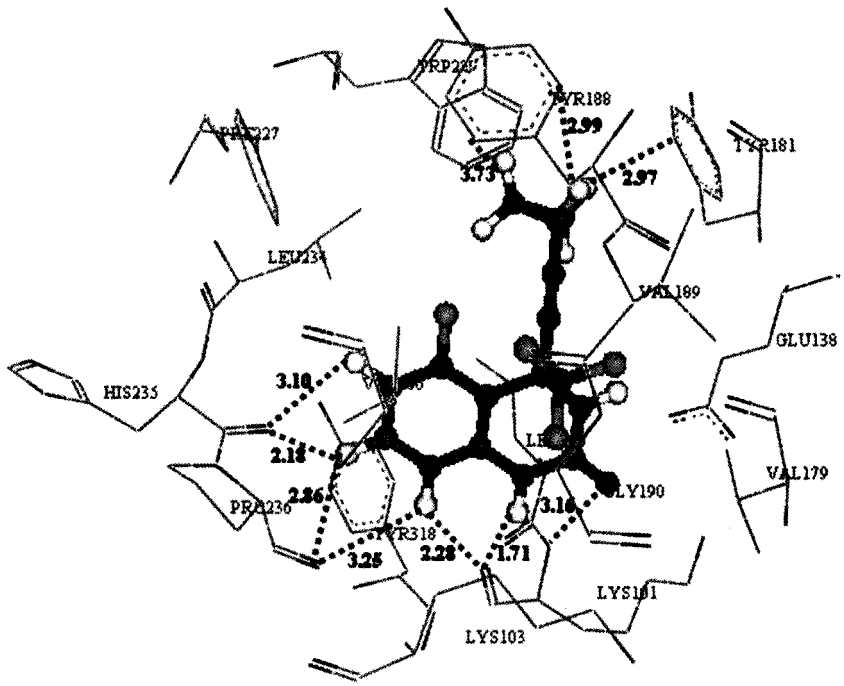

(a)

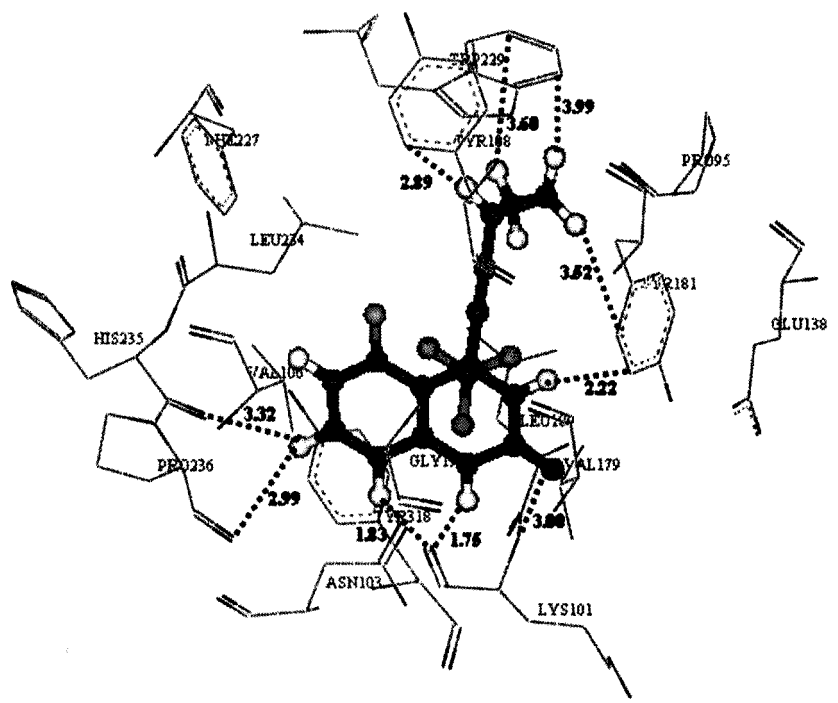

(b)

Figure 36 Compound 25 in WT (a) and K103N binding pocket (b) of HIV-1 RT obtained from molecular docking calculation

Table 17 Interatomic distances of compound 25 and atom of amino acid in the WT and K103N HIV-1 RT binding pockets

Atom of compound and amino acid	Interatomic distance (Å)	
	WT	K103N
6-H(hydrogenbond)		
O(His235)	3.1	**4.22**
H3 (hydrogen bond)		
O(Pro236)	3.25	**4.07**
O(Lys101)	2.28	1.83
H4 (hydrogen bond)		
O(His235)	2.18	3.32
O(Pro236)	2.86	2.99
H2 (hydrogen bond)		
O(Lys101)	1.71	1.75
O1 (hydrogen bond)		
NH(Lys101)	3.16	3.00
Cyclopropyl (Hydrophobic)		
C10		
CD2(Tyr188)	3.96	3.94
CD1(Tyr181)	3.6	**4.72**
CG(Tyr181)	3.74	**4.35**
C12		
CZ2(Trp229)	3.67	**4.06**
CD2(Trp229)	3.48	**4.22**
CG(Trp229)	3.84	**4.79**
NE1(Trp229)	3.54	**4.48**
CD1(Trp229)	3.86	**4.91**
CG(Tyr188)	3.85	**4.86**
CD1(Tyr188)	3.73	**5.11**
CE1(Tyr188)	3.69	**5.44**
CZ(Tyr188)	3.76	**5.53**

4.2.4.2 The lowest activity efavirenz compound against the WT HIV-1 RT

Compound 12 is the lowest activity compound against the WT HIV-1 RT. An analysis for the docked conformation of compound 12 in WT binding pocket reveals that the hydrogen bond between the polar proton (H12, H11, H10) of the benzoxazin-2-one ring and the main chain carbonyl oxygen of His235, Lys101 and Pro236 could be occured (Table 18 and Figure 37a). Moreover, the carbonyl oxygen of the benzoxazin-2-one ring could form hydrogen bond with the backbone-nitrogen atom of Lys101. The alkoxy group shows the hydrophobic interaction with the hydrophobic pocket of Tyr181 and Trp229 (Table 18). In K103N HIV-1 RT binding pocket, the docked conformation of compound 12 loses intermolecular hydrogen bond of H11 with Pro236. The alkoxy group loses the hydrophobic interaction with Trp229 and Tyr188 and some part of Tyr181 (Table 18 and Figure 37b).

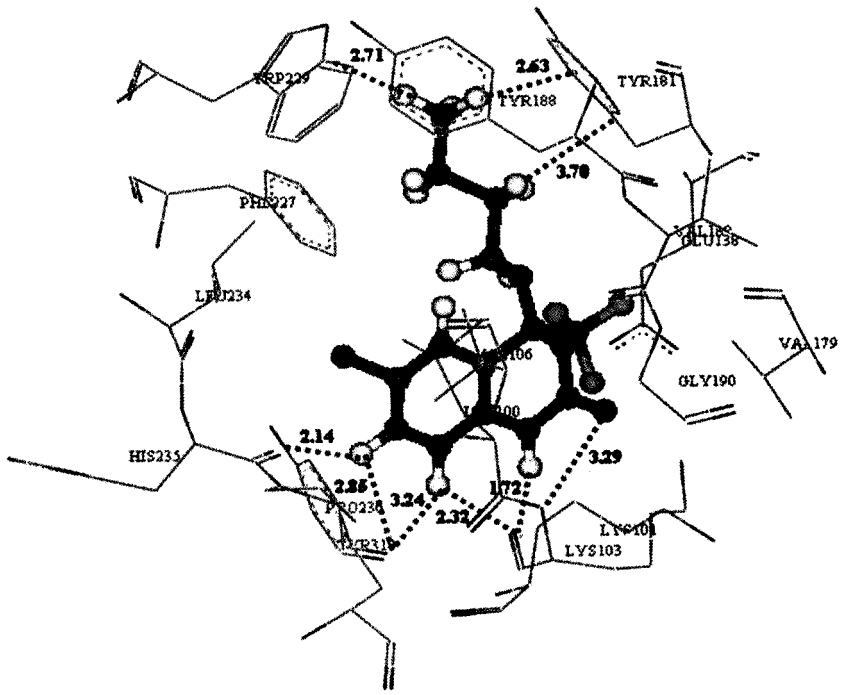

(a)

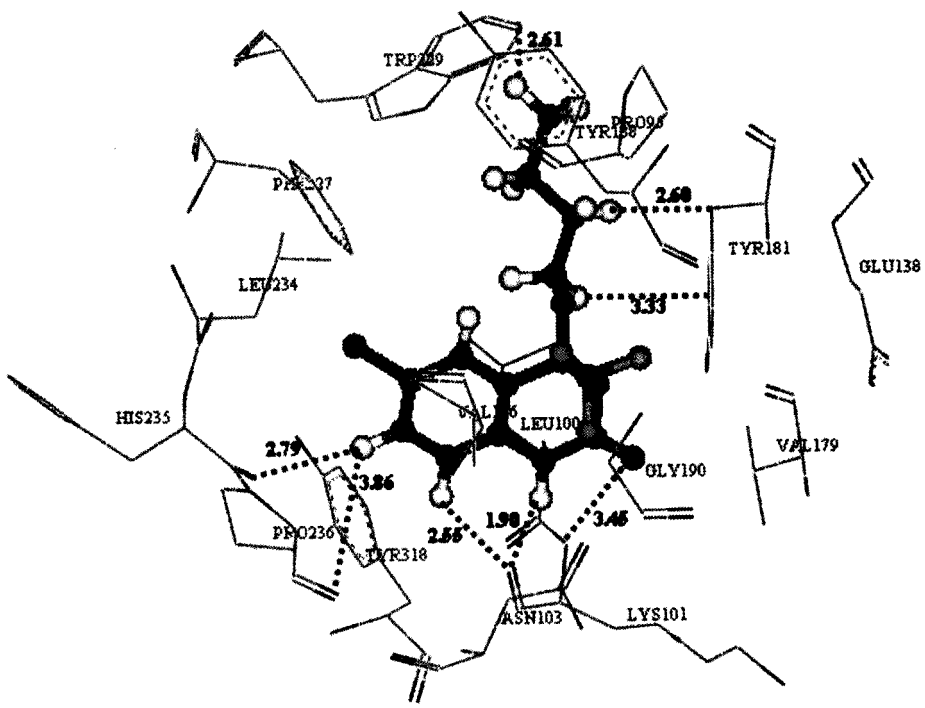

(b)

Figure 37 Compound 12 in WT (a) and K103N (b) binding pockets of HIV-1 RT obtained from molecular docking calculation

Table 18 Interatomic distances of compound 12 and atom of amino acid in the WT and K103N HIV-1 RT binding pockets

Atom of compound and amino acid	Interatomic distance (Å)	
	WT	**K103N**
H12(hydrogen bond)		
O(His235)	2.14	2.79
O(Pro236)	2.85	3.86
H11(hydrogen bond)		
O(Pro236)	3.24	**4.28**
O(Lys101)	2.32	2.55
H10(hydrogen bond)		
O(Lys101)	1.72	1.90
O1 (hydrogen bond)		
NH(Lys101)	3.29	3.45
Alkoxy group		
H3		
CG(Tyr181)	2.92	2.71
CB(Tyr181)	2.96	2.60
CD2(Tyr181)	3.58	3.44
CD1(Tyr181)	3.21	3.07
H8		
CE1(Tyr181)	2.94	**5.19**
CZ(Tyr181)	3.56	**6.04**
CZ2(Trp229)	2.99	**4.79**
CH2(Trp229)	3.56	**4.20**
H7		
CD1(Tyr181)	2.63	**5.07**
CD2(Tyr188)	2.66	**6.14**
H6		
NE1(Trp229)	2.69	**5.33**
CE2(Trp229)	2.71	**4.41**

4.2.4.3 The influence of the C6 substituent of efavirenz derivatives on the WT HIV-1 RT inhibitory activity

Compounds 34, 38 and 25 were selected as examples. The difference between their molecular structures is the substituent on the 6-substituent position (Table 1). Figure 38 depicts the superposition of the binding modes of the compounds in the WT HIV-1 RT binding pocket. At the C6-substituent position, compound 25 shows hydrogen bond between the hydrogen atom on the C6-substituent position with the main chain carbonyl oxygen of His235, whereas, other compounds form the Van der waals interaction with Leu234 on this position(Table 19). This reveals that hydrogen bond occurring on the 6-substituent position. Therefore, compound 25 shows the higher activity than other compounds. On the other hand, the bulky group (MeO) of compound 34 could conflict with Leu234, His235 and Tyr318, resulting in reducing the activity of compound. These results suggest that the hydrogen bond on the 6-substituent position enhance the inhibitory potency, while the bulky group at this position reduces the inhibitory activity potency for against the WT HIV-1 RT.

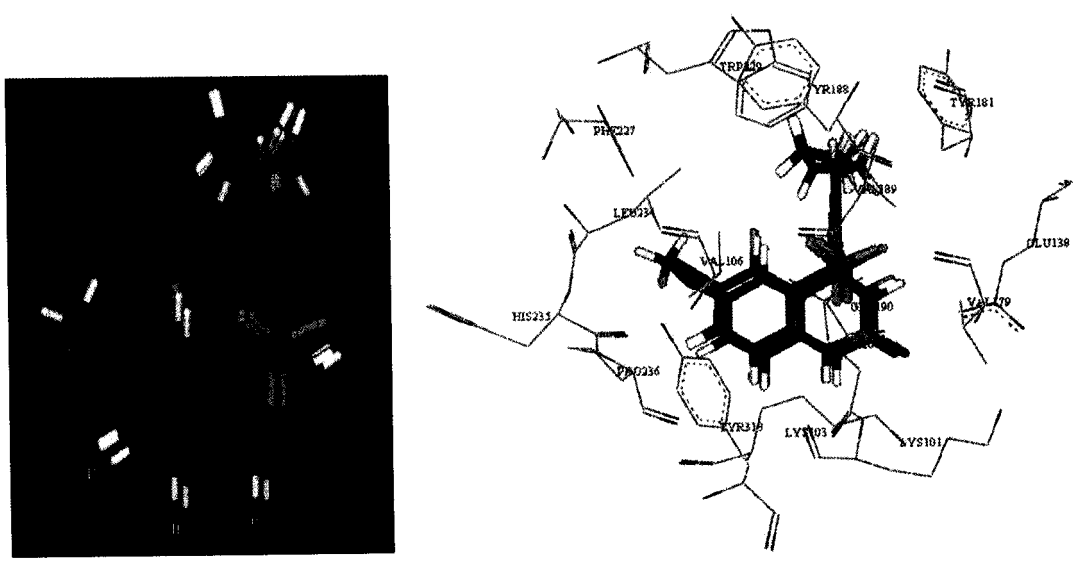

Figure 38 Superposition of compounds 34, 38 and compound 25 in the WT HIV-1 RT binding pocket

Table 19 Interatomic distance comparison of compounds 34, 38 and 25 in the WT HIV-1 RT binding pocket obtained from molecular docking calculation

Atom of compound and amino acid	Interatomic distance (Å)		
	Compound 34	**Compound 38**	**Compound 25**
H18 (hydrogen bond)			
O(His235)	2.59	2.14	2.18
O(Pro236)	2.58	2.94	2.86
H16 (hydrogen bond)			
O(Pro236)	3.46	3.28	3.25
O(Lys101)	1.91	2.35	2.28
H14 (hydrogen bond)			
O(Lys101)	1.80	1.70	1.71
O9 (hydrogen bond)			
NH(Lys101)	3.17	3.12	3.16
6-substituent			
CD1(Leu234)	3.77	5.16	5.26
CA(Leu234)	3.48	4.48	4.80
CG(Leu234)	3.75	4.98	5.11
CB(Leu234)	2.78	3.77	4.03
C(Leu234)	2.71	3.90	4.32
O(Leu234)	**2.47**	3.76	4.31
O(His235) hydrogen bond	-	-	**3.10**
OH(Tyr318)	**2.42**	4.09	**3.85**

4.2.4.4 The influence of the R substituent of efavirenz derivatives on the WT HIV-1 RT inhibitory activity

Compounds 28 and 41 were selected as examples for this study. The only difference between the molecular structures is the R position. Compound 28 shows higher inhibitory activity compound 41 (log (1/C) is 8.68 and 8.21 for compound 28 and 41, respectively). Figure 39 depicts the superposition of the binding mode of compound 28 and compound 41 in the WT HIV-1 RT binding pocket. The cyclopropyl group of compound 28 and the phenyl ring of compound 41 could form the hydrophobic interaction with the aromatic side chain of Tyr188, Tyr181 and Trp229 (Table 20). However, the bulky phenyl substituent could conflict with the aromatic side chain of Trp229, while for the smaller substituent with cyclopropyl group of compound 28, the steric conflict could not occur. The results suggest that the bulky substituent of the R position leads to less inhibitory activity against the WT HIV-1 RT.

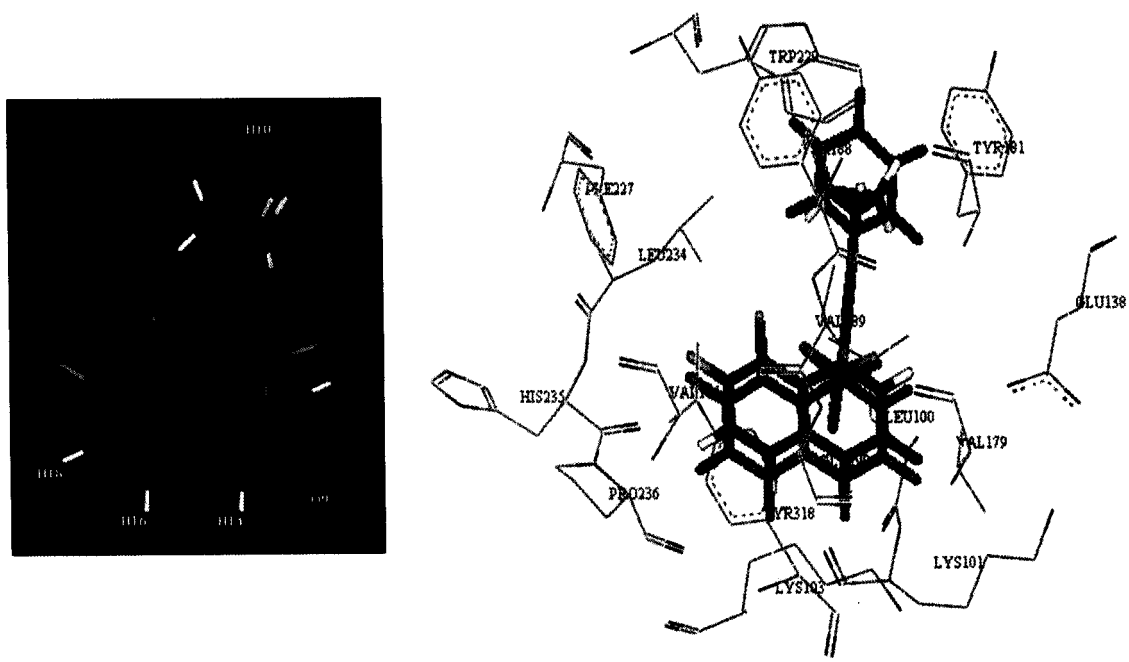

Figure 39 Superposition of compound 28 (color by atom type) and compound 41 (pink) in the WT HIV-1 RT binding pocket

Table 20 Interatomic distance comparison of compounds 28 and 41 in the WT HIV-1 RT binding pocket obtained from molecular docking calculation

Atom of compound and amino acid	Interatomic distance (Å)	
	Compound 28	**Compound 41**
H18 (hydrogen bond)		
O(His235)	2.17	2.58
O(Pro236)	2.88	2.20
H16 (hydrogen bond)		
O(Pro236)	3.25	2.87
O(Lys101)	2.28	2.06
H14 (hydrogen bond)		
O(Lys101)	1.72	1.58
O9 (hydrogen bond)		
NH(Lys101)	3.17	3.26
H10 (steric)		
CZ2(Trp229)	No steric	2.17
CE2(Trp229)	No steric	2.25

4.2.5 Docking analysis of efavirenz derivatives for against K103N HIV-1 RT

4.2.5.1 The highest activity compound against K103N HIV-1 RT

The docked conformation of compound 50, the highest activity compound against K103N HIV-1 RT, in K103N binding pocket is shown in Figure 40a. Numerous favorable interactions found for compound 50 are described as follows. The Van der waals interaction could be formed between methoxy group substituted at C5 position of the benzoxazin-2-one ring and the sidechain of Leu234, Phe227 and Tyr188. There are additional Van der waals interaction between 6-Cl and the sidechain of Leu234, Val106. The hydrophobic interaction between the cyclopropyl group with the aromatic sidechain of Tyr188 and Trp229 could be formed. It is interesting to note that the hydrogen atom (H9) attached to the nitrogen atom on the Z substituent could increase hydrogen-pi (H-π) interaction with the aromatic

sidechain of Tyr181(Table 21).

It is interesting to note that, for compound 50, the docked conformation in the WT binding pocket reveals the possibility of the hydrogen bond formation (Figure 40b). The Van der waals interactions could be also found. Although the H-π interaction was eliminated in the pocket, the cyclopropyl group could match more to the hydrophobic pocket of Tyr188, Trp229 and Tyr181 in the WT binding pocket as show in Figure 40b. This may be the reason that compound 50 shows excellent inhibition against both WT and K103N HIV-1 RT.

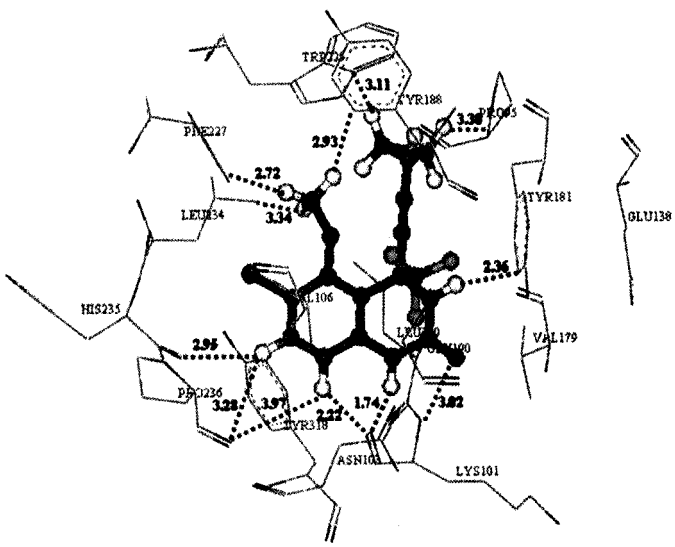

(a)

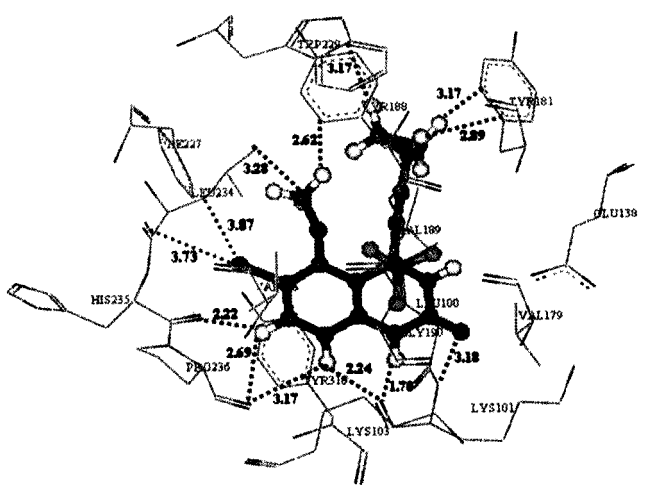

(b)

Figure 40 Compound 50 in the K103N (a) and WT (b) HIV-1 RT binding pockets

Table 21 Interatomic distance comparison of compound 50 in the K103N and WT HIV-1 RT binding pockets

Atom of compound 50 and amino acid	Interatomic distance (Å)	
	K103N pocket	WT pocket
H3 (hydrogen bond)		
O(His235)	2.95	2.22
O(Pro236)	3.28	2.69
H2 (hydrogen bond)		
O(Pro236)	3.97	3.17
O(Lys101)	2.22	2.24
H1 (hydrogen bond)		
O(Lys101)	1.74	1.70
O1 (hydrogen bond)		
NH(Lys101)	3.02	3.18
H9 (H-π)		
CD2(Tyr181)	2.47	**5.96**
CE2(Tyr181)	2.36	**7.14**
CZ(Tyr181)	3.34	**7.87**
CG(Tyr181)	3.50	**5.58**
6 position (Van der waals)		
CD1(Val106)	3.41	3.57
O(His235)	**4.01**	2.89
CB(Leu234)	**4.50**	3.88
O(Leu234)	3.92	3.73
5 position (Van der waals)		
CD1(Leu234)	3.56	3.28
CD2(Leu234)	3.34	**4.39**
CG(Leu234)	3.96	3.95
CB(Phe227)	3.9	**4.21**

Table 21 Interatomic distance comparison of compound 50 in the K103N and WT HIV-1 RT binding pockets (continued)

Atom of compound 50 and amino acid	Interatomic distance (Å)	
	K103N pocket	**WT pocket**
CG(Phe227)	3.63	**4.07**
CD2(Phe227)	2.72	3.32
CE2(Phe227)	3.4	**4.06**
CD1(Tyr188)	2.93	2.62
CE1(Tyr188)	3.54	3.32
CG(Tyr188)	3.53	3.3
CB(Tyr188)	3.84	3.65
Cyclopropyl (hydrophobic)		
C10		
CG(Tyr188)	3.78	3.78
CD2(Tyr188)	3.96	**4.12**
CG(Tyr181)	3.98	3.60
CD1(Tyr181)	**4.27**	3.53
C11		
CG(Tyr181)	3.85	3.83
CD1(Tyr181)	3.62	3.78
C12		
CZ2(Trp229)	3.86	**4.01**
CD2(Trp229)	3.84	**4.13**
CE2(Trp229)	3.75	3.95

4.2.5.2 The lowest activity compound against K103N HIV-1 RT

Compound 22 is the lowest activity compound against K103N HIV-1 RT. Figure 41a shows the binding mode of compound 22 in the K103N HIV-1 RT binding pocket. An analysis for the docked conformation of compound 22 in K103N HIV-1 RT binding pocket reveals that the hydrogen bond between the polar proton (H6, H5, H4) of the benzoxazin-2-one ring and the main chain carbonyl oxygen of His235, Lys101 and Pro236 could be formed. Also, the carbonyl oxygen of the benzoxazin-2-one ring could interact with backbone-nitrogen atom of Lys101 to form hydrogen bond. The alkoxy group shows the hydrophobic interaction with the hydrophobic pocket of Tyr181 and Tyr188. However, this interaction with Trp229 was lost (Table 22 and Figure 41a). Moreover, the Van der waals interaction of F atom on 5, 6-substituent position with the sidechain of Val106 could be observed. On the other hand, the docked conformation of compound 22 in the WT HIV-1 RT binding pocket shows the shorter hydrogen bond distance than in K103N RT. These results may be the reason why compound 22 shows higher activity against WT RT than those of K103N RT (log (1/C) is 8.19 and 5.79 for WT and K103N, respectively).

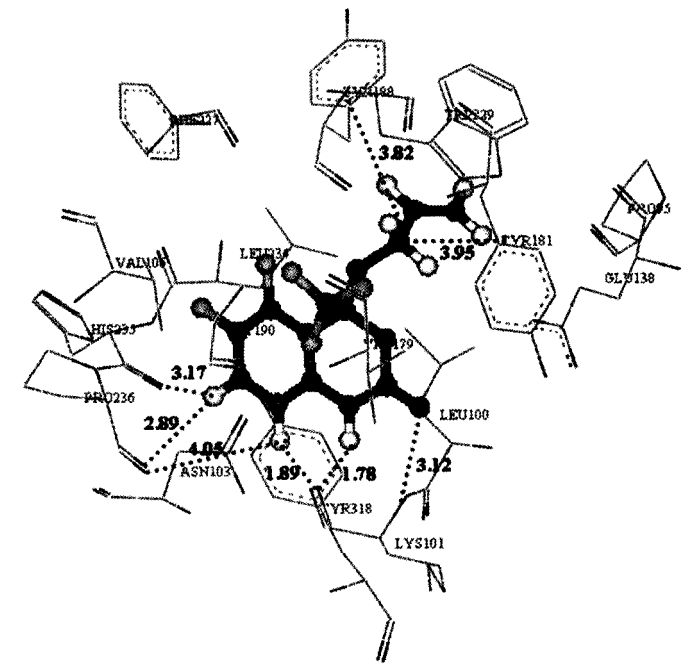

(a)

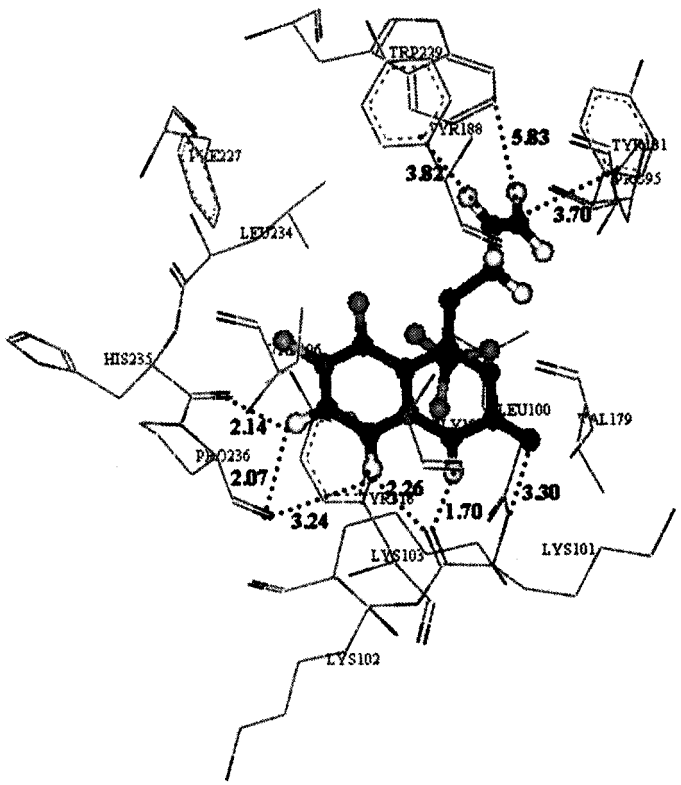

(b)

Figure 41 Compound 22 in K103N (a) and WT (b) HIV-1 RT binding pockets

Table 22 Interatomic distance comparison of compound 22 in the K103N and WT HIV-1 RT binding pockets

Atom of compound and amino acid	Interatomic distance (Å)		Atom of compound and amino acid	Interatomic distance (Å)	
	K103N	WT		K103N	WT
H6 (hydrogen bond)			**Alkoxy group**		
O(His235)	3.17	2.14	**C1**		
O(Pro236)	2.89	2.07	CB(Tyr188)	3.58	3.63
H5 (hydrogen bond)			CB(Tyr181)	3.46	3.46
O(Pro236)	**4.05**	3.24	CG(Tyr181)	3.38	**4.17**
O(Lys101)	1.89	2.26	CD2(Tyr181)	3.37	**5.00**
H4 (hydrogen bond)			**C2**		
O(Lys101)	1.78	1.70	CG(Tyr188)	3.82	3.97
O1 (hydrogen bond)			CD1(Tyr181)	**4.34**	3.83
NH(Lys101)	3.12	3.30	CG(Tyr181)	3.95	3.70
F5			**C3**		
CD1(Val106)	3.64	3.39	CD1(Tyr181)	3.81	3.78
O(His235)	3.99	2.86	CG(Tyr181)	3.87	3.55
F1			CZ2(Trp229)	**4.42**	**5.05**
CD1(Val106)	3.61	3.19	CD2(Trp229)	**4.95**	**5.83**
			CE2(Trp229)	**4.61**	**5.46**

4.2.5.3 The influence of the Z substituent of efavirenz derivatives on the K103N HIV-1 RT inhibitory activity

Compound 38 and 01 were selected as examples. The only difference of their molecular structures is the Z position (Z = NH for compound 38 and Z = O for compound 01). Figure 42 depicts the most similar binding mode of compound 38 and compound 01 in K103N HIV-1 RT binding pocket. Compound 38 shows higher inhibitory activity than compound 01 (log (1/C) is 7.66 and 7.19 for compound 38 and 01, respectively). With regard to the molecular docking conformation, compounds 38 and 01 present the same hydrogen bond interaction as shown in Table 23. The only different interaction is the hydrogen-π interaction of the hydrogen atom on the Z substituent of compound 38 with the aromatic sidechain of Tyr181 amino acid residue, whereas, for compound 01, such an interaction was not found. This is the main reason for the weaker interaction of compound 01. Therefore, the hydrogen-π interaction on the Z position plays an essential rule for enhance the inhibitory activity of K103N HIV-1 RT.

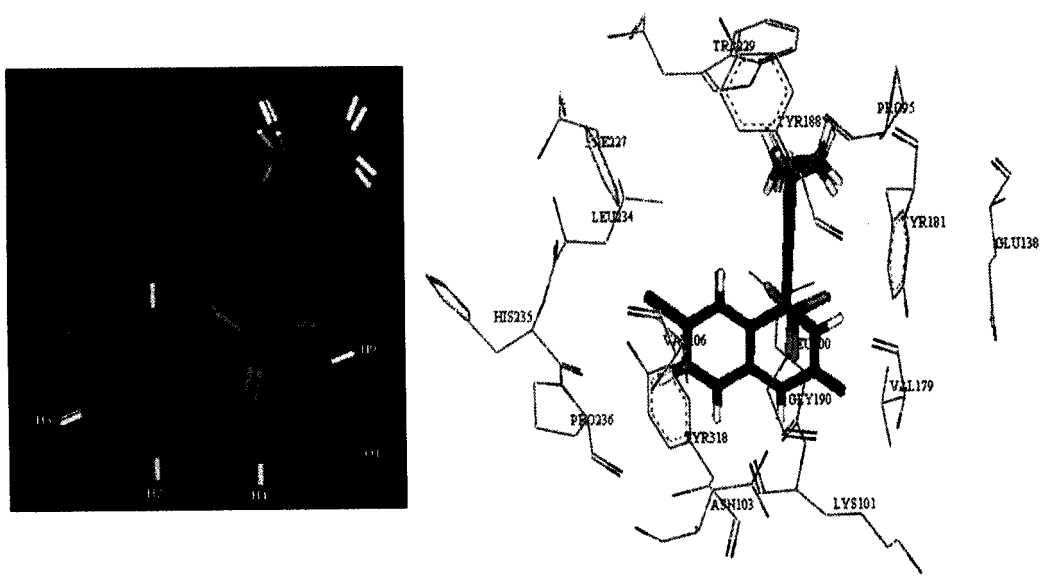

Figure 42 Superposition of compound 38 and compound 01 in K103N HIV-1 RT binding pocket

Table 23 Interatomic distance comparison of compounds 38 and 01 in the K103N HIV-1 RT binding pocket obtained from molecular docking calculation

Atom of compound and amino acid	Interatomic distance (Å)	
	Compound 38	**Compound 01**
H3 (hydrogen bond)		
O(His235)	3.08	3.11
O(Pro236)	3.36	3.25
H2 (hydrogen bond)		
O(Lys101)	1.95	1.89
H4 (hydrogen bond)		
O(Lys101)	1.73	1.75
O1 (hydrogen bond)		
NH(Lys101)	3.04	3.11
H9 (H-π interaction)		
CD2(Tyr181)	2.38	
CE2(Tyr181)	2.19	**No H**
CZ(Tyr181)	3.25	
CG(Tyr181)	3.51	

4.2.5.4 The influence of the R substituent of efavirenz derivatives on the K103N HIV-1 RT inhibitory activity

Compounds 50 and 51 were selected as examples. The only difference between the molecular structures is the R substituent position. The R substituent is cyclopropyl and phenyl ring for compounds 50 and 51, respectively. Figure 43 shows the superposition of the binding mode of compounds 50 and 51 in K103N HIV-1 RT binding pocket, indicating the different binding mode of compounds in K103N HIV-1 RT binding pocket. The bulky phenyl substituent of compound 51 could conflict with the aromatic sidechain of Trp229, while the steric conflict was not found for compound 50 (Table 24). This effect leads to hydrogen-π interaction loss of the hydrogen atom on the Z substituent of compound 51 with the aromatic sidechain of

Tyr181 amino acid residue. Therefore, compound 51 plays the functional inhibitor lower than compound 50 with log (1/C) of 6.95 and 8.12 for compounds 51 and 50, respectively. The results indicate that the bulky R substituent on the bezoxazineone reduces the inhibitory activity against K103N HIV-1 RT.

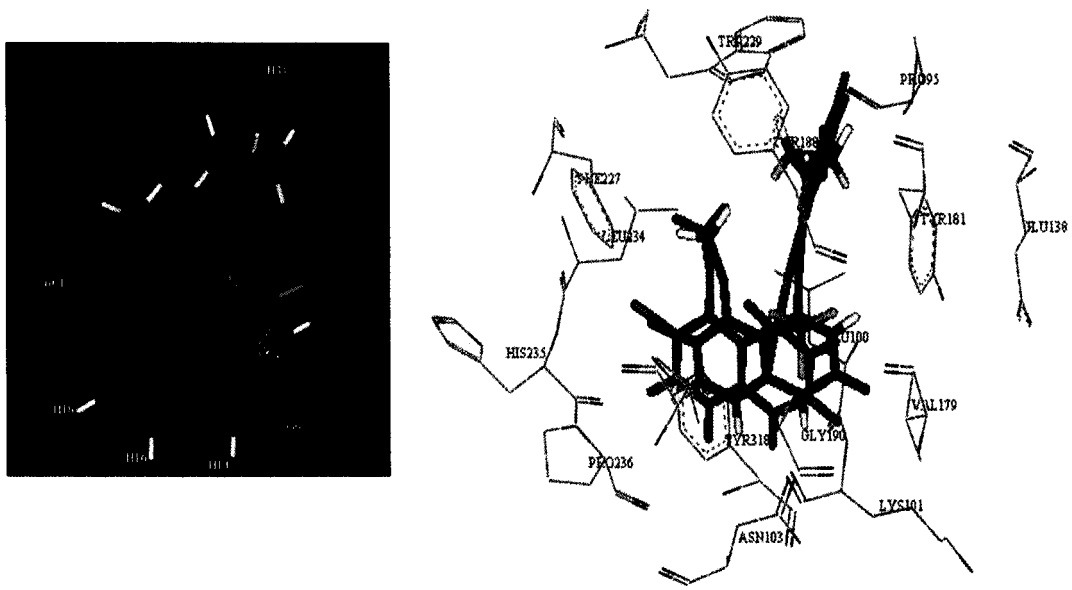

Figure 43 Superposition of compound 50 (color by atom type) and compound 51 (pink) in K103N HIV-1 RT binding pocket

Table 24 Interatomic distance comparison of compounds 50 and 51 in the K103N HIV-1 RT binding pocket obtained from molecular docking calculation

Atom of compound and amino acid	Interatomic distance (Å)	
	compound 50	**compound 51**
H18 (hydrogen bond)		
O(His235)	2.87	2.11
O(Pro236)	3.32	3.37
H16 (hydrogen bond)		
O(Pro236)	3.98	2.96
O(Lys101)	2.22	3.14
H14 (hydrogen bond)		
O(Lys101)	1.74	1.79
O9 (hydrogen bond)		
NH(Lys101)	3.11	3.47
R group (H31)		
CH2(Trp229)	-	2.26
CZ2(Trp229)	-	2.38
Z group (H-π interaction)		
CD2(Tyr181)	2.49	3.44
CE2(Tyr181)	2.44	3.45
CZ(Tyr181)	3.45	**4.50**
CG(Tyr181)	3.53	**4.50**
6Cl (van der waal)		
CD1(Leu234)	4.99	3.52
CD2(Leu234)	4.30	4.47
CG(Leu234)	4.78	4.04
CB(Leu234)	4.28	3.54
CA(Leu234)	4.88	4.04

4.2.5.5 The influence of the C5 substituent position of efavirenz derivatives on the K103N HIV-1 RT inhibitory activity

Taking compounds 50 and 53 as examples for this study, the only difference of the molecular structures is the C5 position with MeO and OH groups for compounds 50 and 53, respectively. The superposition of compounds 50 and 53 in K103N HIV-1 RT binding pocket is shown in Figure 44, showing the similar position and binding mode. However, compound 50 has more the Van der waals interaction of the methoxy group on the C5 position with Leu234, Phe227 and Tyr188 compared with the hydroxyl group of compound 53 (Table 25). Therefore, compound 50 shows a higher inhibitory function more than compound 53 (log (1/C) is 8.12 and 7.55 for compounds 50 and 53, respectively. This result suggests that the Van der waals interaction on the 5 position increase the inhibitory activity for against K103N HIV-1 RT.

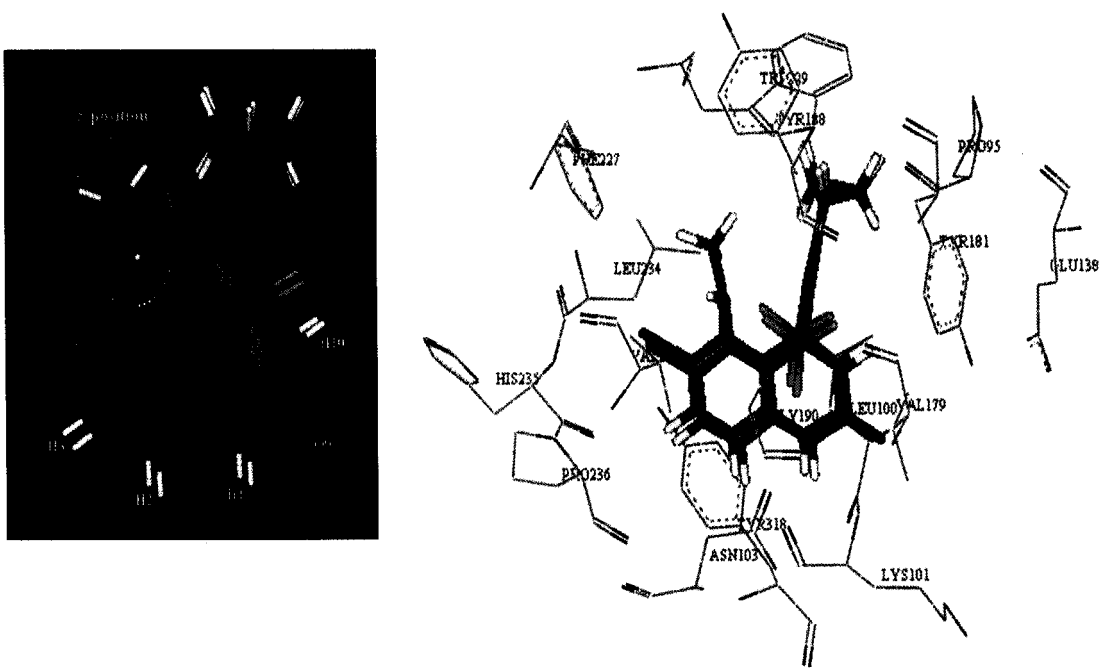

Figure 44 Superposition of compound 50 and compound 53 in K103N HIV-1 RT binding pocket

Table 25 Compare interaction of compound 50 and compound 53 in K103N HIV-1 RT binding pocket obtained from molecular docking calculation

Atom of compound and amino acid	Interatomic distance (Å)	
	compound 50	**compound 53**
H3 (hydrogen bond)		
O(His235)	2.87	3.08
O(Pro236)	3.32	3.18
H2 (hydrogen bond)		
O(Pro236)	3.98	4.18
O(Lys101)	2.22	1.83
H1 (hydrogen bond)		
O(Lys101)	1.74	1.74
O9 (hydrogen bond)		
NH(Lys101)	3.11	3.09
H10 (H-π interaction)		
CD2(Tyr181)	2.49	2.42
CE2(Tyr181)	2.44	2.29
CZ(Tyr181)	3.45	3.33
CG(Tyr181)	3.53	3.51
5 position (MeO, OH)		
CD1(Leu234)	3.52	**5.86**
CD2(Leu234)	3.24	**5.38**
CG(Leu234)	3.89	**5.92**
CD2(Phe227)	2.73	**4.32**
CE2(Phe227)	3.47	**4.27**
CD1(Tyr188)	2.97	**4.45**
CE1(Tyr188)	3.56	**5.42**
CG(Tyr188)	3.58	**4.99**
CG1(Val106)	**4.75**	3.96
CB(Val106)	**4.51**	3.56

4.2.5.6 The influence of the C6 substituent position of efavirenz derivatives on the K103N HIV-1 RT inhibitory activity

Compound 30, 34 and 38 were selected as examples for this study. The C6 substituent of these compounds is F, MeO and Cl for compounds 30, 34 and 38, respectively. Figure 45 depicts the superposition of these compounds in K103N HIV-1 RT binding pocket, which shows that the similar position and the binding mode. Nevertheless, compound 38 shows a rather good functional inhibitor more than the others, log (1/C) is 7.32, 7.40 and 7.66 for compound 30, 34 and 38, respectively because of the Cl atom on the C6 substituent position of compound 38 show more the Van der waals interaction than the methoxy group and F atom (Table 26). Moreover, the methoxy group of compound 34 could be conflict with the sidechain of His235 and Trp229. This suggests that the Van der waals interaction on the C6 substituent position enhance the inhibitory activity of against K103N HIV-1 RT. However, the too large or small substituent on this position could be decrease the inhibitory activity.

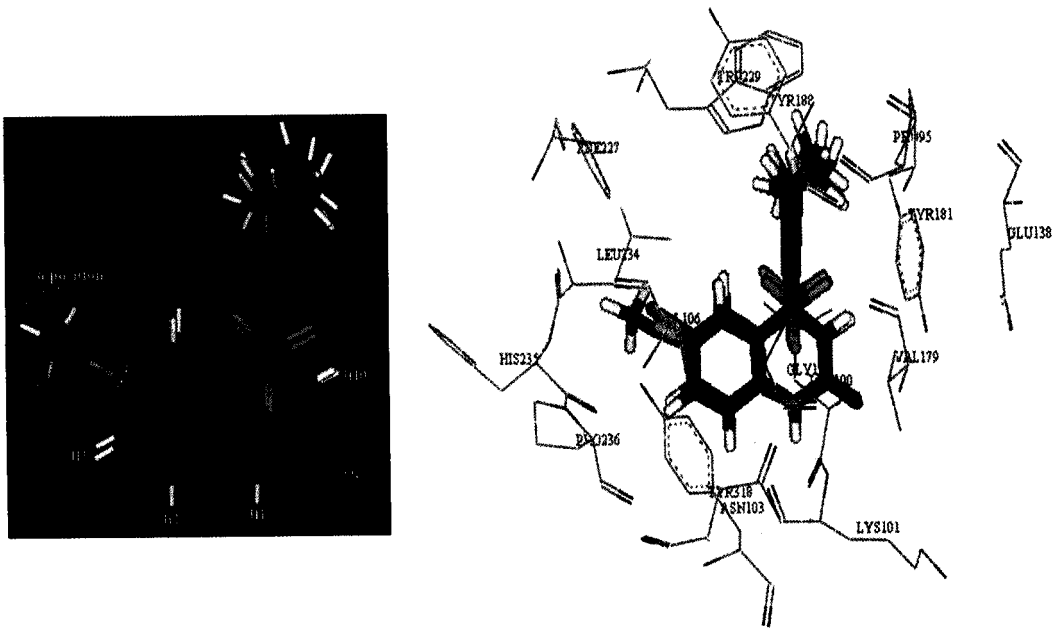

Figure 45 Superposition of compounds 30, 34 and 38 in the K103N HIV-1 RT binding pocket

Table 26 Compare interaction of compounds 30, 34 and 38 in the K103N HIV-1 RT binding pocket obtained from molecular docking calculation

Atom of compound and amino acid	Interatomic distance (Å)		
	compound 30	**compound 34**	**compound 38**
H3 (hydrogen bond)			
O(His235)	3.10	3.04	2.96
O(Pro236)	3.02	3.00	3.36
H2 (hydrogen bond)			
O(Pro236)	4.08	4.07	4.18
O(Lys101)	1.86	1.86	1.95
H1 (hydrogen bond)			
O(Lys101)	1.74	1.74	1.73
O2 (hydrogen bond)			
NH(Lys101)	3.10	3.12	3.04
H10 (H-π interaction)			
CD2(Tyr181)	2.43	2.45	2.38
CE2(Tyr181)	2.34	2.37	2.19
CZ(Tyr181)	3.42	3.43	3.25
CG(Tyr181)	3.54	3.55	3.51
C6 substituent position			
CD2(Phe227)	**4.37**	3.66	3.91
CE2(Phe227)	**4.54**	**4.25**	**4.30**
CG2(Val106)	3.26	**4.46**	3.70
O(His235)	**4.65**	**2.38**	**4.02**
O4(Pro236)	**4.09**	**2.27**	**4.02**

4.2.6 The important interaction of efavirenz derivatives for against the WT and K103N HIV-1 RT

The molecular docking approach was successfully to determine the binding mode and inhibitor-enzyme interactions of efavirenz and its derivative in HIV-1 RT binding pocket. To enhance the inhibitory activity for against the WT HIV-1 RT, the hydrogen bond between the polar atom (H and oxygen carbonyl) on benzoxazin-2-one ring with the main chain of His235, Lys101 and Pro236 could be formed. Particularly, the hydrogen bond at the C6-substituent position seems to be important to against the WT HIV-1 RT. The another important interaction of the WT HIV-1 RT inhibitor is the hydrophobic interaction between the R substituent with the side chain of Tyr181, Tyr188 and Trp229 amino acid residue.

For K103N HIV-1 RT inhibitor, the significant interactions of inhibitor are the hydrogen-π interaction of the NH group on Z position with the aromatic side chain of Tyr181, the Van der waals interaction on the C5, C6-substituent position with surrounding amino acid residue (Phe227, Val106, Leu234 and Tyr188) and the hydrophobic interaction of the R group with the aromatic side chain of Trp229 and Tyr188.

4.3 3D-QSAR analysis

4.3.1 3D-QSAR analysis of WT HIV-1 RT inhibitor

4.3.1.1 CoMFA and CoMSIA models

The statistical parameters of CoMFA and CoMSIA models used in this study are shown in Table 27. These analyses were based on the docking alignment. The CoMFA model obtained from including both steric and electrostatic fields, whereas, the CoMSIA obtained from including steric, electrostatic, hydrophobic, hydrogen donor and hydrogen acceptor fields. The non-cross-validation (r^2) and the cross-validation (r^2_{cv}) of the CoMFA model with an optimum number of components (noc) of three are 0.936 and 0.662, respectively. Regarding the CoMSIA model, the r^2 and r^2_{cv} for the best CoMSIA model with an optimum number of components of six are 0.894 and 0.708, respectively. These statistical parameters suggest that both CoMFA and CoMSIA models for WT HIV-1 RT inhibition are good predictive capabilities. Based on the r^2_{cv} value, the CoMSIA seems to have better predictability than CoMFA. The steric and electrostatic contributions from the best CoMFA model are 63.8 and 36.2%, respectively. The steric, electrostatic, hydrophobic, hydrogen donor and hydrogen acceptor contributions from the best CoMSIA model are 12.2, 19.5, 24.1, 16.8 and 27.3%, respectively.

For the training set, the experimental and predicted activities derived from the best CoMFA and CoMSIA models are shown in Table 28 and Figure 46. This shows a good correlation between the experimental and predicted activities. In the order to evaluate the predictive ability of the resulting two models, the test set was used to predict the inhibitory activities for WT HIV-1 RT inhibition. The comparison of the predicted and experimental activities of the test set is presented in Table 29. The best CoMFA and CoMSIA models predicted the activities of all test compounds within ±1 log unit of the inhibitory activity. This indicates that both models can accurately predict the WT inhibitory affinities.

Table 27 The statistics results of the CoMFA and CoMSIA models for WT HIV-1 RT inhibitors

Statistical results	CoMFA	CoMSIA
r^2_{cv}	0.662	0.708
noc	3	6
s-press	0.145	0.142
r^2	0.936	0.894
S	0.066	0.085
F	83.441	50.844
Contribution		
Steric	63.8	12.2
Electrostatic	36.2	19.5
Hydrophobic	-	24.1
Hydrogen donor	-	16.8
Hydrogen acceptor	-	27.3

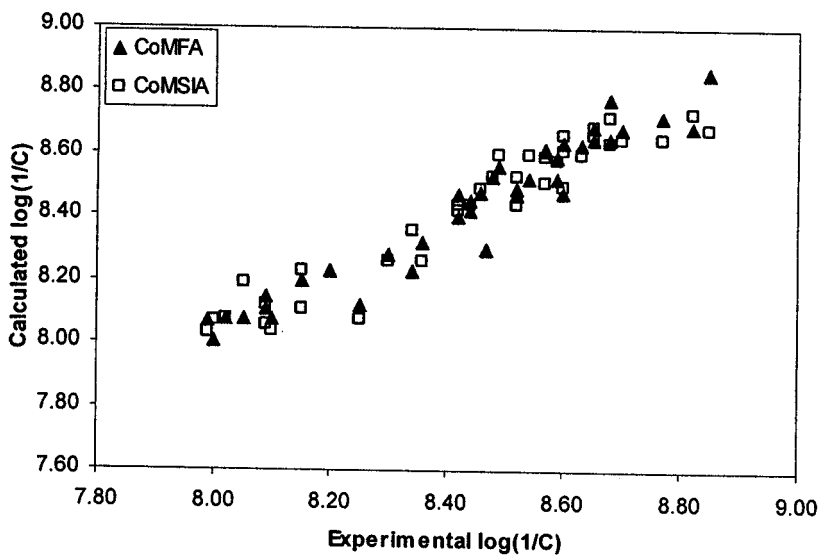

Figure 46 Plots between the predicted and experimental inhibitory affinities of the training set from CoMFA and CoMSIA models of WT HIV1-RT inhibition

Table 28 Predicted log (1/C) WT inhibitory affinities of the training set from CoMFA and CoMSIA models

Compound No.	Exp.	CoMFA		CoMSIA	
		log(1/C)	Residual	log(1/C)	Residual
01	8.77	8.72	0.05	8.65	0.12
02	8.27	8.52	-0.25	8.23	0.04
04	8.42	8.47	-0.05	8.44	-0.02
05	8.42	8.40	0.02	8.42	0.00
06	8.65	8.65	0.00	8.69	-0.04
07	8.60	8.48	0.12	8.50	0.10
08	8.59	8.59	0.00	8.58	0.01
09	8.49	8.56	-0.07	8.60	-0.11
10	8.65	8.69	-0.04	8.66	-0.01
11	8.63	8.63	0.00	8.60	0.03
12	7.99	8.07	-0.08	8.03	-0.04
13	8.00	8.01	-0.01	8.07	-0.07
14	8.36	8.32	0.04	8.26	0.10
15	8.25	8.12	0.13	8.08	0.17
16	8.57	7.87	0.70	8.13	0.44
17	8.50	8.18	0.32	8.02	0.48
18	8.02	8.08	-0.06	8.08	-0.06
20	8.05	8.08	-0.03	8.19	-0.14
21	8.81	8.07	0.74	8.83	-0.02
23	8.20	8.23	-0.03	8.69	-0.49
24	8.82	8.69	0.13	8.73	0.09
25	8.85	8.86	-0.01	8.68	0.17
26	8.52	8.49	0.03	8.53	-0.01
27	8.60	8.68	-0.08	8.61	-0.01
28	8.68	8.78	-0.10	8.72	-0.04
29	8.68	8.65	0.03	8.64	0.04

Table 28 Predicted log (1/C) WT inhibitory affinities of the training set from CoMFA and CoMSIA models (continued)

Compound No.	Exp.	CoMFA		CoMSIA	
		log(1/C)	Residual	log(1/C)	Residual
30	8.70	8.68	0.02	8.65	0.05
31	8.70	8.51	0.19	8.22	0.48
32	8.60	8.64	-0.04	8.66	-0.06
33	8.57	8.62	-0.05	8.59	-0.02
34	8.54	8.52	0.02	8.60	-0.06
35	8.30	8.28	0.02	8.26	0.04
36	8.32	8.66	-0.34	8.58	-0.26
38	8.57	8.61	-0.04	8.51	0.06
40	8.49	8.03	0.46	8.17	0.32
41	8.21	8.42	-0.21	8.25	-0.04
43	8.47	8.30	0.17	8.11	0.36
44	8.48	8.53	-0.05	8.53	-0.05
45	8.15	8.20	-0.05	8.11	0.04
46	8.59	8.52	0.07	8.58	0.01
48	8.52	8.47	0.05	8.44	0.08
49	8.09	8.15	-0.06	8.12	-0.03
50	8.46	8.48	-0.02	8.49	-0.03
51	8.10	8.08	0.02	8.04	0.06
52	8.15	8.21	-0.06	8.23	-0.08
53	8.44	8.42	0.02	8.44	0.00
54	8.44	8.45	-0.01	8.44	0.00
55	8.09	8.11	-0.02	8.06	0.03
56	8.34	8.23	0.11	8.36	-0.02

Table 29 Predicted log (1/C) WT inhibitory affinities of the test set from CoMFA and CoMSIA models

Compound No.	Expt. log(1/C)	CoMFA		CoMSIA	
		Calc. log (1/C)	Residual	Calc. log (1/C)	Residual
03	8.40	8.50	-0.1	8.46	-0.06
19	8.53	7.99	0.54	8.27	0.26
22	8.19	8.73	-0.54	8.58	-0.39
37	8.64	8.43	0.21	8.20	0.44
39	8.42	8.34	0.08	8.54	-0.12
42	8.18	8.27	-0.09	8.23	-0.05
47	8.10	8.63	-0.53	8.47	-0.37

4.3.1.2 CoMFA contour analysis of WT HIV-1 RT inhibitors

The CoMFA contours of steric and electrostatic fields for WT HIV-1 RT inhibitor are shown in Figure 47. Favorable and unfavorable steric interactions are displayed in green and yellow contours, respectively, while blue and red contours illustrate the regions of favored positive and negative charge, respectively. The CoMFA steric field shows a green region surrounding the cyclopropyl group of the compound 25. It indicates that a bulky substituent is preferred to produce higher activity. However, there is a small yellow contour presented close to the green contour, it indicates the limitation of substituent size. From the docking result, it could be found that there are three aromatic sidechains from residues Tyr181, Tyr188, and Trp229 locating near the cyclopropyl group. Therefore, any larger substituent may collide with these residues. On the other hand, too small substituent at this position could not form interaction with these residues and might lead to dropping the inhibitory activity. For example, the inhibitory activity order of compounds is as following; compound 22 $\approx$ compound 41 < compound 28 (Table1). The experimental data supports the explanation of the increased substituent size alkoxy (compound 22), cyclopropyl (compound 28), phenyl (compound 41). This is consistent with the result from molecular docking. The cyclopropyl group can form more interaction with Tyr181, Tyr188, and Trp229 than phenyl and alkoxy groups. The phenyl substituent of compound 41

collides with Trp229, whereas compound 22 loses hydrophobic interaction with Tyr188, and Trp229 because of its smaller R substituent.

The CoMFA for electrostatic contour plot shows red contour located near the C5 and R substituents, which indicate that compounds containing the electron rich group at these positions would be preferable for the binding affinity. The inhibitory activity order of compounds 25 and 27 is the explanation of the negative charge substituent. More electronegativity group at the C5 position can enhance the binding affinity WT HIV-1 RT inhibitors. At the C5 position, compound 25 which has F substituent, shows higher the inhibitory activity than compound 27 (Table 1). The CoMFA contours show minor blue contour near hydrogen atom on the C6-substituent position of the benzoxazin-2-one ring, indicating that more positive charges on this position would increase the activity of inhibitors. This result correlates with the result obtained from molecular docking. The hydrogen atom at the C6-substituent position of compound 25 (the highest activity compound) which could form hydrogen bond with the main chain carbonyl oxygen of His235. Moreover, a blue contour near the NH group of the benzoxazin-2-one ring indicates that the positive charge on this position may increase inhibitory activity. This could be described to the strong hydrogen bond of NH group on the benzoxazin-2-one ring with the oxygen atom of backbone Lys101.

4.3.1.3 CoMSIA contour analysis of WT HIV-1 RT inhibitors

The CoMSIA method defines explicit hydrophobic, hydrogen bond donor and acceptor, steric and electrostatic fields. In this study, the CoMSIA contours of steric and electrostatic fields for WT HIV-1 RT inhibitors are similar to the CoMFA contour. Therefore, the contour interpretation was not discussed in details.

The CoMSIA contour for hydrophobic fields is shown in Figure 48. Magenta contour indicates the regions favorable for hydrophobic groups and the white contour indicates the regions favorable for hydrophilic groups. The cyan contour refers to favored hydrogen donor region, whereas orange contour shows regions favorable for hydrogen acceptor group. The large magenta contour covering around the R substituent (cyclopropyl group) and the 5,6-substituent indicates that the introduction of hydrophobic substituents at these positions would be beneficial for the biological activity. Indeed, the cyclopropyl group of efavirenz could form the hydrophobic interaction with the sidechain of Tyr181, Tyr188, and Trp229 amino acids. The C6-

substituent also appears the minor white contour. It indicates that this position favors both hydrophobic or hydrophilic group, as shown in compound 25 and 01 (Table 1).

The CoMSIA contour for hydrogen donor and acceptor fields are shown in Figure 49. There are two prominent cyan contours close to the NH on benzoxazin-2-one and the Z substituent indicating that the hydrogen donor substituent at these positions will be beneficial for against WT HIV-1 RT. This could be attributed to the strong hydrogen bond between the oxygen atom of backbone of Lys101 and the amide NH of efavirenz. This reveals that the information derived from CoMSIA model correlates with the experimental data. The orange contour observed near the carbonyl oxygen of benzoxazin-2-one ring indicates that this position is favorable for hydrogen acceptor substituent. This is consistent with the experiment that the oxygen atom of carbonyl group could form the hydrogen bond with the backbone Lys101. Another large orange contour closes to the R substituent (cyclopropyl group), which could explain in point of the more electron density of the R substituent.

4.3.1.4 Structural requirement of WT HIV-1 RT inhibitors

The results from CoMFA and CoMSIA models lead to a better understanding of the structural requirement of inhibitor for against WT HIV-1 RT. The red and magenta contours near the C5-substituents indicate that electron withdrawing and hydrophobic groups are preferable. The C6-substituent position located near blue, magenta and white contours suggest that positive charge substituent, hydrophobic or hydrophilic substituent on this position could enhance the inhibitory activity. However, the positive charge at the C6-substituent shows more favorable to higher activity than another group. At the R-substituent position shows green, yellow, magenta and orange contours, which reveal that the bulky group but not too large and electron rich hydrophobic substituent on this position would be beneficial for the biological activity. Moreover, the strong hydrogen bonds from NH group and carbonyl group on benzoxazin-2-one ring play important rule for against WT HIV-1 RT.

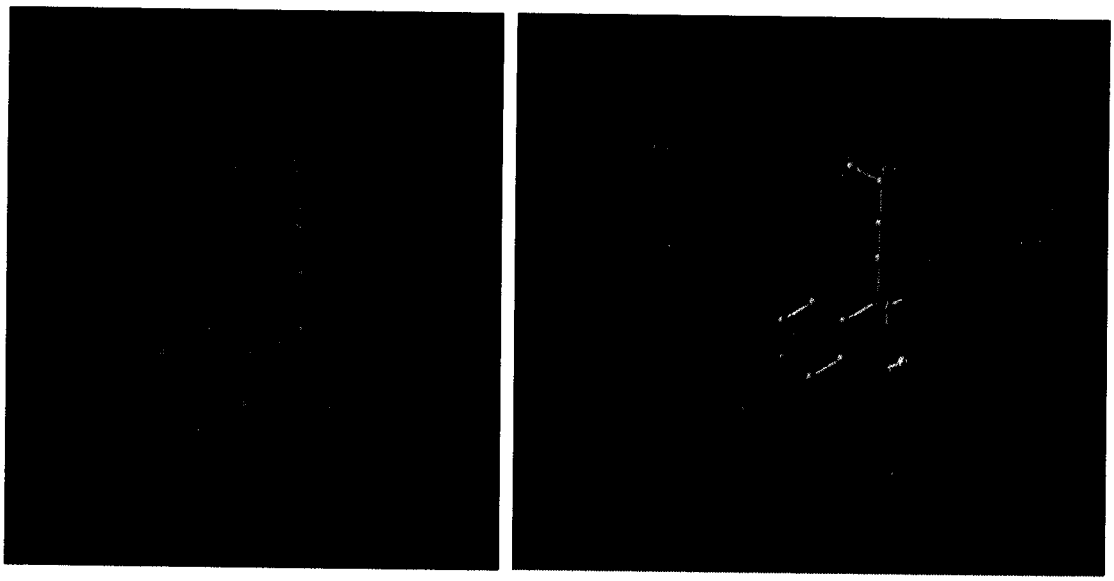

Figure 47 Contour plot of steric and electrostatic fields from CoMFA in combination with compound 25. Favored sterical areas are in green; Unfavored sterical areas are in yellow. Favored positive charge areas are in blue; favored negative charge areas are in red

Figure 48 The CoMSIA contour plot of hydrophobic field in combination with compound 25. Magenta contour show regions favorable for hydrophobic groups; White contour show regions favorable for hydrophilic groups

Figure 49 The CoMSIA contour plot of hydrogen bond donor and acceptor in combination with compound 25. Cyan contour shows regions favorable for hydrogen donor fields; orange contour shows regions favorable for hydrogen acceptor fields

4.3.2 3D-QSAR analysis of K103N HIV-1 RT inhibitor

4.3.2.1 CoMFA and CoMSIA models

The statistical details of CoMFA and CoMSIA analysis are summarized in Table 30. These analyses were based on the docking alignment. The CoMFA model obtained from including both steric and electrostatic fields, whereas, the CoMSIA model obtained from including steric, electrostatic, hydrophobic, hydrogen donor and hydrogen acceptor fields. The r^2 and r^2_{cv} of the CoMFA model, with six optimum number of component are 0.944 and 0.755, respectively. Two statistical values for the CoMSIA model at three components are 0.938 and 0.773, respectively. These statistical indices were reasonably high, indicating that the CoMFA and CoMSIA model might have a powerful predictive ability.

The steric and electrostatic field contributions of CoMFA are 51.2 and 48.8%, respectively. The steric field has greater influence than the electrostatic field. For CoMSIA model, the field contributions steric, electrostatic, hydrophobic, hydrogen bond donor and hydrogen bond acceptor fields are 13.4, 22.3, 20.5, 26.5 and 17.3%, respectively. This indicates that the hydrogen bond donor has the great influence to the inhibitory activities for K103N HIV-1 RT inhibition.

The experimental and predicted activities of the compounds in the training set derived from the best CoMFA and COMSIA models (Table 31 and Figure 50) show a good correlation, which indicate that the two models are high predictability. In order to evaluate the predictive ability of the resulting two models, the same test set as used to predict the inhibitory activities for WT HIV-1 RT inhibition are used. The comparison of the predicted and observed biology activities of the test compounds is present in Table 32. The best CoMFA and CoMSIA models predicted the activities of all test compounds within ±1 log unit of the inhibitory activity. This indicates that both models can accurately predict the K103N HIV-1 RT inhibitory affinities of efavirenz derivatives in the test set.

Table 30 The statistics results of the CoMFA and CoMSIA models for K103N HIV-1 RT inhibitors

Statistical results	CoMFA	CoMSIA
r^2_{cv}	0.755	0.773
noc	6	3
s-press	0.302	0.286
r^2	0.944	0.938
S	0.144	0.155
F	107.318	93.344
Contribution		
Steric	51.2	13.4
Electrostatic	48.8	22.3
Hydrophobic	-	20.5
Hydrogen donor	-	26.5
Hydrogen acceptor	-	17.3

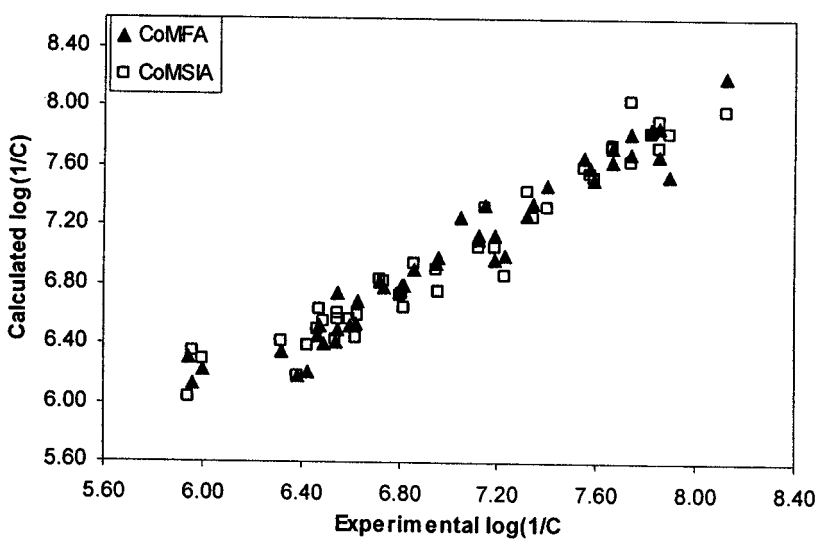

Figure 50 Plots between the predicted and experimental inhibitory affinities of the training set from CoMFA and CoMSIA models of K103N HIV-1 RT inhibitors

Table 31 Predicted log (1/C) K103N inhibitory affinities of the training set from CoMFA and CoMSIA models

Compound No.	Exp. log(1/C)	CoMFA		CoMSIA	
		log(1/C)	Residual	log(1/C)	Residual
01	7.19	7.13	0.06	7.05	0.14
02	5.96	6.13	-0.17	6.35	-0.39
04	6.82	6.80	0.02	6.64	0.18
05	6.49	6.40	0.09	6.55	-0.06
06	7.23	7.00	0.23	6.86	0.37
07	6.43	6.21	0.22	6.39	0.04
08	6.48	6.52	-0.04	6.63	-0.15
09	6.55	6.74	-0.19	6.6	-0.05
10	6.81	6.80	0.01	6.74	0.07
11	6.86	6.90	-0.04	6.95	-0.09
12	6.00	6.23	-0.23	6.29	-0.29
13	6.54	6.41	0.13	6.43	0.11
14	6.63	6.68	-0.05	6.59	0.04
15	6.39	6.18	0.21	6.19	0.20
16	7.08	6.45	0.63	6.34	0.74
17	6.51	7.56	-1.05	6.53	-0.02
18	6.62	6.53	0.09	6.44	0.18
20	5.94	6.30	-0.36	6.04	-0.10
21	7.19	6.97	0.22	6.67	0.52
23	6.74	6.78	-0.04	6.82	-0.08
24	7.85	7.68	0.17	7.73	0.12
25	7.05	7.26	-0.21	7.65	-0.60
26	7.82	7.85	-0.03	7.82	0.00
27	7.2	7.71	-0.51	7.41	-0.21
28	7.89	7.54	0.35	7.83	0.06
30	7.32	7.27	0.05	7.43	-0.11

Table 31 Predicted log (1/C) K103N inhibitory affinities of the training set from CoMFA and CoMSIA models (continued)

Compound No.	Exp. log(1/C)	CoMFA		CoMSIA	
		log(1/C)	Residual	log(1/C)	Residual
31	6.96	6.99	-0.03	6.75	0.21
32	7.15	7.34	-0.19	7.33	-0.18
33	7.74	7.69	0.05	7.64	0.10
34	7.4	7.48	-0.08	7.32	0.08
35	6.32	6.35	-0.03	6.41	-0.09
36	7.74	7.82	-0.08	8.05	-0.31
38	7.66	7.73	-0.07	7.74	-0.08
40	6.55	6.50	0.05	6.56	-0.01
41	6.72	6.82	-0.1	6.83	-0.11
43	6.8	6.77	0.03	6.72	0.08
44	7.59	7.51	0.08	7.53	0.06
45	6.60	6.52	0.08	6.56	0.04
46	7.57	7.59	-0.02	7.55	0.02
48	7.66	7.64	0.02	7.73	-0.07
49	6.47	6.45	0.02	6.49	-0.02
50	8.12	8.20	-0.08	7.98	0.14
51	6.95	6.95	0.00	6.9	0.05
52	6.86	7.28	-0.42	6.99	-0.13
53	7.55	7.67	-0.12	7.6	-0.05
54	7.12	7.13	-0.01	6.2	0.92
55	7.34	7.35	-0.01	7.25	0.09
56	7.12	7.11	0.01	7.05	0.07

Table 32 Predicted log (1/C) K103N inhibitory affinities of the test set from CoMFA and CoMSIA models

Compound No.	Expt. log(1/C)	CoMFA		CoMSIA	
		Calc.log (1/C)	Residual	Calc. log (1/C)	Residual
03	6.94	6.28	0.66	6.58	0.36
19	6.97	6.46	0.51	6.23	0.74
22	5.79	7.42	-1.63	6.43	-0.64
37	7.14	6.76	0.38	6.72	0.42
39	7.25	7.79	-0.54	7.48	-0.23
42	6.49	6.51	-0.02	6.54	-0.05
47	7.74	7.78	-0.04	7.81	-0.07

4.3.2.2 CoMFA contour analysis of K103N HIV-1 RT inhibitor

The CoMFA contours of steric and electrostatic fields from the final non-cross-validated analysis were plotted as 3D colored contour maps (Figure 51). The compound 50 (the highest activity compound) was used in the contours for analysis. The sterical favored and unfavored areas are in green and yellow, respectively, while blue and red contours illustrate the regions of positive charge favored and negative charge favored, respectively. The R-substituent position near the green and yellow contours suggests that the R substituent should be bulky group but not too large due to the limitation by volume of the binding pocket. This is consistent with the result from experimental data and molecular docking. It could be found that the aromatic sidechains from residues Tyr181 and Trp229 are located near this position. Therefore, any larger substituent may collide with these residues leading to dropping the inhibitory activity. The inhibitory activity order of compound 28 and 41 is the explanation of the substituent size (Table 1), which increase substituent size from cyclopropyl (compound 28) to phenyl (compound 41). The cyclopropyl group forms hydrophobic interaction with Tyr188 and Trp229, whereas the phenyl group of compound 41 collides with Trp229. This result brings compound 28 (log 1/C = 7.89) shows higher the inhibitory activity more than compound 41 (log 1/C = 6.72).

The C5-substituent position shows green and red contours. This suggests that bulky and high negative charge substituent would be increase the molecular inhibitory activity, which consistent with the experimental data. This could explain that compound 47, 36 and 53 with Cl, F and OH substituents at the C5-substituent position of the benzoxazin-2-one ring are less active than compound 50 bearing MeO group (Table 1). In docking investigation, it was found that the MeO substituent could form the Van der waals interaction with the sidechain of Leu234, Phe227 and Tyr188 amino acid residues. The other substituents could form the Van der waals interaction with the only side chain of Val106. This reveals that steric and electrostatic at this position are favorable to the inhibitory activity compound.

Another region of sterically favored green contour near the C6-substituent indicates that bulky substituents in this position could increase the molecular inhibitory activity. This could explain that compound 38 with Cl substituents at the C6-substituent position of the benzoxazin-2-one ring are more active than compound 30 bearing F atom (Table 1). The docking results reveal that Cl atom of compound 38 could form Van der waals interaction with the sidechain of Phe227 and Val106 more than F atom of compound 30. However, the too bulky group could conflict with the main chain carbonyl oxygen of His235 and Pro236. This result could explain compound 34 bearing MeO group at this position showing less active than compound 38 and compound 30.

The electrostatically favored blue contour located near and the Z substituent indicating that the positive charge at this position would play a favorable role for activity. This indication agrees with the experimental data that the inhibitors with the replacement of an oxygen atom by the NH group at this position always show higher potency active against K103N RT. Taking compound 38 and compound 01 are examples (Table 1). From molecular docking study, it reveals that NH on this position could form the hydrogen-π interaction with the aromatic sidechain of Tyr181 amino acid residue, whereas, compound 01 could not found such an interaction. Moreover, there is a large blue contour near the NH on the benzoxazin-2-one ring indicates that the positive charge on this position may increase inhibitory activity. This could be described to the strong hydrogen bond between the main chain carbonyl oxygen of Lys101 and the NH of compound. The red contour finds near the carbonyl oxygen group indicating that this

position favorable to negative charge. This is consistent with the experiment that the carbonyl oxygen on benzoxazin-2-one ring of the crystal structure of efavirenz could form the hydrogen bond with the amide back bone of Lys101 amino acid residue.

4.3.2.3 CoMSIA contour analysis of K103N HIV-1 RT inhibitor

The CoMSIA contours for hydrophobic field, hydrogen donor and hydrogen acceptor fields are shown in Figures 52 and 53. The CoMSIA contours of steric and electrostatic fields for K103N HIV-1 RT inhibitor are not discussed in this topic because the obtained contours are similar to the steric and electrostatic fields of the CoMFA contour.

The hydrophobic favored large magenta contour locates around the C5 and C6 substituents indicating that the hydrophobic substituents at these positions would be beneficial for the biological activity. Another minor magenta contour locates near the R substituent suggesting that this position is favorable for the hydrophobic group. This information correlates with the obtained docking result that the R group could form hydrophobic interaction with Tyr188 and Trp229.

The minor cyan contour close to the Z substituent corresponding the hydrogen donor substituent exists at these positions. This is consistent with the docking study and the electrostatic contour of the CoMFA model. The hydrogen atom attached to the nitrogen atom on the Z substituent could from hydrogen-π interaction with the aromatic sidechain of Tyr181. This interaction enhances the biological activity of K103N RT inhibition. Molecules occupying the NH group on the Z position reveal high affinities, whereas the O atom on the Z position shows low affinities (Table 1). The orange contour exists near the carbonyl oxygen of benzoxazin-2-one ring indicating that the carbonyl oxygen is favorable for hydrogen acceptor. This is consistent with the experimental data that the carbonyl oxygen of efavirenz could form the hydrogen bond with the amide back bone of Lys101 amino acid residue. There is another large orange region close to the R substituent, which could explain in point of the electron rich of the R substituent.

4.3.2.4 Structural requirement of inhibitor for against K103N HIV-1 RT

The results from CoMFA and CoMSIA models could suggest the structural requirement of inhibitor for against K103N HIV-1 RT. The substituents at the C5 position of efavirenz derivatives near red, green and magenta contours indicate that the bulky electron withdrawing and hydrophobic group is favorable to activity. The C6-substituent position

near green contour and magenta contour suggests that the bulky hydrophobic group is required on this position for enhance the inhibitory activity. At the R substituent position, the green, yellow, magenta and orange contours reveal that the bulky group but not too large and electron rich hydrophobic substituent on this position would be beneficial for the biological activity. At the Z substituent position, the NH group plays important rule for against K103N HIV-1 RT. Moreover, the strong hydrogen bond of NH and carbonyl oxygen group on benzoxazin-2-one ring is favorable of the inhibitory activity.

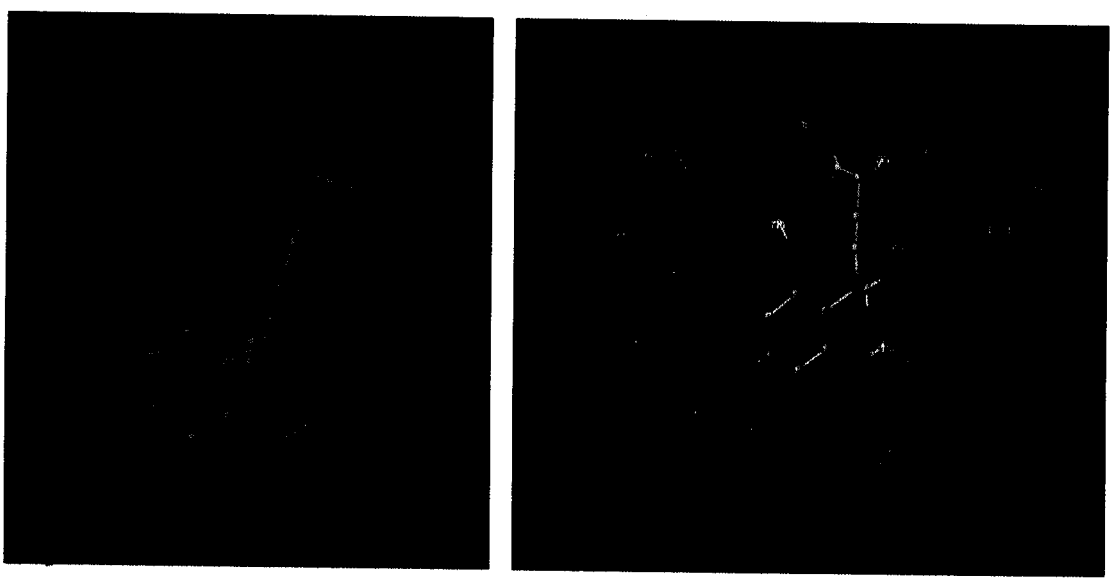

Figure 51 Contour plot of steric and electrostatic fields from CoMFA in combination with compound 50. Sterical favored areas are in green; Sterical unfavored areas are in yellow. Positive charge favored areas are in blue; negative charge favored areas are in red

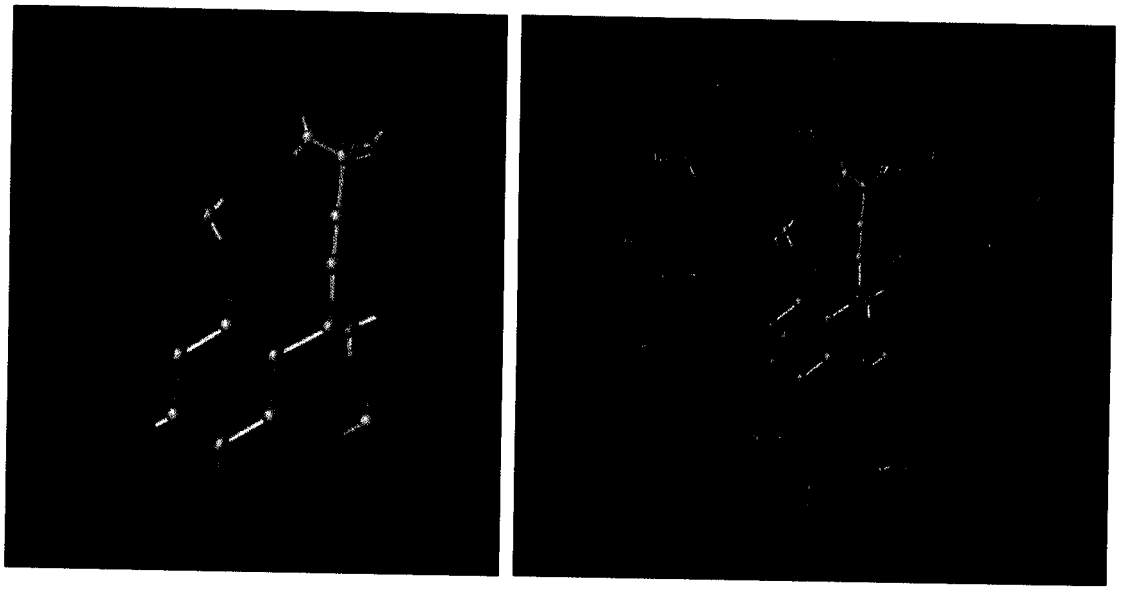

Figure 52 CoMSIA contour plot of hydrophobic field combine with compound 50. Magenta contour show regions favorable for hydrophobic groups; White contour show regions favorable for hydrophilic groups

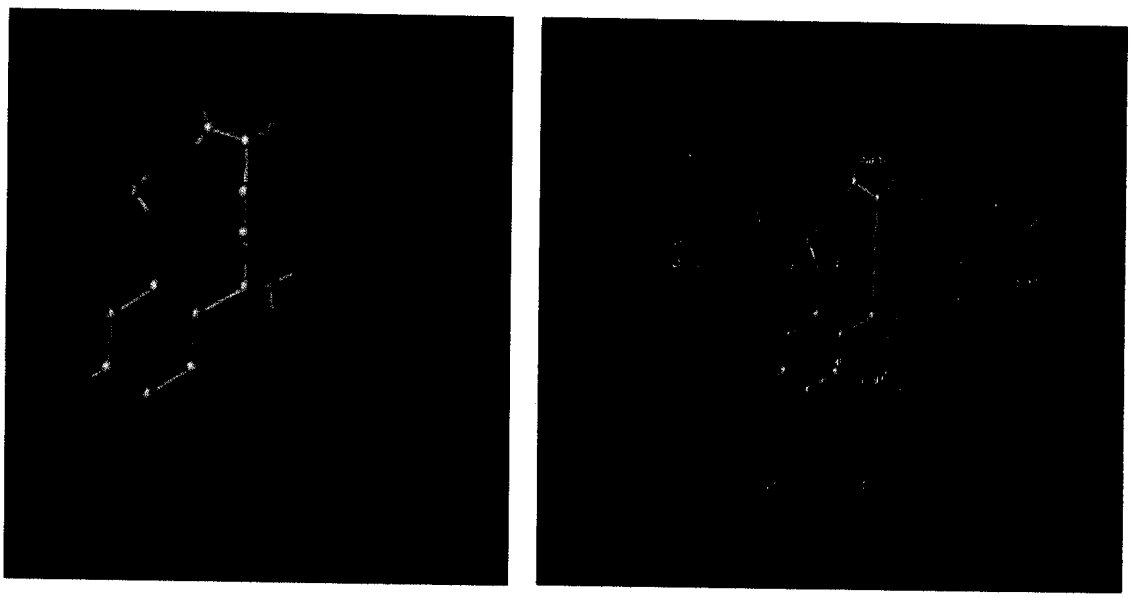

Figure 53 CoMSIA contour plot of hydrogen bond donor and acceptor fields combine with compound 50. Cyan and purple contours show regions favorable and unfavorable for hydrogen donor fields, respectively. Orange and white contours show regions favorable and unfavorable for hydrogen acceptor fields, respectively

4.4 Design of new HIV-1 RT inhibitors

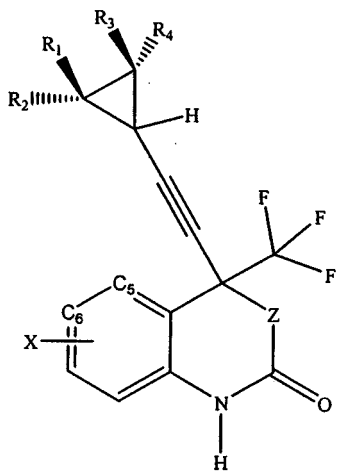

Figure 54 The structure, numbering and defined substituents used for new inhibitor design

The results obtained from CoMFA and CoMSIA models are successful to suggest the structural requirement of inhibitor active against WT and K103N HIV-1 RT. For WT HIV-1 RT inhibition, the positive charge substituent is required on the C6-substituent to form hydrogen bond with His235. The hydrophobic or hydrophilic substituent is required on this position to form the Van der waals interaction with Val106. At the C5-substituent, the electron withdrawing and hydrophobic groups are required. The bulky groups but not too large and electron rich group are required at the R substituent to form the hydrophobic interaction with Tyr181, Tyr188 and Tpr229. On the Z substituent, the NH group is required.

Structural requirements for the K103N HIV-1 RT inhibition are as following; the NH group is required on the Z position to form the hydrogen-π interaction with the aromatic sidechain of Tyr181. At the C5-substituent, the bulky electron withdrawing and hydrophobic groups are required to form Van der waals interaction with Leu234, Phe227 and Tyr188. According to the C6-substituent position, the bulky hydrophobic group but not too large is required to form Van der waals interaction with Val106 and Phe227. At the R substituent, the bulky group but not too large and electron rich hydrophobic group are required to form the hydrophobic interaction with Trp229 and Tyr188.

In this study, new HIV-1 RT inhibitors have been designed based on the results derived from QSAR models and molecular docking methods. The structure, numbering and

defined substituents used for new inhibitor design is shown in Figure 54. Structure and calculated inhibitory activities of new proposed inhibitors for against WT and K103N HIV-1 RT are shown in Tables 33 and 34, respectively.

The design novel compounds for WT and K103N HIV-1 RT inhibitors have been performed in following steps.

Compound 25, the highest potency against WT HIV-1 RT, was used as the starting compound for the modification. Firstly, in the order to examine the R-substituent, compounds WT-D01 – WT-D15 were constructed and their inhibitory activities were predicted. The results show that the CH_3, Cl and CN groups on the R_2 position on the cyclopropyl ring give high potent activity, as shown by compounds WT-D02, WT-D13, and WT-D15. For the next examination, compounds WT-D16 – WT-D23 were constructed to examine the C5-substituent. It was found that the OH and F groups are the group required on this position. For the last step, the combination of the best substituent for each position and the replacement NH group with oxygen atom on the starting compound were performed. Compounds WT-D24 – WT-D33 were constructed and their inhibitory activities were predicted. The results show that all compounds show highly potent affinity, as shown in Table 33.

For the design novel compounds for K103N HIV-1 RT inhibitors, compound 50 (the highest potency against K103N HIV-1 RT) was employed as the starting compound for the modification. Firstly, in the order to evaluate the R-substituent, compounds MT-D01 – MT-D12 were constructed and their inhibitory activities were predicted. The results indicate that the CH_3, Cl and CN groups on the R_4 position on the cyclopropyl ring give high potent activity, as shown by compounds MT-D02, MT-D09 and MT-D11. For the next step, compounds MT-D13 – MT-D23 were constructed to examine the C5-substituent. It was found that the ethyl group, methyl group and methoxy group are the optimum size requirement on this position. The variation of the C6-substituent was further evaluated, therefore, compounds MT-D24 – MT-D30 were constructed. The results show that these compounds show potent affinity lower than compound 50, as shown in Table 34. Therefore, the Cl atom is an optimum group on this position. For the last step, the combination of the best substituent for each position on the starting compound was performed. Compounds MT-D31 – MT-D41 were constructed. The results show that compounds MT-D31, MT-D32, MT-D34 – MT-D39 and MT-D41 show highly potent

affinity, as shown in Table 34.

In the summary, the design of new inhibitors active against WT HIV-1 RT found that compounds WT-D27 – WT-D33 show the highly active against WT HIV-1 RT. For K103N HIV-1 RT, compounds MT-D02, MT-D04, MT-D05, MT-D09 – MT-D11, MT-D13, MT-D17, MT-D21, MT-D31, MT-D32, MT-D34 – MT-D39 and MT-D41 seem to be highly active against K103N HIV-1 RT.

Table 33 Structure and predicted inhibitory activity of new design WT HIV-1 RT inhibitors

Cpds No.	X	R	Z	Log (1/C)		
				Exp.	CoMFA	CoMSIA
Compound 25	**5-F**	CC-cyclopropyl	**NH**	**8.85**	**8.86**	**8.68**
WT-D01	5-F	CC-cyclopropyl-R_1-CH_3	NH		8.71	8.57
WT-D02	**5-F**	**CC-cyclopropyl-R_2-CH_3**	**NH**		**8.91**	**8.69**
WT-D03	5-F	CC-cyclopropyl-R_3-CH_3	NH		8.44	8.63
WT-D04	5-F	CC-cyclopropyl-R_4-CH_3	NH		8.63	8.74
WT-D05	5-F	CC-cyclopropyl-R_2-CH_2CH_3	NH		8.75	8.67
WT-D06	**5-F**	**CC-cyclopropyl-R_2-CH_2OH**	**NH**		**8.86**	**8.62**
WT-D07	5-F	CC-cyclopropyl-R_2-CH_2CN	NH		8.81	8.67
WT-D08	5-F	CC-cyclopropyl-R_1-OH	NH		8.78	8.81
WT-D09	5-F	CC-cyclopropyl-R_2-OH	NH		8.84	8.66
WT-D10	5-F	CC-cyclopropyl-R_3-OH	NH		8.72	8.92
WT-D11	5-F	CC-cyclopropyl-R_4-OH	NH		8.74	8.77
WT-D12	**5-F**	**CC-cyclopropyl-R_2-CH_2OCH_3**	**NH**		**8.87**	**8.54**
WT-D13	**5-F**	**CC-cyclopropyl-R_2-Cl**	**NH**		**8.92**	**8.73**
WT-D14	**5-F**	**CC-cyclopropyl-R_2-F**	**NH**		**8.86**	**8.74**

Table 33 Structure and predicted inhibitory activity of new design WT HIV-1 RT inhibitors (continued)

Cpds No.	X	R	Z	Log (1/C)		
				Exp.	CoMFA	CoMSIA
WT-D15	**5-F**	**CC-cyclopropyl-R_2-CN**	**NH**		**8.91**	**8.68**
WT-D16	**5-OH**	**CC-cyclopropyl**	**NH**		**8.86**	**8.58**
WT-D17	5-CN	CC-cyclopropyl	NH		8.75	8.54
WT-D18	5-CH_3	CC-cyclopropyl	NH		8.69	8.62
WT-D19	5-OCH_2F	CC-cyclopropyl	NH		8.81	8.66
WT-D20	5-$OCHF_2$	CC-cyclopropyl	NH		8.81	8.64
WT-D21	5-OCF_3	CC-cyclopropyl	NH		8.81	8.63
WT-D22	5-OCH_3	CC-cyclopropyl	NH		8.82	8.58
WT-D23	5-CH_3	CC-cyclopropyl	NH		8.74	8.64
WT-D24	**5-OH**	**CC-cyclopropyl-R_2-CH_3**	**NH**		**8.91**	**8.59**
WT-D25	**5-OCH_2F**	**CC-cyclopropyl-R_2-CH_3**	**NH**		**8.86**	**8.58**
WT-D26	**5-OH**	**CC-cyclopropyl-R2-Cl**	**NH**		**8.92**	**8.62**
WT-D27	**5-F**	**CC-cyclopropyl-R_2-CH_3**	**O**		**9.09**	**8.87**
WT-D28	**5-F**	**CC-cyclopropyl-R_2-Cl**	**O**		**9.10**	**8.91**
WT-D29	**5-F**	**CC-cyclopropyl-R_2-CN**	**O**		**9.08**	**8.86**

Table 33 Structure and predicted inhibitory activity of new design WT HIV-1 RT inhibitors (continued)

Cpds No.	X	R	Z	Log (1/C)		
				Exp.	CoMFA	CoMSIA
WT-D30	5-F	CC-cyclopropyl	O		9.04	8.86
WT-D31	5-OH	CC-cyclopropyl-R_2-CH_3	O		9.09	8.77
WT-D32	5-OH	CC-cyclopropyl-R_2-Cl	O		9.10	8.80
WT-D33	5-OH	CC-cyclopropyl	O		9.04	8.76

Table 34 Structure and predicted inhibitory activity of new design K103N HIV-1 RT inhibitors

Cpds No.	X	R	Z	Log (1/C)		
				Exp.	CoMFA	CoMSIA
Compound 50	**5-OMe, 6-Cl**	**CC-cyclopropyl**	**NH**	**8.12**	**8.20**	7.98
MT-D01	5-OMe, 6-Cl	CC-cyclopropyl-R_2-CH_3	NH		8.19	8.06
MT-D02	**5-OMe, 6-Cl**	**CC-cyclopropyl-R_4-CH_3**	**NH**		**8.29**	**8.04**
MT-D03	5-OMe, 6-Cl	CC-cyclopropyl-R_2-CH_2CH_3	NH		8.18	8.08
MT-D04	**5-OMe, 6-Cl**	**CC-cyclopropyl-R_4- CH_2CH_3**	**NH**		**8.25**	**8.04**
MT-D05	**5-OMe, 6-Cl**	**CC-cyclopropyl-R_2,R_4-CH_3**	**NH**		**8.28**	**8.02**
MT-D06	5-OMe, 6-Cl	CC-cyclopropyl-R_2-OCH_3	NH		8.17	7.81
MT-D07	5-OMe, 6-Cl	CC-cyclopropyl-R_4-OCH_3	NH		8.14	7.98
MT-D08	5-OMe, 6-Cl	CC-cyclopropyl-R_2-Cl	NH		8.19	8.06
MT-D09	**5-OMe, 6-Cl**	**CC-cyclopropyl-R_4-Cl**	**NH**		**8.29**	**8.02**
MT-D10	**5-OMe, 6-Cl**	**CC-cyclopropyl-R_2,R_4-CH_3, Cl**	**NH**		**8.29**	**8.11**
MT-D11	**5-OMe, 6-Cl**	**CC-cyclopropyl-R_4-CN**	**NH**		**8.29**	**8.00**
MT-D12	5-OMe, 6-Cl	CC-cyclopropyl-R_2-CN	NH		8.19	7.96
MT-D13	**5-OCH_2F, 6-Cl**	**CC-cyclopropyl**	**NH**		**8.28**	**8.01**
MT-D14	5-$OCHF_2$, 6-Cl	CC-cyclopropyl	NH		8.19	8.08

Table 34 Structure and predicted inhibitory activity of new design K103N HIV-1 RT inhibitors (continued)

Cpds No.	X	R	Z	Log (1/C)		
				Exp.	CoMFA	CoMSIA
MT-D15	5-OCF_3, 6-Cl	CC-cyclopropyl	NH		8.19	8.08
MT-D16	5-CH_2CN, 6-Cl	CC-cyclopropyl	NH		8.09	7.09
MT-D17	**5-CH_2CH_3, 6-Cl**	**CC-cyclopropyl**	**NH**		**8.28**	**8.07**
MT-D18	5-CH_2CH_2F, 6-Cl	CC-cyclopropyl	NH		8.18	8.04
MT-D19	5-CH_2CHF_2, 6-Cl	CC-cyclopropyl	NH		8.17	8.11
MT-D20	5-CH_2CF_3, 6-Cl	CC-cyclopropyl	NH		8.16	8.18
MT-D21	**5-CH_3, 6-Cl**	**CC-cyclopropyl**	**NH**		**8.28**	**7.90**
MT-D22	5-CH_2F, 6-Cl	CC-cyclopropyl	NH		8.05	7.86
MT-D23	5-CHF_2, 6-Cl	CC-cyclopropyl	NH		8.05	7.88
MT-D24	5-CF_3, 6-CH_2 F	CC-cyclopropyl	NH		8.05	7.95
MT-D25	5-OMe, 6-CN	CC-cyclopropyl	NH		8.20	7.92
MT-D26	5-OMe, 6-CH_3	CC-cyclopropyl	NH		8.09	7.95
MT-D27	5-OMe, 6-CH_2F	CC-cyclopropyl	NH		8.09	7.87
MT-D28	5-OMe, 6-CHF_2	CC-cyclopropyl	NH		8.09	7.90
MT-D29	5-OMe, 6-CF_3	CC-cyclopropyl	NH		8.09	8.06

Table 34 Structure and predicted inhibitory activity of new design K103N HIV-1 RT inhibitors (continued)

Cpds No.	X	R	Z	Log (1/C)		
				Exp.	CoMFA	CoMSIA
MT-D30	5-OMe, 6-OH	CC-cyclopropyl	NH		8.06	7.78
MT-D31	**5-OCH_2F, 6-CN**	**CC-cyclopropyl-R_4-CH_3**	**NH**		**8.27**	**8.02**
MT-D32	**5-CH_2CH_3, 6-CN**	**CC-cyclopropyl-R_4-CH_3**	**NH**		**8.29**	**8.07**
MT-D33	5-CH_3, 6-CN	CC-cyclopropyl-R_4-CH_3	NH		8.09	7.91
MT-D34	**5-OCH_2F, 6-Cl**	**CC-cyclopropyl-R_4-CH_3**	**NH**		**8.28**	**8.07**
MT-D35	**5-CH_2CH_3, 6-Cl**	**CC-cyclopropyl-R_4-CH_3**	**NH**		**8.30**	**8.13**
MT-D36	**5-CH_3, 6-Cl**	**CC-cyclopropyl-R_4-CH_3**	**NH**		**8.33**	**7.97**
MT-D37	**5-OMe, 6-CN**	**CC-cyclopropyl-R_4-CH_3**	**NH**		**8.28**	**7.99**
MT-D38	**5-OCH_2F, 6-CN**	**CC-cyclopropyl-R_4-Cl**	**NH**		**8.28**	**7.99**
MT-D39	**5-CH_2CH_3, 6-CN**	**CC-cyclopropyl-R_4-Cl**	**NH**		**8.30**	**8.05**
MT-D40	5-CH_3, 6-CN	CC-cyclopropyl-R_4-Cl	NH		8.10	7.85
MT-D41	**5-OMe, 6-CN**	**CC-cyclopropyl-R_4-Cl**	**NH**		**8.29**	**7.89**

As the previous study, the molecular docking approach shows high ability for searching the binding mode and inhibitor-enzyme interactions of efavirenz and its derivative in HIV-1 RT binding pocket. Moreover, the docking approach enables to derive beneficial guidelines for the design of the novel efavirenz compounds with higher anti-HIV–1 RT activities against WT and K103N RT. Therefore, in order to ensure the new inhibitors of the design favor to energetic binding interaction with the receptor, the molecular docking approach was performed on the set of highly active compounds of the design for against WT and K103N HIV-1 RT. The results show that the calculated binding energy of these compounds could be comparable with the highest activity compound and efavirenz for both WT and K103N RT (Tables 35 and 36). These suggest that the designed inhibitors could strongly bind the receptor.

To identify and predict the interaction of the highest activity compound of the design for against WT and K103N HIV-1 RT in corresponding receptors, the molecular docking calculations were performed on the highest activity compounds of the design. In the WT HIV-1 RT binding pocket, the results show that the highest activity compounds of the design (WT-D28 and WT-D32) could form the hydrophobic interaction of the R substituent with the aromatic sidechain of Trp227 more than compound 25 as shown in Figure 55. These results support that compounds WT-D28 and WT-D32 show higher inhibitory activity than compound 25. For K103N HIV-1 RT binding pocket, the highest activity compound of the design (MT-D36) shows that the hydrophobic interactions between the methyl group on the R substituent and the aromatic sidechain of Try181 are more favorable for the binding affinity than that of the hydrogen atom on the R substituent of compound 50 (Figure 56). This could explain that why MT-D36 shows higher inhibitory activity than compound 50. Moreover, these results suggest that the interactions of the designed inhibitors correspond with the predicted inhibitory from CoMFA and CoMSIA models.

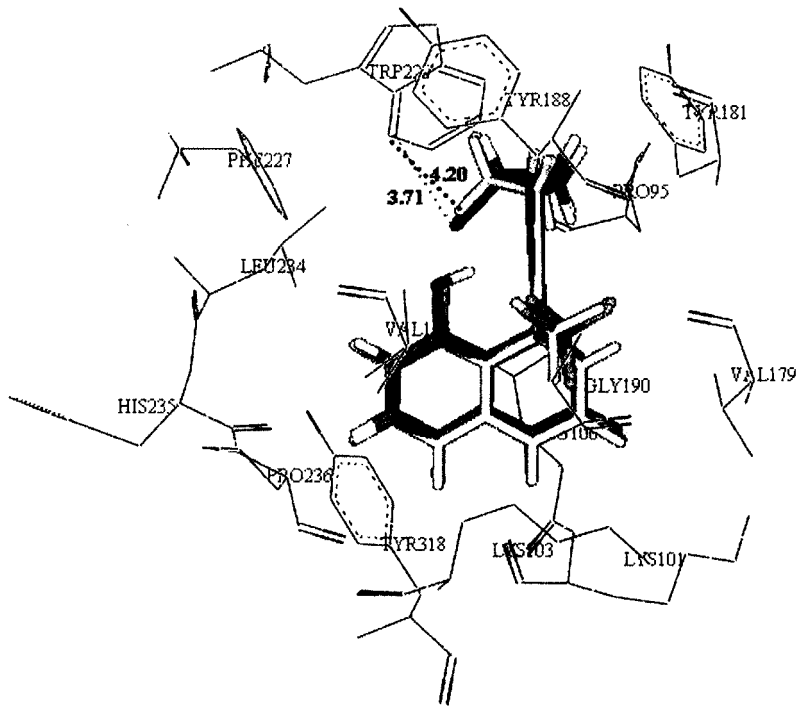

Figure 55 Compound 25 (yellow), WT-D28 and WT-D32 (color by atom type) in WT HIV-1 RT binding pocket

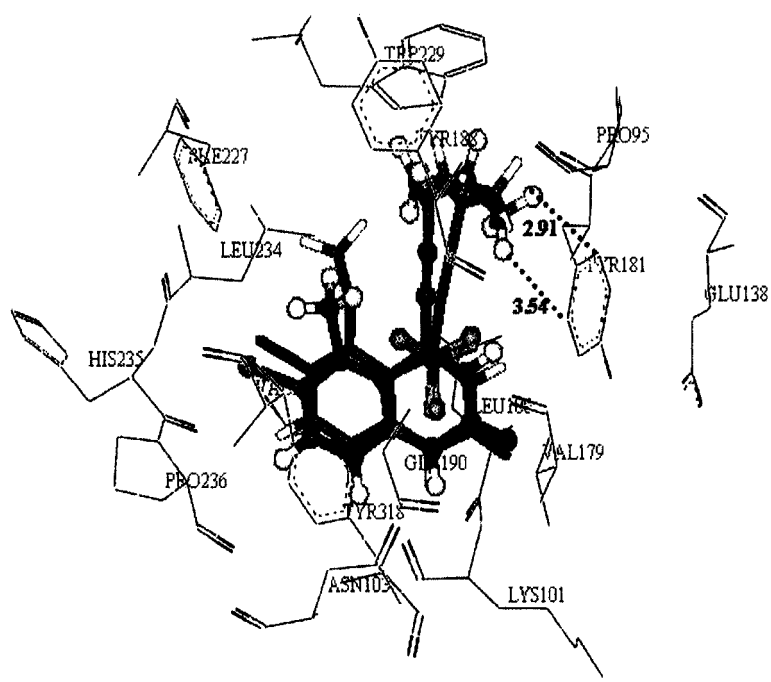

Figure 56 Compound 50 (stick) and MT-D36 (ball and stick) in K103N HIV-1 RT binding pocket

Table 35 Docking results of the proposed inhibitors active against WT HIV-1 RT

Compd. No.	Log 1/C from CoMFA model	Calculated binding energy (kcal/mol)
Compound 01	8.72	-13.19
Compound 25	8.86	-12.73
WT-D27	9.09	-12.22
WT-D28	9.10	-12.78
WT-D29	9.08	-12.40
WT-D30	9.04	-11.78
WT-D31	9.09	-11.83
WT-D32	9.10	-12.03
WT-D33	9.04	-11.32

Table 36 Docking results of the proposed inhibitors active against K103N HIV-1 RT

Compd. No.	Log 1/C from CoMFA model	Calculated binding energy (kcal/mol)
Compound 01	7.13	-13.19
Compound 25	8.20	-13.39
MT-D02	8.29	-13.35
MT-D09	8.29	-12.88
MT-D10	8.29	-12.88
MT-D11	8.29	-11.77
MT-D32	8.29	-13.42
MT-D35	8.30	-12.52
MT-D36	8.33	-13.72
MT-D39	8.30	-12.70
MT-D41	8.29	-13.04

CHAPTER 5

CONCLUSIONS

On the basis of various methods of quantum chemical calculations, the conformational analysis of the HIV-1 RT inhibitor of efavirenz and selected derivatives has been performed. The obtained 2D and 3D PES for these compounds derived from high level of calculations could provide the role of molecular flexibility of the structures and give additional information according to the preferable conformation. The calculated preferable conformations agree well with the binding conformation derived from the X-ray crystallographic data and the docked conformation. Consecutively, the molecular docking calculations and 3D-QSAR analyses were successfully intergated to investigate the interaction and the relationship between structural requirements of efavirenz derivatives for WT and K103N HIV-1 RT. The potential binding orientation of the efavirenz inhibitors in the binding pockets could be identified, by using molecular docking studies. The docking results provide additional insight into essential inhibitor-enzyme interactions for efavirenz derivatives and different types of wild type and mutant type of HIV-1 RT. Based on the docking conformations, the reliable and predictive CoMFA and CoMSIA models of efavirenz derivatives for the WT and K103N RT inhibition were derived. The QSAR models are successfully used to highlight different characteristics for different type of WT and K103N HIV-1 RT. The suggestions obtained from all docking and 3D-QSAR models reinforce each other and also show good accordance with inhibitor-receptor complex derived by experimental data. Evidently, in the present study, molecular modeling with the combination of structure-based and ligand-based drug design approaches integrated with quantum chemical calculations has been proven as attractive and efficient tools for better understanding of the key structural element for enhancing the interaction between efavirenz compounds and the WT and K103N HIV-1 RT. Consequently, the obtained results enable to provide beneficial guidelines to design novel efavirenz compounds with higher anti-HIV–1 RT activities against WT and K103N RT.

REFERENCES

REFERENCES

Barreca, M.L. and et al. "Comparative Molecular Field Analysis (CoMFA) and Docking Studies of Non-nucleoside HIV-1 RT Inhibitors (NNIs)", Bioorganic & Medicinal Chemistry. 7: 2283-2292; 1999.

Bacheler, L. and et al. "Genotypic Correlates of Phenotypic Resistance to Efavirenz in Virus Isolates from Patients Failing Nonnucleoside Reverse Transcriptase Inhibitor Therapy", The Journal of Virology. 75: 4999-5008; 2001.

Chen, H.F. and et al. "Computational Studies and Drug Design for HIV-1 Reverse Transcriptase Inhibitors of 3',4'-di-O-(S)-Camphanoyl-(+)-cis-Khellactone (DCK) Analogs", Journal of Computer-Aided Molcelar Design. 19(4): 243-58; 2005.

Chen, H.F. and et al. "Comparative Study of Nonnucleoside Inhibitors with HIV-1 Reverse Transcriptase Based on 3D-QSAR and Docking", SAR and QSAR in Environmental Research. 14(5-6): 455-474; 2003.

Cocuzza, A.J. and et al. "4,1-Benzoxazepinone Analogues of Efavirenz (Sustiva™) as HIV-1 Reverse Transcriptase Inhibitors", Bioorganic &Medicinal Chemistry Letters. 11: 1389 –1392; 2001.

Cocuzza, A.J. and et al. "Synthesis and Evaluation of Efavirenz (Sustiva) Analogues as HIV-1 Reverse Transcriptase Inhibitors: Replacement of the Cyclopropylacetylene Side Chain", Bioorganic & Medicinal Chemistry Letters. 11(9): 1177-9; 2001.

Conway, B. and et al. "Development of Drug Resistance in Patients Receiving Combinations of Zidovudine, Didanosine and Nevirapine", AIDS. 15: 1269-1274; 2001.

Corbett, J.W. and et al. "Inhibition of Clinically Relevant Mutant Variants of HIV-1 by Quinazolinone non-Nucleoside Reverse Transcriptase Inhibitors", Journal of Medicinal Chemistry. 43(10): 2019-30; 2000.

Corbett, J.W. and et al. "3,3a-Dihydropyrano[4,3,2-de]quinazolin-2(1H)-ones are Potent Non-Nucleoside Reverse Transcriptase Inhibitors", Bioorganic & Medicinal Chemistry Letters. 11: 211-214; 2001.

REFERENCES (CONTINUED)

Evans, D.B. and et al. "A Recombinant Ribonuclease H Domain of HIV-1 Reverse Transcriptase that is Enzymatically Active", Journal of Biological Chemistry. 266: 20583-20585; 1991.

Font, M. and et al. "Structure-activity Relationships in Quinoline Reissert Derivatives with HIV-1 Reverse Transcriptase Inhibitory Activity", Drug Design Discovery. 14(4): 259-72; 1997.

Frisch, M. J. and et al. Gaussian 03, Revision C.02, Gaussian, Inc., Wallingford CT, 2004.

Hannongbua, S. and et al. "3D-Quantitative Structure-Activity Relationships of HEPT Derivatives as HIV-1 Reverse Transcriptase Inhibitors, Based on *Ab Initio* Calculations", Journal of Chemical Information and Computer Sciences. 41(3): 848-855; 2001.

Hannongbua, S. and et al. "Quantitative Structure-activity Relationships and Comparative Molecular Field Analysis of TIBO Derivatised HIV-1 Reverse Transcriptase Inhibitors", Journal of Computer-Aided Molcelar Design. 13(6): 563-577; 1999.

Hannongbua, S., S. Prasithichokekul and P. Pungpo. "Conformational Analysis of Nevirapine, a Non-Nucleoside HIV-1 Reverse Transcriptase Inhibitor, Based on Quantum Mechanical Calculations", Journal of Computer-Aided Molcelar Design. 15(11): 997-1004; 2001.

Hannongbua, S. and et al. "Molecular Calculations on the Conformation of the HIV-1 Reverse Transcriptase Inhibitor (+)-(S)-4,5,6,7-Tetrahydro-8-Chloro-5-Methyl-6-(3-Methyl-2-Butenyl)-Imidazo[4,5,1-jk][1,4] Benzodiazepine-2(1H)-Thione (8-Chloro-TIBO)", Monatshefte Chemie. 132(10): 1157-1169; 2001.

Heeres, J. and et al. "Design, Synthesis, and SAR of a Novel Pyrazinone Series with Non-Nucleoside HIV-1 Reverse Transcriptase Inhibitory Activity", Journal of Medicinal Chemistry. 48(6): 1910-1918; 2005.

REFERENCES (CONTINUED)

Hopkins, A.L. and et al. "Complexes of HIV-1 Reverse Transcriptase with Inhibitors of the HEPT Series Reveal Conformational Changes Relevant to the Design of Potent Non-Nucleoside Inhibitors", Journal of Medicinal Chemistry. 39(8): 1589-1600; 1996.

Hsiou, Y. and et al. "Structures of Tyr188Leu Mutant and Wild-type HIV-1 Reverse Transcriptase Complexed with the Non-Nucleoside Inhibitor HBY 097: Inhibitor Flexibility is a Useful Design Feature for Reducing Drug Resistance", Journal of Molecular Biology. 284(2): 313-23; 1998.

Kalyan, D. and et al. "Roles of Conformational and Positional Adaptability in Structure-based Design of TMC125-R165335 (Etravirine) and Related Non-Nucleoside Reverse Transcriptase Inhibitors that are Highly Potent and Effective Against Wild-type and Drug-Resistant HIV-1 Variants", Journal of Medicinal Chemistry. 47(10): 2550-60; 2004.

Kohlstaedt, L.A. and et al. "Crystal Structure at 3.5 Å Resolution of HIV-1 Reverse Transcriptase Complexed with an Inhibitor", Science. 256(5065): 1783-90; 1992 .

Kroeger, S. and et al. "Molecular Modeling Studies of HIV-1 Reverse Transcriptase Nonnucleoside Inhibitors: Total Energy of Complexation as a Predictor of Drug Placement and Activity", The Protein Society. 4(10): 2203-22; 1995.

Lawtrakul, L. and et al. "Conformational Study of the HIV-1 Reverse Transcriptase Inhibitor 1-[(2-Hydroxyethoxy)Methyl]-6-(Phenylthio)Thymine (HEPT)", Journal of Biological Chemistry. 380(2): 265-7; 1999.

Markwalder, J.A. and et al. "Synthesis and Biological Activities of Potential Metabolites of the non-Nucleoside Reverse Transcriptase Inhibitor Efavirenz", Bioorganic & Medicinal Chemistry Letters. 11(5): 619-22; 2001.

Martino, G.D. and et al. "Novel 1-[2-(diarylmethoxy)Ethyl]-2-Methyl-5-Nitroimidazoles as HIV-1 Non-Nucleoside Reverse Transcriptase Inhibitors. A Structure-activity Relationship Investigation", Journal of Medicinal Chemistry. 48: 4378-4388; 2005.

REFERENCES (CONTINUED)

Medina-Franco, J.L. and et al. "Flexible Docking of Pyridinone Derivatives into the Non-Nucleoside Inhibitor Binding Site of HIV-1 Reverse Transcriptase", Bioorganic & Medicinal Chemistry Letters. 12(23): 6085-95; 2004.

Medina-Franco, J.L. and et al. "Docking-based CoMFA and CoMSIA Studies of Non-Nucleoside Reverse Transcriptase Inhibitors of the Pyridinone Derivative Type", Journal of Computer-Aided Molcelar Design. 18(5): 345-360; 2004.

Mei, Y. and et al. "Quantum Study of Mutational Effect in Binding of Efavirenz to HIV-1 RT", Proteins. 59(3): 489-95; 2005.

Miller, V. and et al. "The M184V Mutation in HIV-1 Reverse Transcriptase (RT) Conferring Lamivudine Resistance does not Result in Broad Cross-resistance to Nucleoside Analogue RT Inhibitors", AIDS. 12: 705-712; 1998.

Morris, G.M., D.S. Goodsell and A.J. Olson. The Scripps Research Institute, AutoDock 3.05, 2000.

Nowak, M.A. and R.M. May. "Mathematical Biology of HIV Infections: Antigenic Variation and Diversity Threshold", Mathematical Biosciences. 106: 1–21; 1991.

Patel, M. and et al. "Synthesis and Evaluation of Quinoxalinones as HIV-1 Reverse Transcriptase Inhibitors", Bioorganic & Medicinal Chemistry Letters. 10(15): 1729-31; 2000.

Patel, M. and et al. "Synthesis and Evaluation of Benzoxazinones as HIV-1 Reverse Transcriptase Inhibitors. Analogs of Efavirenz (SUSTIVA)", Bioorganic & Medicinal Chemistry Letters. 9(22): 3221-4; 1999.

Patel, M. and et al. "Synthesis and Evaluation of Analogs of Efavirenz (SUSTIVA) as HIV-1 Reverse Transcriptase Inhibitors", Bioorganic & Medicinal Chemistry Letters. 9(19): 2805-10; 1999.

Pungpo, P. and S. Hannongbua. "Three-Dimensional Quantitative Structure-activity Relationships Study on HIV-1 Reverse Transcriptase Inhibitors in the Class of Dipyridodiazepinone Derivatives, using Comparative Molecular Field Analysis", Journal of Molecular Graphics & Modelling. 18(6): 581-590; 2000.

REFERENCES (CONTINUED)

Pungpo, P. and et al. "Computer-aided Molecular Design of Highly Potent HIV-1 RT Inhibitors: 3D-QSAR and Molecular Docking Studies of Efavirenz Derivatives", SAR and QSAR in Environmental Research. 17(4): 353-70; 2006.

Pungpo, P., S. Hannongbua and P. Wolschann. "Hologram Quantitative Structure-activity Relationships Investigations of Non-Nucleoside Reverse Transcriptase Inhibitors", Current Medicinal Chemistry. 10(17): 1661-77; 2003.

Ragno, R. and et al. "Computer-aided Design, Synthesis, and Anti-HIV-1 Activity in Vitro of 2-Alkylamino-6-[1-(2,6-Difluorophenyl)Alkyl]-3,4-Dihydro-5-Alkylpyrimidin-4(3H)-Ones as Novel Potent Non-Nucleoside Reverse Transcriptase Inhibitors, also Active Against the Y181C Variant", Journal of Medicinal Chemistry. 47(4): 928-34; 2004.

Ragno, R. and et al. "Docking and 3-D QSAR Studies on Indolyl Aryl Sulfones. Binding Mode Exploration at the HIV-1 Reverse Transcriptase Non-Nucleoside Binding Site and Design of Highly Active N-(2-Hydroxyethyl)carboxamide and N-(2-Hydroxyethyl)carbohydrazide Derivatives", Journal of Medicinal Chemistry. 48: 213-223; 2005.

Ranise, A. and et al. "Structure-Based Design, Parallel Synthesis, Structure-Activity Relationship, and Molecular Modeling Studies of Thiocarbamates, New Potent Non-Nucleoside HIV-1 Reverse Transcriptase Inhibitor Isosteres of Phenethylthiazolylthiourea Derivatives", Journal of Medicinal Chemistry. 48(11): 3858-3873; 2005.

Rawal, R.K. and et al. "Molecular Docking Studies on 4-Thiazolidinones as HIV-1 RT Inhibitors", Journal of Molecular Modeling. 13: 155–161; 2007.

Ren, J. and et al. "Structural Basis for the Resilience of Efavirenz (DMP-266) to Drug Resistance Mutations in HIV-1 Reverse Transcriptase", Structure. 8(10): 1089-94; 2000.

REFERENCES (CONTINUED)

Rodriguez-Barrios, F., J. Balzarini and F. Gago. "The Molecular Basis of Resilience to the Effect of the Lys103Asn Mutation in Non-nucleoside HIV-1 Reverse Transcriptase Inhibitors Studied by Targeted Molecular Dynamics Simulations", Journal of the American Chemical Society. 127(20): 7570-8; 2005.

Saenoon, S., S. Hannongbua and P. Wolschann. "Structural Flexibility of Non-Nucleoside HIV-1 Reverse Transcriptase Inhibitor: 9-Cl TIBO as Explained by Potential Energy Surface and 13C and 1H NMR Calculations, Based on *ab initio* and Density Functional Study", Journal of Chemical Information and Computer Sciences. 43(5): 1412-1422; 2003.

Saparpakorn, P., S. Hannongbua and D. Rognan. "Design of Nevirapine Derivatives Insensitive to the K103N and Y181C HIV-1 Reverse Transcriptase Mutantsdagger", SAR and QSAR in Environmental Research. 17(2): 183-94; 2006.

Tripos Associates Inc., St. Louis, MO, Alchemy2000, 1998.

Sudbeck, E.A. and et al. "Structure-based Design of Novel Dihydroalkoxybenzyloxo pyrimidine (DABO) Derivatives as Potent Non-Nucleoside Inhibitors of HIV Reverse Transcriptase", Book of Abstracts, 216th ACS National Meeting, Boston. 1998.

Tantillo, C. and et al. "Locations of Anti-AIDS Drug Binding Sites and Resistance Mutations in the Three-dimensional Structure of HIV-1 Reverse Transcriptase. Implications for Mechanisms of Drug Inhibition and Resistance", Journal of Molecular Biology. 243: 369; 1994.

Torti, C. and et al. "Distribution of K103N and/or Y181C HIV-1 Mutations by Exposure to Zidovudine and Non-nucleoside Reverse Transcriptase Inhibitors", Journal of Antimicrobial Chemotherapy. 48: 113-116; 2001.

Tummino, P.J. and et al. "Competitive Inhibition of HIV-1 Protease by Biphenyl Carboxylic Acids", Archives of Biochemistry and Biophysics. 316(1): 523-528; 1995.

REFERENCES (CONTINUED)

Vig, R. and et al. "Rational Design and Synthesis of Phenethyl-5-Bromopyridyl Thiourea Derivatives as Potent Non-Nucleoside Inhibitors of HIV Reserve Transcriptase", Bioorganic & Medicinal Chemistry. 6(10): 1789-97; 1998.

Weinzinger, P., S. Hannongbua and P. Wolschann. "Molecular Mechanics PBSA Ligand Binding Energy and Interaction of Efavirenz Derivatives with HIV-1 Reverse Transcriptase", Journal of Enzyme Inhibitor Medicinal Chemistry. 20(2): 129-34; 2005.

Wodarz, D. and et al. "Dynamics of Macrophage and T Cell Infection by HIV", Journal of Theoretical Biology. 196: 101–113; 1999.

Young, S.D. and et al. "L-743,726 (DMP-266): a Novel, Highly Potent Nonnucleoside Inhibitor of the Human Immunodeficiency Virus Type 1 Reverse Transcriptase", Antimicrobial Agents and Chemotherapy. 39(12): 2602-2605; 1995.

Zhou, Z. and J.D. Madura. "CoMFA 3D-QSAR Analysis of HIV-1 RT Nonnucleoside Inhibitors, TIBO Derivatives Based on Docking Conformation and Alignment", Journal of Chemical Information and Computer Sciences. 44(6): 2167-2178; 2004.

Zhang, Z. and et al. "Towards Discovering Dual Functional Inhibitors Against Both Wild Type and K103N Mutant HIV-1 Reverse Transcriptase: Molecular Docking and QSAR Studies on 4,1-Benzoxazepinone Analogues", Journal of Computer-Aided Molecular Design. 20: 281–293; 2006.

APPENDIX

POSTER CONTRIBUTIONS TO CONFERENCES

INTERNATIONAL CONFERENCE

1. Pornpan Pungpo, Auradee Punkvang, Patchareenart Saparpakorn, Peter Wolschann and Supa Hannongbua. Theoretical Investigations on Potent HIV-1 Reverse Transcriptase Inhibitors of Efavirenz Analogues by Using Conformational Analysis, Molecular Docking and 3D-QSAR Studies. *The XIIth International Congress of Quantum Chemistry (XII-ICQC2006), 21-26 May, 2006, Kyoto, Japan.*
2. Pornpan Pungpo, Auradee Punkvang, Patchreenart Saparpakorn and Supa Hannongbua. The Investigation on the Interactions between HIV-1 RT Inhibitors of Efavirenz Analogues and HIV-1 RT, Based on Molecular Docking Calculations. *International Conference on Modeling in Chemical and Biological Engineering Sciences. 26-27 Octuber, 2006, Bangkok, Thailand.*

NATIONAL CONFERENCE

1. Auradee Punkvang, Patchreenart Saparpakorn, Supa Hannongbua and Pornpan Pungpo. Conformational Analysis of HIV-1 Reverse Trancriptase Inhibitor (S)-6-Chloro–4-(Cyclopropylethenyl)-1,4–Dihydro-4-(Trifluoromethyl)-2H-3,1-Benzoxazin-2-One (Efavirenz) and Its Derivtives, by Using Quantum Chemical Calculations. *The 32nd Congress on Science and Technology of Thailand, October, 10-12, 2006, Bangkok, Thailand.*
2. Auradee Punkvang, Patchreenart Saparpakorn, Supa Hannongbua and Pornpan Pungpo. Theoretical Investigation of Highly Potent HIV-1 RT Inhibitors in The Class of Efavirenz Derivatives, Based on Quantum Chemical Calculations and Molecular Modeling. *The 6th National Symposium on Graduate Research 13-14 October 2006, Bangkok, Thailand.*
3. Pornpan Pungpo, Auradee Punkvang, Patchreenart Saparpakorn and Supa Hannongbua. Identification of Binding and Interaction for HIV-1 RT Inhibitors in the Class of Efavirenz Derivatives in the Binding Pocket of WT and K103N HIV-1 RT by Using Molecular Docking Studies. *The first annual symposium of Protien Research Society of THAILAND "Challenges in Protein Research in Thailand" 24-25 October, 2006, Bangkok, Thailand.*

4. Pornpan Pungpo, Auradee Punkvang, Patchreenart Saparpakorn and Supa Hannongbua. Understanding the Interaction and the structure–Activity Correlation of Efavirenz Derivatives and WT and K103N HIV-1 RT by Molecular Docking and 3D-QSAR Approaches. *The 8th International Meeting "Molecular Epidemiology and Evolutionary Genetics of Infectious Disease" (MEEGID VIII). 30 November – 2 December, 2006, Bangkok, Thailand.*
5. Pornpan Pungpo, Auradee Punkvang, Patchreenart Saparpakorn and Supa Hannongbua. A Combined Approach of Docking and 3D QSAR Studies of Efavirenz Derivatives as Highly Potent HIV-1 RT Inhibitors. *The 11th Annual National Symposium on Computational Science and Engineering. 28-30 March October, 2007, Phuket , Thailand.*

Theoretical Investigations on potent HIV-1 reverse transcriptase inhibitors of efavirenz analogues by using conformational analysis, molecular docking and 3D-QSAR studies

Pornpan Pungpo[1], Anuadee Punkvang[1], Patchareenart Saparpakorn[2], Peter Wolschann[3] and Supa Hannongbua[1]

[1]Department of Chemistry, Faculty of Science, Ubonratchathani University, Ubonratchathani, Thailand 34190

[2]Department of Chemistry, Faculty of Science, Kasetsart University, Bangkok, 10900

[3]Institute for Theoretical Chemistry, University of Vienna, Vienna, AUSTRIA

The reverse transcriptase (RT) of human immunodeficiency virus type 1 (HIV-1) has been the target of several antiviral therapeutic agent used in the treatment of the acquired immune deficiency syndrome (AIDS) for a number of years. Efavirenz, a potent non-nucleoside reverse transcriptase inhibitor (NNRTI), has been approved for the treatment of HIV infections. Although HIV infection is generally well controlled by efavirenz containing regimens, efavirenz induces drug resistance variants of HIV-1, both in cell culture and in patients. The K103N mutation is the most frequent mutation observed within RT resulting from therapeutic interventions involving NNRTIs. Since the current available drugs cannot cover enough to completely eradicate HIV within the AIDS patient, there is a continuing need to identify improved agents within each class in order to provide the optimum clinical benefit.

The starting geometry of efavirenz compound was taken from X-ray crystallographic data. The conformational analysis of efavirenz was investigated by various method methods of quantum chemical calculations: AM1, PM3, HF/3-21G, HF/6-31G** and B3LYP/6-31G**. For molecular docking and 3D-QSAR studies, 56 efavirenz derivatives were constructed and fully geometrical optimized by HF/3-21G calculations. For molecular docking calculations, Autodock program was used to investigate the potential binding orientations of several efavirenz derivatives in the binding pocket. Based on the docked binding conformations, 3D-QSAR methods based on CoMFA and CoMSIA were applied to determine relationships between structural properties and HIV-1 inhibitions.

Conformational analysis

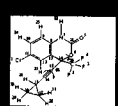

Fig 1

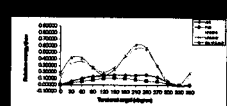

Fig 2

Fig 3

The rotational potential along the C–C bond connecting the cyclopropyl side chain to the heterocyclic ring system as were calculated by using various calculations, semiempirical (AM1, PM3), *ab initio* (HF/3-21G, HF/6-31G**) DFT calculations. Based on HF and B3LYP results, two pronounced energetic local minima were found at the similar region, whereas AM1 and PM3 calculations seem to be not accurate enough to obtain helpful information regarding conformational analysis of this molecules. The geometry of compound is mainly determined by the rigid aromatic ring system and the positions of the side chains. The conformation minimum for dihedral angle α is 330 degree close to the geometry of the molecule complexed with HIV-1 RT. The superimposition of X-ray crystal structure of efavirenz and calculated conformational structures indicates that B3LYP/6-31G** results gives the most similar conformation to the geometry obtained from the X-ray structure.

Molecular docking studies

Fig 4

Fig 5

Based on the binding conformations derived from docking calculations, the obtained CoMFA and CoMSIA models are satisfying based on both statistical significance and predictive ability. CoMFA model reveals the importance of steric and electrostatic interactions through contour maps. The resulting CoMSIA models enhance the understanding of steric, electrostatic, hydrophobic, electron donor and acceptor requirements for ligands binding to the WT and K103N HIV-1 RT. The CoMSIA models enhance the understanding of steric, electrostatic, hydrophobic, electron donor and acceptor requirements for ligands binding to HIV-1RT. The analysis derived by CoMFA and CoMSIA support each other and clearly highlight different characteristics for different types of wild type and mutant type HIV-1 RT.

WT K103N

Fig 6

Fig 7

To validate the docking method used, Autodock 3.0 was applied to dock the efavirenz compound back into the WT and K103N HIV-1 RT binding pocket. The rmsd of the docked pose from the X-ray pose of efavirenz in the binding pockets are less than 1 Å indicating the parameters used for the docking simulations are reasonable in reproducing the X-ray structure. Therefore, Autodock method and its parameters could be extended to search the binding conformations in the binding pocket for all compounds in the data set. The best docked conformations of all efavirenz compounds shows the similar binding conformation of these inhibitors in the binding pockets suggesting that they interact with WT and K103N HIV-1 RT in a similar way. The common core structures of all derivatives were superimposed each other well. Moreover, the results derived from docking analysis give additional information and help

WT K103N

Fig 8

Fig 9

In the present study, the performance of conformational analysis on efavirenz inhibitor provides the most energetical favorable structure and give helpful information into the conformational possibilities, the range of flexibility of the molecule. The molecular docking and 3D-QSAR methods were successfully combined to investigate the relationship between structural properties and HIV-1 inhibitions. The best binding conformations of efavirenz derivatives were determined using docking calculations. Based on the binding conformations and their alignments inside the binding pocket, highly reliable and predictive 3D-QSAR models were obtained. The results obtained from the models agree well with the interactions of the ligand-receptor complexes derived by the experimental data. Accordingly, the information obtained from the QSAR results can be integrated to identify the structural requirements of efavirenz derivatives for designing new inhibitors with enhancing WT and K103N HIV-1 RT inhibitory activity.

The grants providing by the Thailand Research Fund (TRG5880015, BRG/15/2000) and the Golden Jubilee Ph.D. program (CHE-PHD-47-B-1) are gratefully acknowledged for research supports. Partial supports from the XII ICQC 2006 for attending the conress is acknowledged. Special thanks due to S. Suramitr for his helpful suggestion on conformational analysis.

A081

Theoretical Investigations on potent HIV-1 reverse transcriptase inhibitors of efavirenz analogues by using conformational analysis, molecular docking and 3D-QSAR studies

Pornpan Pungpo[1], Oradee Pankwang[1], Patchreenart Saparpakorn[2], Peter Wolschann[3] and Supa Hannongbua[2]

[1]*Faculty of Science, Ubonratchathani University, Ubonratchathani, Thailand*

[2]*Faculty of Science, Kasetsart University, Bangkok, Thailand*

[3]*Institute of Theoretical Chemistry, University of Vienna, Vienna, AUSTRIA*

Conformational analysis of HIV-1 reverse transcriptase inhibitor (s)-6-chloro-4-(cyclopro -pylethynyl)-1,4-dihydro-4-(trifluoromethyl)-2H-3, 1-benzoxazin -2- one or efavirenz has been investigated, based on high level of calculations, ab initio and DFT theory. The starting geometry of efavirenz was taken from x-ray crystallographic data. The rotational potential energy surface along the single bond between carbon atom of CF 3 group and atoms in the heterocyclic ring and in the cyclopropylethynyl group were examined. The comparison of the calculated energy minimum conformers and the bound conformer in the X-ray HIV-1 RT shows that the conformation in the pocket is close to an energy minimum structure and the deviation are caused by the interaction with the complementary protein surface. In addition, molecular docking calculations were performed to locate the binding orientations and conformations of the inhibitors in the binding pocket of K103N HIV-1 RT. The starting geometry was obtained from X-ray crystallographic data. 58 efavirenz derivatives were constructed and fully optimized by *ab-initio* molecular orbital method at HF/3-21G level. The very similar binding conformations of these inhibitors show that they interact with K103N HIV-1 RT in a very similar way. Based on the molecular alignment of conformations obtained from molecular docking procedures, the high predictive 3D-QSAR models were produced by using CoMFA and CoMSIA approaches. The CoMFA models reveal the importance of steric and electrostatic interactions through contour maps. The resulting CoMSIA models enhance the understanding of steric, electrostatic, hydrophobic, electron donor and acceptor requirements for ligands binding to the K103N HIV-1 RT. Consequently, the results obtained from structure-based and ligand-based design approaches can be integrated to identify the structural requirements of HIV-1 RT inhibitors in the class of efavirenz compounds. The principle derived from the present study provides a beneficial guideline to design and predict new and more potent compounds active against K103N HIV-1 RT.

The Investigation on the Interactions between HIV-1 RT Inhibitors of Efavirenz Analogues and HIV-1 RT, Based on Molecular Docking Calculations

Porupan Pangpo[1], Anvadee Pankvang[1], Patchreenart Saparpakorn[1] and Supa Hannongbua[2]
[1] Faculty of Science, Ubonratchathani University, Ubonratchathani, Thailand, 34190
[2] Faculty of Science, Kasetsart University, Bangkok, Thailand, 10900

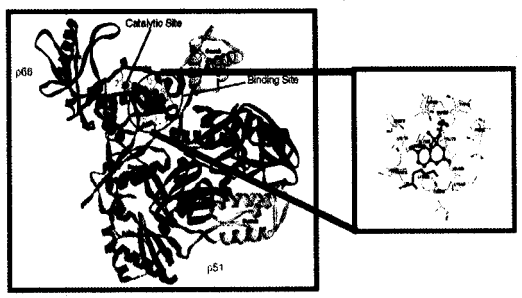

Figure 1. X-ray crystallograpic structure of efavirenz/ WT HIV-1 RT complexes and its binding pocket.

RESULTS

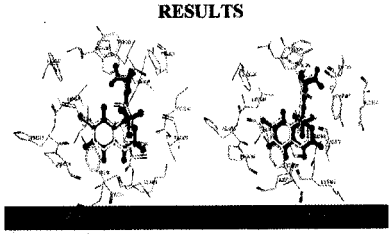

Figure 2. Comparison of X-ray pose orientation of efavirenz (yellow) and the docked conformation of efavirenz (green) in the WT and K103 HIV-1 RT binding pocket.

INTRODUCTION

Efavirenz is a second-generation non-nucleoside inhibitor of HIV-1 reverse transcriptase (RT) that has recently been approved for use against HIV-1 infection. However, the efficacy of the inhibitor is significantly reduced by the appearance of drug-resistant mutant viruses of HIV-1 RT, in particular the Lys103-Asp mutation (K103N). Therefore, the investigation on structural requirement for higher inhibition on the viral replication of the mutant HIV-1 RT is still required. As the availability of X-ray crystallographic structures of efavirenz in complex with both wild-type and K103N HIV-1 RT are available, docking studies have been performed for efavirenz derivatives in the WT and K103N HIV-1 RT binding pocket in order to gain an insight into the potential binding orientation and the interaction of efavirenz derivatives with HIV-1 RT.

METHODS OF CALCULATIONS

The starting geometry of efavirenz was taken from X-ray crystallographic data. A set of 58 efavirenz compounds were constructed and fully optimized by *ab-initio* molecular orbital method at HF/3-21G level. Docking studies were carried out using Autodock 3.0 for efavirenz derivatives in the WT and K103N HIV-1 RT binding pocket.

Table 1. The structures and inhibitory activities of selected efavirenz derivatives.

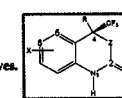

No.	X	R	Z	Exp. IC50 WT RT	Exp. IC50 K103N RT
1 (Efavirenz)	6-Cl	CC-cyclopropyl	O	8.77	7.19
2	5-F	CC-cyclopropyl	NH	8.85	7.05
3	6-Cl	$OCH_2CHCHCH_2$(cis)	O	8.36	6.63
4	5-MeO,6-Cl	CC-cyclopropyl	NH	8.46	8.12
5	6-F	CC-2-pyridyl	NH	8.30	6.32

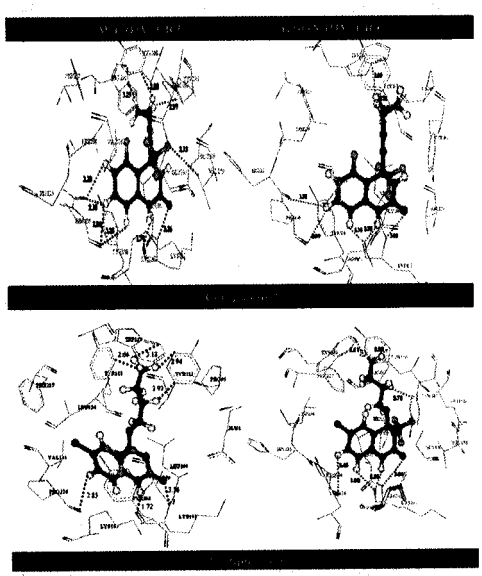

Figure 3. Docked conformations of efavirenz derivatives in WT and K103N HIV-1 RT binding pocket

CONCLUSIONS

- The docking method can be successfully applied to provide the potential binding mode of efavirenz derivatives in WT and K103N HIV-1 RT binding pocket.
- For the higher active compound dealing with WT inhibition, hydrogen-bond interaction between 6-H position of the benzoxazin-2-one ring and oxygen atom of His235 is required, whereas hydrogen-pi interaction between the hydrogen atom attached to the nitrogen atom on the Z substituent and the phenyl ring of Tyr 181 are necessary for mutant type inhibition.
- The docking results gave good insights into the HIV-1 RT-ligand interactions. This information provides beneficial guideline to design new more potent compounds active against both WT and K103N HIV-1 RT.

ACKNOWLEDGEMENTS

- Thailand Research Fund (MRG4880001, BRG478007)
- The Golden Jubilee Ph.D. program (3.C.KU/45/B.1)

A-CBES168

International Conference on Modeling in Chemical and Biological Engineering Sciences

The investigation on the interactions between HIV-1 RT inhibitors of efavirenz analogues and HIV-1 RT, based on molecular docking calculations

Pornpan Pungpo[1*], Oradee Pankwang[1], Patchreenart Saparpakorn[2] and Supa Hannongbua[2]

[1]*Faculty of Science, Ubonratchathani University, Ubonratchathani, Thailand, 34190*
[2]*Faculty of Science, Kasetsart University, Bangkok, Thailand, 10900*

Structure-based inhibitor design approach, based on computational docking studies, has been applied to model the potential binding modes of 58 efavirenz derivatives in the binding pocket of WT and K103N HIV-1 RT. The results show that the Autodock 3.0 method reveals a good ability to reproduce the X-ray bound conformation with rmsd less than 0.6 Å for both WT and mutant enzymes. The docking calculations of all efavirenz derivatives in the data set were, consecutively, performed toelucidate their orientations in the binding pockets. The results derived from docking analysis give additional information and further probes the inhibitor-enzyme interactions. The correlation of the results obtained from docking models and the inhibitory activities validate each other and lead to better understanding of the structural requirements for the activity. Therefore, these results are informative to improve the development of more efficient HIV-1 RT inhibitors, especially, active against mutant enzyme.

*Corresponding author
Tel. 66-45-288400 ext. 4114
e-mail; pornpan_ubu@yahoo.com

Conformational Analysis of HIV-1 Reverse Tranceriptase Inhibitor (S)-6-Chloro-4-(Cyclopropylethenyl)-1,4-Dihydro-4-(Trifluoromethyl)-2H-3,1-Benzoxazin-2-One (Efavirenz) and Its Derivtives, by Using Quantum Chemical Calculations

Amadee Panket[1], Patchreenart Saparpakorn[2], Supa Hannongbua[2] and Pornpan Pungpo[1]

[1]Department of Chemistry, Faculty of Science, Ubonratchathani University, Ubonratchathani, 34190
[2]Department of Chemistry, Faculty of Science, Kasetsart University, Bangkok, 10900

INTRODUCTION

The Human Immunodeficiency Virus Type I (HIV-1) was identified as the etiologic agent of the Acquired Immune Deficiency Syndrome (AIDS). The HIV-1 reverse transcriptase (HIV-1 RT) has been the active target of several antiviral therapeutic agent used in the treatment of AIDS. Efavirenz is one of the most specific and potent non-nucleoside reverse transcriptase inhibitors (NNRTIs) of HIV-1 RT currently used for clinically AIDS treatment. The important features of this compound are presenting the butterfly-like shape in the complex of bound HIV-1 RT/Efavirenz and high flexibility of structure. These reasons lead us to investigate the conformational analysis of Efavirenz and its derivatives.

METHODOLOGY

Conformational analysis of efavirenz compound and its derivatives (the best compound active against WT and K103N HIV-1 RT) were investigated based on various method of quantum chemical calculations. AM1, PM3, HF/3-21G, HF/6-31G* and B3LYP/6-31G*. The starting geometry of (-) 6-chloro-4-(cyclopropylethenyl)-1,4-dihydro-4-(trifluoromethyl)-2H-3,1-benzoxazin-2-one or efavirenz compound was taken from the complex X-ray crystal structure of the HIV-1 RT and efavirenz (pdb code: 1FK9). The fully geometry optimization were performed at the HF/3-21G level. The potential energy surfaces at the side chains of the molecules were examined. The calculated conformations were then compared to the results of X-ray investigation on efavirenz associated with HIV-1 RT and the docked conformation obtained from molecular docking calculations based on AUTODOCK 3.0 program.

RESULTS AND DISCUSSION

I. Conformational Analysis of Efavirenz compound

The rotational potential along the C-C bond connecting the cyclopropyl side chain to the heterocyclic ring (see Scheme 1) of efavirenz compound (Figure 1a) were calculated by using various calculations. Based on HF and B3LYP result, two pronounced energetic local minima were found at the similar region, whereas AM1 and PM3 calculations seem to be not accurate enough to obtain helpful information regarding conformational analysis of this molecule (Figure 1b). The superimposition of X-ray crystal structure of efavirenz and docked conformation derived from docking calculations and calculated lowest energy conformation obtained from all methods of calculations indicates that B3LYP/6-31G* results give the most similar conformation to the geometry obtained from the X-ray structure (Figure 1c).

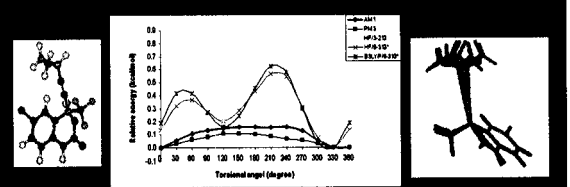

II. The best efavirenz derivative active against wild type HIV-1 RT

The rotational potential profile (Figure 2b) of the alpha angle shows that the global minimum is 140 degree obtained from all methods of calculations. However the energy barrier between the local minima is very small. The superimposition of docked conformation and calculated lowest energy conformation are similar for all methods and different from the docked conformation (Figure 2c).

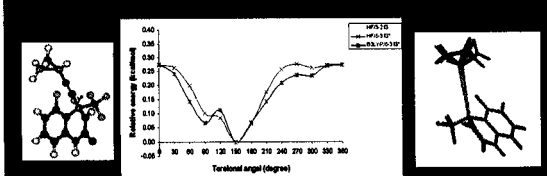

III. The best efavirenz derivative active against K103N HIV-1 RT

Figure 3 shows the structure of the best efavirenz derivative active against K103N HIV-1 RT. The rotational potential profile of the alpha angle show that the global minimum at 270 degree for HF/6-31G* and B3LYP/6-31G* and at 60 degree for HF/3-21G (Figure 3a). The superimposition of docked and calculated lowest energy conformation obtained from all calculation method show that HF/3-21G result gives more similar conformation to the docked conformation (Figure 3b). Another the rotational potential of the methoxy side chain to the heterocyclic ring (see Scheme 2) were calculated. Two local minima were announced at 60 degree and 300 degree and the energy barrier between the local minima is very large ranging from 10 to kcal/mol (Figure 3d). The superimposition of docked conformation and lowest energy conformation obtained from all method of calculations show that B3LYP/6-31G* results correspond well to the docking conformation (Figure 3b).

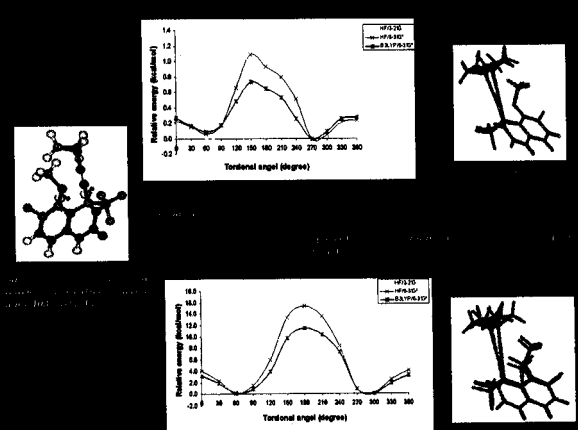

ACKNOWLEDGEMENTS

The Thailand Research Fund (TRF) is acknowledged for its financial support.

Abstract: Al(III)PO_4•H_2O and its deutearated analogues have been synthesized and investigated by FT-IR and FT-Raman spectroscopy. Vibrational bands are identified in relation to the crystal structure in terms of the fundamental vibrating units namely PO_4^{3-}, H_2O, AlO_4 and AlO_6. The vibrational modes of PO_4^{3-} ion and H_2O molecules are analyzed based on the correlation field splitting. Three FTIR bands of OH stretching of HOH are observed at 3447, 3369, and 3121 cm^{-1}. The band at 3369 cm^{-1} is assigned to weakly hydrogen bonded water and the band at 3121 cm^{-1} to strong hydrogen bonded water. The OD stretching bands of deuterated analogues are observed at 2551, 2499 and 2376 cm^{-1} which resemble the spectral profile of OH stretching of HOH region. Two HOH bending are observed at 1662, 1639 cm^{-1} and HOD bending at 1491, 1455 cm^{-1}. These doublet bands indicate two types of water molecules with different hydrogen bonding strengths. The bands at 3369 and 3121 cm^{-1} lead to the estimation of $R_{O_w...O}$ by using a Libowitzky type function that found to be 2.778 and 2.680 Å. The correlation function for the estimation is in the form $v_1 = 3592 - 304 \times 10^9 \exp(R_{O_w...O}/0.1321)$, $R^2 = 0.96$ [Libowitzky, 1999].

C4_C0259 CONFORMATIONAL ANALYSIS OF HIV-1 REVERSE TRANSCRIPTASE INHIBITOR(S)-6-CHLORO-4-(CYCLOPROPYLETHYNYL)-1,4-DIHYDRO-4-(TRIFLUOROMETHYL)-2H-3,1-BENZOXAZIN-2-ONE (EFAVIRENZ) AND ITS DERIVATIVES, BY USING QUANTUM CHEMICAL CALCULATIONS

Auradee Punkvang[1*], Patchareenart Saparpakorn[2], Supa Hannongbua[2] and Pompan Pungpo[1]
[1] Department of Chemistry, Faculty of Science, Ubonratchathani University, Ubonratchathani, 34190
[2] Department of Chemistry, Faculty of Science, Kasetsart University, Bangkok, 10900
E-mail address: Punkvang@yahoo.com

Abstract: Conformational analysis of HIV-1 reverse transcriptase inhibitor (s)-6-chloro-4-(cyclopropylethynyl)-1,4-dihydro-4-(trifluoromethyl)-2H-3, 1-benzoxazin-2-one (efavirenz) and its derivatives (the best compounds active against WT and K103N HIV-1 RT) were investigated based on various methods of quantum chemical calculations, AM1, PM3, HF/3-21G, HF/6-31G* and B3LYP/6-31G*. The starting geometry of efavirenz was taken from X-ray crystallographic data. The rotational potentials along the single bond between the cyclopropylethynyl group and atoms in the heterocyclic ring (alpha dihedral angle) for all derivatives were examined. Moreover, the rotational potentials of the methoxy side chain to the heterocyclic ring system (beta dihedral angle) were also considered. The comparison of the calculated energy minimum conformations with the X-ray HIV-1 RT/efavirenz complexed structure and the docked conformations derived by docking calculations. The results show that based on HF and B3LYP calculations, the energetical favorable conformers were found at the similar regions, whereas AM1 and PM3 calculations seem to be not accurate enough to obtain helpful information of conformational analysis of this molecules. For the alpha dihedral angles of efavirenz derivatives, the energetical favorable conformation obtained from B3LYP/6-31G* show high correspondence to the conformation in the X-ray crystallographic structure, whereas the energy minimum conformer obtained from HF/3-21G is good agreement with the docking conformer. Whereas, for the beta dihedral angle, it is interesting to note that an energy minimum conformation obtained from B3LYP/6-31G* calculation is the most similar to the docking conformer. Consequently, the comparative conformational analysis provide beneficial information concerning the conformational possibilities and the range of flexibility which is related to the biological behaviors of efavirenz derivatives to inhibit WT and K103N HIV-1 RT.

C4_C0265 Theoretical study of structure and energetic of a novel pyrrolidinyl PNA binding to DNA

Khatcharin Siriwong,[a,*] Parawan Chuichay,[b] Suwipa Saen-oon,[c] Tirayut Vilaivan[c] and Supot Hannongbua[c]
[a] Department of Chemistry, Faculty of Science, Khon Kaen University, Khon Kaen 40002, Thailand
[b] Department of Physics, Faculty of Science, Kasetsart University, 50 Phahon Yothin Road, Cha-tuchak, Bangkok 10900, Thailand
[c] Department of Chemistry, Faculty of Science, Chulalongkorn University, Phayathai Road, Paturnwan, Bangkok 10330, Thailand

Abstract: -Molecular dynamics (MD) simulations have been used to study the structure of a novel pyrrolidinyl PNA binding to DNA (PNA×DNA) for both parallel and antiparallel configurations in aqueous solution. A DNA duplex (DNA×DNA) was also carried out for comparison. B-like form was used as a model for all starting structures. MD trajectories were generated for 2 ns using AMBER 8 package. Furthermore, Molecular Mechanics-Generalized Born/surface area (MM-GBSA) approach and normal-mode analysis have been used as the postprocess to evaluate the binding free energy of the double strand. As a result, the trajectories show a stability of duplexes during the simulation time period. Both DNA×DNA and PNA×DNA(antiparallel) duplexes remain in canonical B as their starting structures, whereas a distortion from B-like is observed in PNA×DNA(parallel) duplex. As shown by the radial distribution function, the distance of the first solvation shell of PNA strand is larger than that of DNA strand because of a hydrophobic property of PNA. MM-GBSA result shows that PNA×DNA(antiparallel) is the most stability and parallel fashion is more stable than DNA duplex, which are in agreement with the experimental data.

C4_C0266 THEORETICAL INVESTIGATIONS ON STRUCTURAL ELECTRONIC AND OPTICAL PROPERTIES OF CARBAZOLE-CAPPED MOLECULES AS NOVEL BLUE LIGHT-EMITTING HOLE-TRANSMITTING MATERIALS, BASED ON QUANTUM CHEMICAL CALCULTIONS

Pompan Pungpo[1*], Songwut Suramitr[2] and Siriporn Jungsuttiwong[1]
[1]Department of Chemistry, Faculty of Science, Ubonratchathani University, Ubonratchathani, 34190
[2]Department of Chemistry, Faculty of Science, Kasetsart University, Bangkok, 10900
E-mail address: pompan_ubu@yahoo.com

Abstract: The conformational analysis and electronic properties for carbazole-capped molecules as novel blue light-emitting

Conformational Analysis of HIV-1 Reverse Transcriptase Inhibitors (S)-6Chloro-4(Cycloptopyl ethynyl)-1,4-Dihydro-4-(Trifluoromethyl) 2H-3, 1-Benzoxazin-2 One (Efavirenz) and Its Derivatives, by Using Quantum Chemical Calculations

Autsadee Punkvang[1], Patchreenart Saparpakorn[2], Supa Hannongbua[2] and Pornpan Pungpo[1]

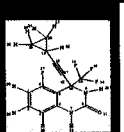

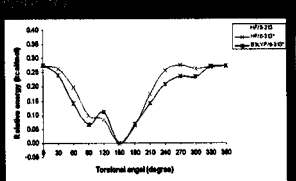

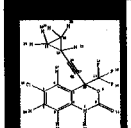

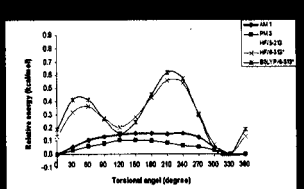

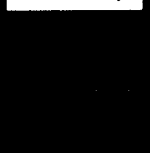

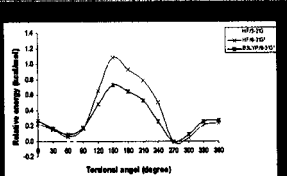

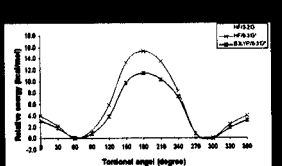

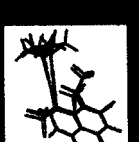

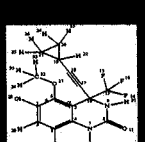

Title **CONFORMATIONAL ANALYSIS OF HIV-1 REVERSE TRANSCRIPTASE INHIBITOR (S)-6-CHLORO-4-(CYCLOPROPYLETHYNYL)-1,4-DIHYDRO-4-(TRIFLUOROMETHYL)-2H-3, 1-BENZOXAZIN-2-ONE (EFAVIRENZ) AND ITS DERIVATIVES, BY USING QUANTUM CHEMICAL CALCULATIONS**

Author *Auradee Punkvang*[1]

Advisor *Pornpan Pungpo*[1], *Supa Hannongbua*[2]

Affiliation [1]*Department of Chemistry, Faculty of Science, Ubonratchathani University, Ubonratchathani, 34190*

[2]*Department of Chemistry, Faculty of Science, Kasetsart University, Bangkok, 10900*

E-mail Address *punkvang@yahoo.com*

Keywords -

Abstract Conformational analysis of HIV-1 reverse transcriptase inhibitor (S)-6-chloro-4-(cyclopropylethynyl)-1,4-dihydro-4-(trifluoromethyl)-2H-3,1-benzoxazin-2-one (efavirenz) and its derivatives (the best compounds active against WT and K103N HIV-1 RT) were investigated based on various methods of quantum chemical calculations, AM1, PM3, HF/3-21G, HF/6-31G* and B3LYP/6-31G*. The starting geometry of efavirenz was taken from x-ray crystallographic data. The rotational potentials along the single bond between the cyclopropylethynyl group and atoms in the heterocyclic ring (alpha dihedral angle) for all derivatives were examined. Moreover, the rotational potentials of the methoxy side chain to the heterocyclic ring system (beta dihedral angle) were also considered. The comparison of the calculated energy minimum conformations with the x-ray HIV-1 RT/efavirenz complexed structure and the docked conformations derived by docking calculations were performed. The results show that based on HF and B3LYP calculations, the energetically favorable conformers were found at the similar regions, whereas AM1 and PM3 calculations seem to be not accurate enough to obtain helpful information of conformational analysis of these molecules. For the alpha dihedral angles of efavirenz derivatives, the energetical favorable conformation obtained from B3LYP/6-31G* show high correspondence to the conformation in the X-ray crystallographic structure, whereas the energy minimum conformer obtained from HF/3-21G is good agreement with the docking conformer. For the beta dihedral angle, it is interesting to note that an energy minimum conformation obtained from B3LYP/6-31G*calculation is the most similar to the docking conformer. Consequently, the comparative conformational analysis of the efavirenz compounds and its derivatives provides fundamental information concerning the conformational possibilities and the range of flexibility which is related to the biological behaviors of efavirenz derivatives to inhibit WT and K103N HIV-1 RT.

Identification of Binding and Interaction for HIV-1 RT Inhibitors in the Class of Efavirenz Derivatives in the Binding Pocket of WT and K103N HIV-1 RT by Using Molecular Docking Studies

Pornpan Pungpo[1], Auradee Punkvang[1], Patchreenart Saparpakorn[2] and Supa Hannongbua[2]
[1]Faculty of Science, Ubonratchathani University, Ubonratchathani, Thailand, 34190
[2]Faculty of Science, Kasetsart University, Bangkok, Thailand, 10900

INTRODUCTION

Efavirenz, a potent non-nucleoside reverse transcriptase inhibitor (NNRTI), has been approved for the clinical use. However, the effectiveness of the inhibitor is limited, as rapid resistant strains of the virus emerged. Mainly, amino acid substitutions at the position 103 and 108 are responsible for the emergence of resistant virus not only for efavirenz but also for NNRTIs. Thus, it is necessary to find new and more effective inhibitors that remain active across these virus mutations.

Figure 1. (a) The efavirenz-WT HIV-1 RT complexed X-ray crystallographic structure and its HIV-1 RT binding pocket.

The availability of X-ray crystallographic structures of efavirenz in complex with both wild type and K103N HIV-1 RT leads to an understanding of some structural factors that confer resilience to drug resistance mutation. In the present study, in order to gain an insight into the potential binding orientation and the interaction of efavirenz derivatives with HIV-1 RT and, consequently, to improve the development of more efficient HIV-1 RT inhibitors, especially, active against mutant enzyme, docking studies have been performed for efavirenz derivatives in the WT and K103N HIV-1 RT binding pocket.

METHODS OF CALCULATIONS

The starting geometry of efavirenz was taken from X-ray crystallographic data. A set of 58 efavirenz compounds, obtained from the experimental data, were built and fully optimized by *ab initio* calculations at HF/3-21G level. Docking studies were carried out using GOLD and Autodock 3.0 for efavirenz derivatives in the WT and K103N HIV-1 RT binding pocket.

Table 1. Summary of selected structures and their inhibitory activities of efavirenz derivatives.

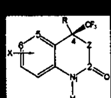

No.	X	R	Z	Exp. log(1/C)	
				WT RT	K103N RT
1 (Efavirenz)	6-Cl	CC-cyclopropyl	O	8.77	7.19
2	[illegible]	CC-cyclopropyl	NH	[illegible]	[illegible]
3	6-Cl	[illegible]	O	[illegible]	[illegible]
4	[illegible]	CC-cyclopropyl	NH	[illegible]	[illegible]
5	[illegible]	CC-2-pyridyl	NH	[illegible]	[illegible]

RESULTS AND DISCUSSION

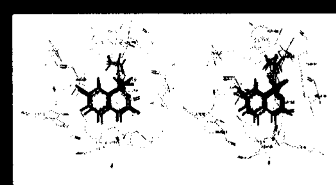

Autodock GOLD

Compound

Docked conformations of efavirenz derivatives in WT HIV-1 RT binding pocket.

Autodock GOLD

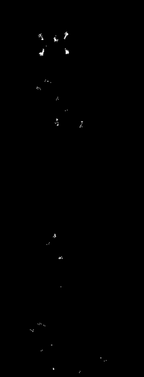

Compound

Docked conformations of efavirenz derivatives in K103N HIV-1 RT binding pocket.

CONCLUSIONS

The docking methods both GOLD and Autodock 3.0 programs can be successfully used to provide the potential binding mode of efavirenz derivatives in WT and K103N HIV-1 RT binding pocket.

For the higher active compound against WT HIV-1 RT, hydrogen bond interaction is needed, whereas hydrogen pi interaction plays important role for K103N HIV-1 RT inhibition.

Molecular docking analysis can support each other and give beneficial guideline in the applicability of structure-activity relationships in drug design.

ACKNOWLEDGEMENTS

Thailand Research Fund (MRG4880001, BRG4-800...)
The Golden Jubilee Ph.D. program (3.C.KU/48/B.1)

Understanding the interaction and the structure–activity correlation of efavirenz derivatives and WT and K103N HIV-1 RT by molecular docking and 3D-QSAR approaches

Pornpan Pungpo[1], Auradee Punkvang[1], Patchreenart Saparpakorn[2] and Supa Hannongbua[2]

[1]Faculty of Science, Ubonratchathani University, Ubonratchathani, Thailand, 34190

[2]Faculty of Science, Kasetsart University, Bangkok, Thailand, 10900

INTRODUCTION

AIDS, caused by HIV infection, is still one of the most important challenges for the chemotherapy of the early 21st century. The number of drugs against this disease is slowly increasing but the chemotherapy is far from being solved. Efavirenz, a potent non-nucleoside reverse transcriptase inhibitor (NNRTI), has been approved for the treatment of infections (SustivaTM). However, the effectiveness of the inhibitor is limited, as rapid resistant strains of the virus emerged. Mainly, amino acid substitutions at the position 103 and 108 are responsible for the emergence of resistant virus not only for efavirenz but also for NNRTIs. Therefore, there is an urgent need for the development of new and more effective inhibitors active against the currently resistant viral strains. In the present study, docking studies by using GOLD and Autodock 3.0 and 3D-QSAR studies based on CoMFA and CoMSIA were performed to understand the interaction and the structure–activity relationship of efavirenz derivatives between a with WT and K103N HIV-1 RT.

RESULTS

I. Docking Results

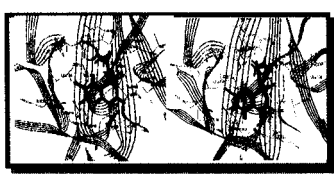

Figure 1. The conformations of docked efavirenz by using GOLD (red) and Autodock (blue) and compared with the orientation of X-ray pose (Ball and Stick color).

Table 1. Selected structures and their inhibitory activities efavirenz derivatives.

no.	X	R	Z	exp. log(1/C) WT RT	exp. log(1/C) K103N RT
1 (Efavirenz)	6-Cl	CC-cyclopropyl	O	8.77	7.19
2	5-F	CC-cyclopropyl	NH	8.85	7.86
3	6-Cl	$OCH_2CHClCH_2$(cis)	O	8.26	6.43
4	5-Me,6-Cl	CC-cyclopropyl	NH	8.46	8.12
5	6-F	CC-2-pyridyl	NH	8.30	6.82

II. 3D-QSAR Results

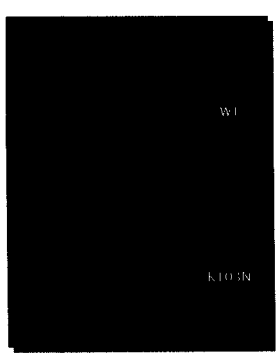

Figure 5. Superimposition of docked efavirenz derivatives in WT and K103N HIV-1 RT.

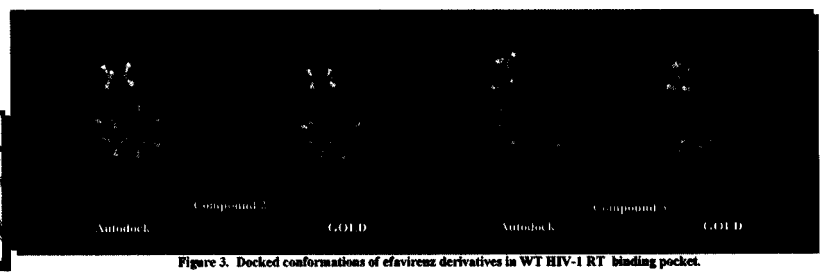

Figure 3. Docked conformations of efavirenz derivatives in WT HIV-1 RT binding pocket.

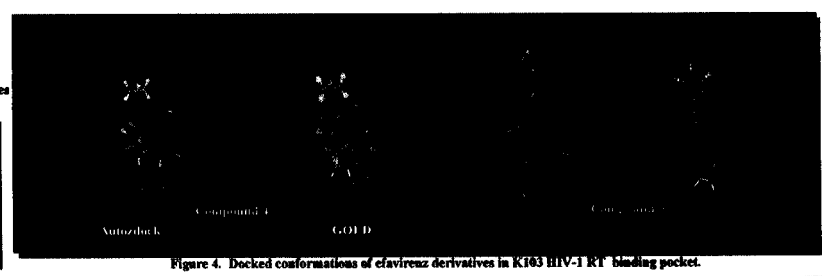

Figure 4. Docked conformations of efavirenz derivatives in K103 HIV-1 RT binding pocket.

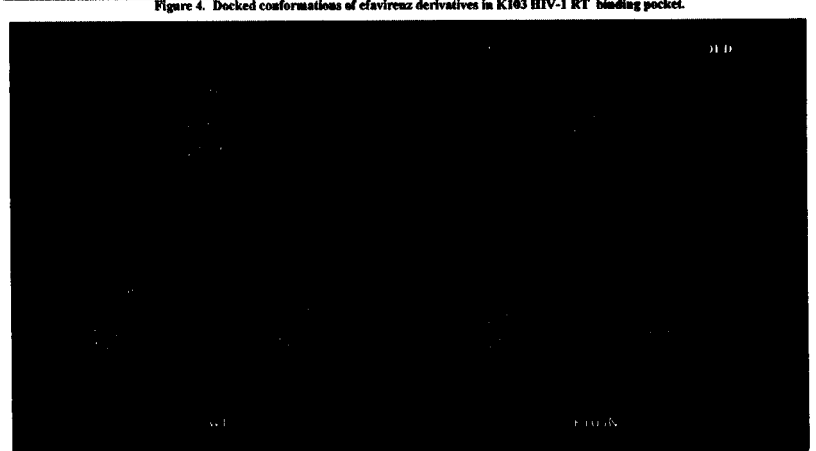

Figure 6 . CoMFA and CoMSIA contour maps of efavirenz derivatives for WT and K103N HIV-1 RT inhibitory activities.

CONCLUSIONS

- The molecular docking and 3D-QSAR methods were successfully combined to investigate the interaction and relationship between structural properties of efavirenz derivatives and HIV-1 inhibitions.
- For the higher active compound against WT HIV-1 RT, hydrogen-bond interaction is needed, whereas hydrogen-pi interaction plays important role for K103N HIV-1 RT inhibition.
- Based on the binding conformations and their alignments inside the binding pocket, highly reliable and predictive 3D-QSAR models were obtained.
- The results obtained from the models agree well with the interactions of the ligand-receptor complexes derived by the experimental data.
- The information obtained from the QSAR results can be integrated to identify the structural requirements of efavirenz derivatives for designing new inhibitors with enhancing WT and K103N HIV–1 RT inhibitory activity.
- The principle derived from the present study provides a beneficial guideline to design and predict new and more potent compounds active against K103N HIV-1 RT.

ACKNOWLEDGEMENTS

- TRF (MRG4880001, BRG478007)
- RGJ Ph.D. program (3.C.KU/45/B.1)

A Combined Approach of Docking and 3D QSAR Studies of Efavirenz Derivatives as Highly Potent HIV-1 RT Inhibitors

Pornpan Pungpo[1], Auradee Punkvang[2], Patchreenart Saparpakorn[3] and Supa Hannongbua[4]

[1,2]Faculty of Science, Ubonratchathani University, Ubonratchathani, Thailand, 34190

[3,4]Faculty of Science, Kasetsart University, Bangkok, Thailand, 10900

Introduction

Efavirenz is a second-generation non-nucleoside inhibitor of HIV-1 reverse transcriptase (RT) that has recently been approved for use against HIV-1 infection [1]. However, the efficacy of the inhibitor is significantly reduced by the appearance of drug-resistant mutant viruses of HIV-1 RT, in particular the Lys103-Asp mutation (K103N). The developments of compounds with the high ability to inhibit both HIV-1 RT need to understand the inhibitory molecular mechanic and structural requirement of inhibitors. In the present study, docking studies have been performed for efavirenz derivatives in the WT and K103N HIV-1 RT binding pocket in order to gain an insight into the potential binding orientation and the interaction of efavirenz derivatives with HIV-1 RT. Moreover, 3D-QSAR studies using comparative molecular field analysis (CoMFA) and comparative similarity indices analysis (CoMSIA) were used to better understand the binding model and the relationship between the physicochemical properties of efavirenz derivatives.

Computational details

The starting geometry of efavirenz was taken from x-ray crystallographic of wild-type RT (1FK9) and K103N RT (1FKO). A set of 56 efavirenz compounds [2-4] were considered and fully optimized by *ab-initio* molecular orbital method at HF/3-21G level. For molecular docking calculations, autodock 3.0 program was used to investigate the potential binding orientations of several efavirenz derivatives in the binding pocket. The conformation with the lowest binding free energy was selected for the structural alignment in 3D-QSAR analyses. CoMFA and CoMSIA studies were applied to determine relationships between structural properties and HIV-1 inhibitions, based on the docked binding conformations.

Results and Discussion

1. Docking analysis

To validate the docking method used, Autodock 3.0 was applied to dock the efavirenz compound back into the WT and K103N HIV-1 RT binding pocket. The rmsd of the docked pose from the X-ray pose of efavirenz compound in the WT and K103N RT binding pockets are less than 1 Å indicating the parameters used for the docking simulations are reasonable in reproducing the X-ray structure. Therefore, Autodock method and its parameters could be extended to search the binding conformations in the binding pocket for all compounds in the data set. The obtained docking conformations were shown in Figure 1. For the highest active compound for WT inhibition, the hydrogen bond between 6-H position of the benzoxazin-2-one ring with the main-chain carbonyl oxygen could be possible to form. In case of highest active compound for K103N inhibition, the replacement of oxygen atom with N-H group on the benzoxazin-2-one ring could increases H-π interaction to Tyr181. These additional interactions seem to be favorable to the binding activity. In contrast, too bulky substituents attached to the C4 position on the ring lead to steric conflict with the amino acid residues Tyr181, Tyr188 and Trp229 in both WT and K103N binding pockets. It could be the main reason for the weaker interactions resulting in least inhibitory activity of compounds 12 and 2. The docking results gave good insights into the HIV-1 RT-ligand interactions.

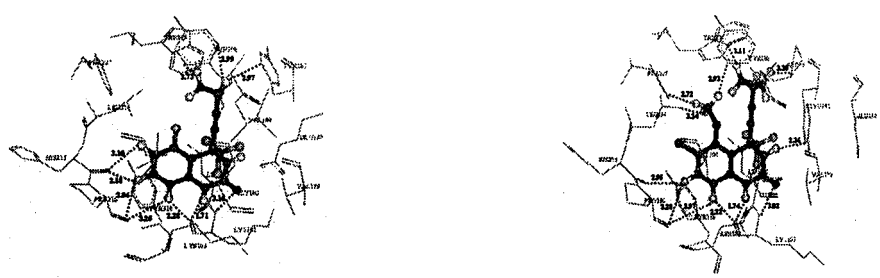

Figure 1. Docked conformations of efavirenz derivatives in WT and K103N HIV-1 RT binding pocket

2

2. QSAR Analysis

Based on the docked alignmemts, all QSAR models obtained are satisfying based on both statistical significance and predictive abilty as indicated by cross-validated r^2 values (r^2_{cv}). The models with r^2_{cv} of 0.662 and 0.708 for CoMFA and CoMSIA were derived based on WT inhibition. For K103N inhibition, the high predictive models with r^2_{cv} of 0.755 and 0.773 for CoMFA and CoMSIA were obtained. The CoMFA and CoMSAI contour maps for WT and K103N RT inhibition are shown in Figures 2-4. CoMFA model reveals the importance of steric and electrostatic interactions through contour maps Figures 2a and 2b. The resulting CoMSIA models enhance the understanding of hydrophobic, electron donor and acceptor requirements for ligands binding to the WT and K103N HIV-1 RT as presented in Figures 3a,3b,4a and 4b. The analysis derived by CoMFA and CoMSIA support each other and clearly highlight different characteristics for different types of wild type and mutant type HIV-1 RT.

Figure 2a. CoMFA contour maps for WT inhibition

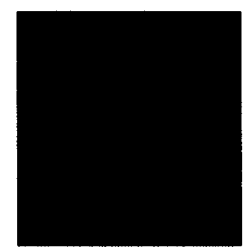

Figure 2b. CoMFA contour maps for K103N inhibition

Figure 3a. CoMSIA hydrophobic contour maps for WT inhibition

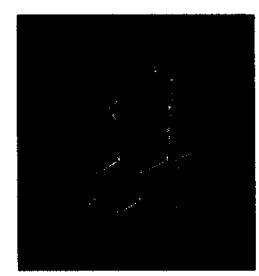

Figure 3b. CoMSIA hydrophobic contour maps for K103N inhibition

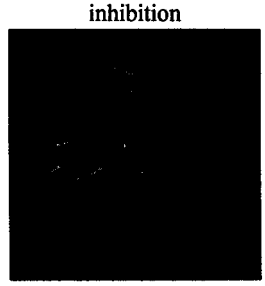

Figure 4a. CoMSIA hydrogen donor and acceptor contour maps for WT inhibition

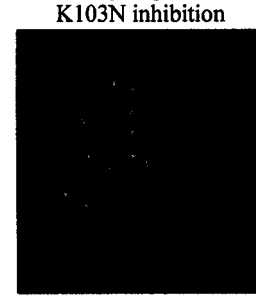

Figure 4a. CoMSIA hydrogen donor and acceptor contour maps for K103N inhibition

Conclusion

In the present study, the molecular docking and 3D-QSAR methods were successfully combined to investigate the relationship between structural properties and HIV-1 inhibitions. The best binding conformations of efavirenz derivatives were determined using docking calculations. Based on the binding conformations and their alignments inside the binding pocket, highly reliable and predictive 3D-QSAR models were obtained. The results obtained from the models agree well with the interactions of the ligand-receptor complexes derived by the experimental data. Accordingly, the information obtained from the QSAR results can be integrated to identify the structural requirements of efavirenz derivatives for designing new inhibitors with enhancing WT and K103N HIV–1 RT inhibitory activity.

3

Acknowledgements

The grants provided by the Thailand Research Fund (TRG4880001 and BRG4780007) are gratefully acknowledged. We thank LCAC,the National Electronics and Computer Technology (HPCC/NECTEC) for providing computational resources.

Reference

[1] Young, S.D., *et al. Antimicrob. Agents Chemother.*, 39, (1995), 2602.
[2] Corbett, J.W., *et al. J. Med. Chem.*, 43, (2000), 2019-30.
[3] Corbett, J.W., *et al. Bioorg. Med. Chem. Lett.*, 11, (2001) 211-214.
[4] Cocuzza, A.J., *et al. Bioorg. Med. Chem. Lett.*, 11, (2001), 1177-1179.
[5] Cocuzza, A.J.,.*et al. Bioorg. Med. Chem. Lett.*, 11, (2001), 1389-1392.

PUBLICATIONS

1. Pornpan Pungpo, Auradee Punkvang, Patchreenart Saparpakorn and Supa Hannongbua. Understanding the interaction and the structure activity correlation of HIV-1 RT inhibitors of efavirenz derivatives and WT and K103N HIV-1 RT using molecular docking, 3D-QSAR approaches and quantum chemical calculations, accepted for publication as a chapter in *Drug design reserach trend, Nova Science Publishers, Inc., 2007.*

Understanding the interaction and the structure–activity correlation of HIV-1 RT inhibitors of efavirenz derivatives and WT and K103N HIV-1 RT using molecular docking, 3D-QSAR approaches and quantum chemical calculations

Pornpan Pungpo[1*], *Auradee Punkvang*[1], *Patchreenart Saparpakorn*[2] *and*

Supa Hannongbua[2]

[1]*Faculty of Science, Ubonratchathani University, Ubonratchathani, Thailand, 34190*

[2]*Faculty of Science, Kasetsart University, Bangkok, Thailand, 10900*

Molecular docking and 3D-QSAR analyses were performed to understand the interaction between a series of efavirenz derivatives with WT and K103N HIV-1 RT. To model the potential binding modes of efavirenz derivatives in the binding pocket of WT and K103N HIV-1 RT, molecular docking approaches by using GOLD and Autodock 3.05 programs were performed. The results show that the docking results obtained from both methods reveal a good ability to reproduce the X-ray bound conformation with rmsd less than 1.0 Å for both WT and mutant enzymes. The docking calculations of all efavirenz derivatives in the data set were, consecutively, performed to elucidate their orientations in the binding pockets. The results derived from docking analysis give additional information and further probes the inhibitor-enzyme interactions. The correlation of the results obtained from docking models and the inhibitory activities validate each other and lead to better understanding of the

structural requirements for the activity. Therefore, these results are informative to improve the development of more efficient HIV-1 RT inhibitors, especially, active against mutant enzyme. Based on the molecular alignment of conformations obtained from molecular docking procedures, the high predictive 3D-QSAR models were produced by using CoMFA and CoMSIA approaches. The CoMFA models reveal the importance of steric and electrostatic interactions through contour maps. The resulting CoMSIA models enhance the understanding of steric, electrostatic, hydrophobic, electron donor and acceptor requirements for ligands binding to the K103N HIV-1 RT. Moreover, quantum chemical calculations were carried out to analyze the interaction energies of the selected inhibitors with the individual amino acids in the binding pocket. The obtained results show the important interactions of inhibitors with the enzyme at the residue level. Consequently, the results obtained from structure-based, ligand-based design approaches and quantum chemical calculations can be integrated to identify the structural requirements of HIV-1 RT inhibitors in the class of efavirenz compounds. The principle derived from the present study provides a gainful guideline to design and predict new and more potent compounds active against WT and K103N HIV-1 RT.

VITAE

NAME : Miss Auradee Punkvang

BIRTH DATE : July 04, 1980

BIRTH PLACE : Ubonratchathani, Thailand

NATIONALITY : Thai

EDUCATION

: YEAR	INSTITUTION	DEGREE
2000-2003	Ubonrajathanee University	B.Sc. (Chemistry)

PUBLICATIONS

1. Pornpan Pungpo, Auradee Punkvang, Patchreenart Saparpakorn and Supa Hannongbua. Understanding the interaction and the structure activity correlation of HIV-1 RT inhibitors of efavirenz derivatives and WT and K103N HIV-1 RT using molecular docking, 3D-QSAR approaches and quantum chemical calculations, accepted for publication as a chapter in *Drug design reserach trend, Nova Science Publishers, Inc., 2007.*

POSTER CONTRIBUTIONS TO CONFERENCES

INTERNATIONAL CONFERENCE

1. Pornpan Pungpo, Auradee Punkvang, Patchareenart Saparpakorn, Peter Wolschann and Supa Hannongbua. Theoretical Investigations on Potent HIV-1 Reverse Transcriptase Inhibitors of Efavirenz Analogues by Using Conformational Analysis, Molecular Docking and 3D-QSAR Studies. *The XIIth International Congress of Quantum Chemistry (XII-ICQC2006), 21-26 May, 2006, Kyoto, Japan.*
2. Pornpan Pungpo, Auradee Punkvang, Patchreenart Saparpakorn and Supa Hannongbua. The Investigation on the Interactions between HIV-1 RT Inhibitors of Efavirenz Analogues and HIV-1 RT, Based on Molecular Docking Calculations. *International Conference on*

Modeling in Chemical and Biological Engineering Sciences. 26-27 Octuber, 2006, Bangkok, Thailand.

NATIONAL CONFERENCE

1. Auradee Punkvang, Patchreenart Saparpakorn, Supa Hannongbua and Pornpan Pungpo. Conformational Analysis of HIV-1 Reverse Trancriptase Inhibitor (S)-6-Chloro–4-(Cyclopropylethenyl)-1,4–Dihydro-4-(Trifluoromethyl)-2H-3,1-Benzoxazin-2-One(Efavirenz) and Its Derivtives, by Using Quantum Chemical Calculations. *The 32nd Congress on Science and Technology of Thailand, October, 10-12, 2006, Bangkok, Thailand.*
2. Auradee Punkvang, Patchreenart Saparpakorn, Supa Hannongbua and Pornpan Pungpo. Theoretical Investigation of Highly Potent HIV-1 RT Inhibitors in The Class of Efavirenz Derivatives, Based on Quantum Chemical Calculations and Molecular Modeling. *The 6th National Symposium on Graduate Research 13-14 October 2006, Bangkok, Thailand.*
3. Pornpan Pungpo, Auradee Punkvang, Patchreenart Saparpakorn and Supa Hannongbua. Identification of Binding and Interaction for HIV-1 RT Inhibitors in the Class of Efavirenz Derivatives in the Binding Pocket of WT and K103N HIV-1 RT by Using Molecular Docking Studies. *The first annual symposium of Protien Research Society of THAILAND "Challenges in Protein Research in Thailand" 24-25 October, 2006, Bangkok, Thailand.*
4. Pornpan Pungpo, Auradee Punkvang, Patchreenart Saparpakorn and Supa Hannongbua. Understanding the Interaction and the structure–Activity Correlation of Efavirenz Derivatives and WT and K103N HIV-1 RT by Molecular Docking and 3D-QSAR Approaches. *The 8th International Meeting "Molecular Epidemiology and Evolutionary Genetics of Infectious Disease" (MEEGID VIII). 30 November – 2 December, 2006, Bangkok, Thailand.*
5. Pornpan Pungpo, Auradee Punkvang, Patchreenart Saparpakorn and Supa Hannongbua. A Combined Approach of Docking and 3D QSAR Studies of Efavirenz Derivatives as Highly Potent HIV-1 RT Inhibitors. *The 11th Annual National Symposium on Computational Science and Engineering. 28-30 March October, 2007, Phuket , Thailand.*